IDENTIFICATION OF A KEY REGULATORY PATHWAY IN BONE REGENERATION USING A NOVEL MOUSE FRACTURE MODEL

by

MICHAELE BETH MANIGRASSO

A Dissertation submitted to the

Graduate School-New Brunswick

Rutgers, The State University of New Jersey

and

The Graduate School of Biomedical Sciences

University of Medicine and Dentistry of New Jersey

in partial fulfillment of the requirements

for the degree of

Doctor of Philosophy

Graduate Program in Biomedical Engineering

written under the direction of

James Patrick O'Connor, PhD

and approved by

_____

_____

_____

_____

_____

New Brunswick, New Jersey

October 2007

ABSTRACT OF THE DISSERTATION

IDENTIFICATION OF A KEY REGULATORY PATHWAY IN BONE REGENERATION USING A NOVEL MOUSE FRACTURE MODEL

By Michaele Beth Manigrasso

Dissertation Director:
James Patrick O'Connor, PhD

Fracture healing is the complex biological process that restores broken bones to their original shape and function. While the fracture repair process follows a definitive sequence of events, not all the molecular or chemical pathways are completely understood. The development of animals with targeted mutations has allowed for the examination of specific fracture healing pathways, making the use of the mouse model an increasingly valuable tool in the field of orthopaedics. Additionally, evaluating the healing tissues using a torsional mechanical testing protocol is more reproducible and provides a better estimate of the biomechanical properties. Therefore, the first section of this dissertation is focused on the development and characterization of a murine femoral fracture model suitable for torsional mechanical testing. The model developed was tested using radiography, histology and mechanical testing and was shown to be

comparable to other published femoral fracture models. After validation of this model, the next experiment focused on exploring how a complex phenotype, such as bone mineral density, may affect bone healing. Using inbred strains of mice with established bone mineral density values, the radiographic, histologic and biomechanical analyses of the healing femurs were evaluated. This data showed that having a high bone mineral density actually results in lower mechanical properties and therefore may be deleterious to fracture repair. Finally, this mouse fracture model was used to see how altering the arachidonic acid pathway affects fracture healing. Using genetically modified mice and the fracture and mechanical testing protocols as described, the role of the arachidonic acid pathway in fracture repair was examined. This data showed that either inhibition or acceleration of fracture repair is achieved by manipulating this pathway.

Dedication

For My Mother,

Love Always, Your Michaele

I would first like to thank and remember my mother, Dolores Manigrasso. This was the hardest page to write and the last one completed. While I am saddened that you didn't get the chance to see the end of all of this, I know I was loved more than any one little girl deserved or needed. I am truly grateful for having the opportunity of being your daughter, even if it was only for a short time. I promise you that I will keep my head up and take my chances on everyday. I love and miss you very much.

I would also like to acknowledge and thank my father, James Manigrasso. If I had to bet money on who would have my back during all of this, I would have lost and lost big. I want to thank you for showing up and for backing this horse. I won't forget it. I suppose this means I can no longer stick you in that nursing home. Oh well, I guess you will have to live with me. I love you, Daddy.

To my committee, thank you for the all of the support and guidance.

Last, but never least, I would like to say thank you to my husband, Jay Geiger. I would like to thank you for all the support these past three years and for loving me in spite of everything I do. I couldn't have picked a better man to secure my financial future. Always remember, these are better days.

Table of Contents

LIST OF TABLES

LIST OF FIGURES

1.0.0 Introduction

1.1.0 Biology of Fracture Repair

Fracture healing is a complex biological process that restores broken bones to their original shape and function. Though the molecular and cellular pathways that govern fracture healing are not completely understood, the fracture repair process follows a definitive, multistage, chronological, and spatial sequence of events involving the recruitment of cells to the fracture site and the expression of particular genes during these stages (1-4). Clinically, fracture healing has been broadly divided into two different processes: direct or primary fracture healing and indirect or secondary fracture healing.

1.1.1 Indirect Fracture Healing

Indirect fracture healing is the natural biological process to restore broken bones to their original shape and function. This repair process is characterized by responses from the periosteum and surrounding external soft tissues with the subsequent formation of a fracture callus (2,5,6). Formation of the callus is generally enhanced by limited motion of the broken bone ends at the fracture site and is inhibited by rigid fixation of the broken bone (7). Secondary fracture healing forms new bone through intramembranous ossification and endochondral ossification. Intramembranous ossification is the direct formation of bone, without first forming cartilage, from committed osteoprogenitor and undifferentiated mesenchymal cells residing in the periosteum (2). This results in the formation of what is histologically referred to as the “hard callus”.

Endochondral ossification involves the recruitment, proliferation, and differentiation of undifferentiated mesenchymal cells into cartilage. This newly formed cartilage eventually becomes calcified and is replaced by bone during the process of endochondral ossification (2).

In 1975, Cruess and Dumont proposed a sequence of three overlapping stages to characterize the fracture healing cascade (8). The first stage was defined as the inflammatory reaction stage, followed by the reparative stage and finally bone remodeling stage. This scheme was based largely on descriptive histology. Other groups have divided fracture healing into as many as five phases or stages (2,7,9). For simplicity, the three stages as proposed by Cruess and Dumont will be discussed. It should be noted that none of these events are independent. In fact, the stages overlap with the results of the earlier stages affecting the progress of the later stages.

1.1.1.1 The Inflammatory Reaction Stage

The inflammatory reaction stage is the period immediately following bone fracture and is the initiating event of the fracture repair process. Due to the disruption of skeletal integrity, normal vascular structures, and nutrient flow at the fracture site, there is a reduction in oxygen tension and a disruption of the bone marrow architecture. This causes the infiltration of inflammatory cells, macrophages, and degranulation of platelets and results in the formation of a blood clot, or hematoma (2,10). This clot serves as a reservoir for cytokines and growth factors that begin the healing cascade (11). Inflammatory cells and

platelets within this clot release important factors needed for chemotaxis, proliferation, angiogenesis and differentiation of mesenchymal cells into osteoblasts or chondrocytes (11,12). The hematoma also establishes a fibrin network that provides a pathway for further cell migration (8). While not all pathways are known, it is presumed that various growth factors responsible for regulating cell migration and differentiation, which are normally trapped in the bone matrix, get released into the local environment during this time (13,14).

1.1.1.2 The Reparative Stage

Within a few days after fracture, intramembranous bone formation begins. Cells in high cellular density regions become differentiated and take on an osteoblastic phenotype (10). Additionally, osteoblasts lining the cortical bone surface become activated and periosteal pre-osteoblasts divide and begin to differentiate (2). This results in the formation of woven bone, or hard callus, near the peripheral edges of the fracture site.

At the same time, granulation tissue is formed between the bone fragments as the hematoma is removed by macrophages and giant cells. This granulation tissue will begin to be replaced by cartilage that spans the fracture gap and is referred to as soft callus. It is the soft callus that provides the initial stabilization of the fracture site. This newly formed cartilage callus is initially characterized by high levels of type II collagen expression. As the chondrocytes of the soft callus located near the woven bone of the hard callus start to become elongated, they form elaborate vesicular structures. As the chondrocytes mature,

they become hypertrophic and express type X collagen similar to the hypertrophic chondrocytes of the growth plate (15-18). Matrix vesicles bud from these chondrocytes and begin to detach from the cytoplasmic processes as they migrate to the extracellular matrix. It is here that they appear to deposit proteolytic enzymes responsible for breaking down the cartilage as it is prepared for calcification (19). Phosphatases, also contained in matrix vesicles, are also released to help degrade phosphodiesters. The phosphodiesters release phosphate ions needed for calcium precipitation used in ossification (15). The mineralization of the soft callus proceeds in an organized manner with hypertrophy of chondrocytes and calcification beginning at the interface between the maturing cartilage and newly formed woven bone. After the cartilage calcifies, angiogenesis begins. Angiogenesis introduces a blood supply to the fracture site and is crucial for the progression of fracture healing. Growth factors that stimulate angiogenesis, such as fibroblast growth factor (FGF) and vascular endothelial growth factor (VEGF) are present in the fracture site and potentially enhance the healing process by affecting chondrocytes and osteoblasts (20-22). As osteoblastic progenitors are brought into the area with the new blood vessels, osteoclasts begin to resorb the calcified tissue. Chondrocytes in the area are removed by a combination of apoptotic cell death and some cell necrosis. However, there is no transdifferentiation of chondrocytes to osteoblasts (23). Vascularization is necessary during this stage and is thought to be necessary for recruitment of osteoblastic progenitors necessary for bone deposition (24). The

osteoblastic progenitors differentiate into osteoblasts that produce the woven bone to unite the fracture ends.

1.1.1.3 The Bone Remodeling Stage

The final stage of the fracture healing is characterized by the remodeling of the woven bone to reform the intramedullary canal and restore the mechanical strength of the healing bone to that of intact bone. During remodeling, the fracture callus diminishes until the bone regains its normal dimensions (25). Also, the bones overall mechanical properties are enhanced by replacing the mechanically poor woven bone with the mechanically stronger and more mature lamellar bone. Osteoclasts resorb the woven bone which osteoblasts then replace with lamellar bone. This process is responsive to the local mechanical environment and allows the collagen fibers in the lamellar bone to be oriented in alignment with the mechanical stresses of the bone (9).

1.1.2 Direct Fracture Healing

Primary fracture healing is an artificial process that arises by surgical manipulation of the bone fragments. Primary fracture healing is sometimes referred to as direct fracture healing. For primary fracture healing to occur, bone on both sides of the fracture site must be juxtaposed to reestablish mechanical continuity. This process only occurs when there is an anatomic restoration of the fracture fragments using rigid internal fixation. This rigid fixation results in a substantial decrease in the interfragmentary strain (7). This decrease in strain

allows bone resorbing cells to directly reestablish new haversian systems. The haversian systems generated provide pathways for new blood vessels, along with endothelial and perivascular mesenchymal cells, to infiltrate the damaged area. It is these endothelial and perivascular mesenchymal cells that become the osteoprogenitor cells for osteoblasts. This results in the formation of discrete remodeling units that aid in restoring bone tissue continuity across the fracture (7). Additionally, the removal of the periosteum during surgery results in little to no periosteal response. Subsequently, there is very little fracture callus formation observed (2,5-7) and healing proceeds by normal osteonal remodeling. As an increasing number of osteons span the fracture site, the two sides become united.

1.2.0 Gene Expression During Fracture Healing

While the fracture repair process is relatively well described, little is understood about the coordinated regulation of events leading to successful fracture repair. It is clear that fracture repair involves the regulation of cellular chemotaxis, proliferation, and differentiation and that these events are regulated by growth factor signaling. Many signaling molecules are involved in secondary fracture healing that help contribute to the success in the initiation and control of these biological processes. These include the transforming growth factor- beta superfamily, pro-inflammatory cytokines and multiple angiogenic factors (12,26-28).

1.2.1 Transforming Growth Factor Beta (TGF-β) Superfamily

The TGF-β superfamily is a large group of growth and differentiation factors that includes transforming growth factor-beta (TGF-β), bone morphogenetic proteins (BMP's) as well as growth differentiation factors (GDFs), activins and inhibins. These factors are made as high molecular weight precursors that are activated by proteolytic enzymes and act on serine/threonine kinase membrane receptors located on target cells (28,29). Specific members of this superfamily help promote various stages of intramembranous and endochondral bone ossification during fracture healing (1).

1.2.1.1 Transforming Growth Factor Beta (TGF-β)

During the initial inflammatory phase, platelets release TGF-β (11,30). Due to the time of expression, it is thought to play a role in callus formation (11,30). TGF-β is also produced by osteoblasts and chondrocytes and is stored in the bone matrix (31). Its effect is mediated through Type-1 and Type-2 serine/threonine kinase receptors and is responsible for activating the Smad-2 and Smad-3 pathways (32). TGF-β enhances proliferation of mesenchymal stem cells, pre-osteoblasts, osteoblasts and chondrocytes (31). TGF-β induces the production of collagen, proteoglycans, osteopontin, osteonectin, alkaline phostphatase as well as other extracellular proteins (4). While the main role of TGF-β is thought to be during chondrogenesis (20), it may also initiate signaling for BMP synthesis by osteoprogenitor cells and may inhibit osteoclastic activation and promote osteoclast apoptosis (30,33).

1.2.1.2 Bone Morphogenetic Proteins (BMPs)

Bone morphogenetic proteins (BMPs) are pleiotropic morphogens that play a critical role in differentiation, growth and apoptosis of multiple cell types, including osteoblasts, chondrocytes and epithelial cells. BMPs bind to type II serine/threonine kinase receptors which transphosphorylate type-I receptors initiating the Smad intracellular signaling cascade that regulates the transcription of target genes (34-37).

Cheng et al. proposed an osteogenic hierarchical model of BMPs. In summary, this model suggested BMP-2, -6 and -9 may be the most potent to induce osteoblast differentiaton from cells of mesenchymal origin while most other BMPs (excluding BMP-3 and -13) can promote the end differentiation of committed osteoblastic precursor cells and osteoblasts (38). BMPs are also involved in the sequential cascade of events, including chemotaxis, cell proliferation and differentiation, angiogenesis and extracellular matrix production, necessary for chondrogenesis (3,34).

Another important function of BMPs is to stimulate the synthesis and secretion of other necessary bone and angiogenic growth factors, specifically insulin-like growth factor (IGF) and vascular- endothelial growth factor (VEGF) (39). BMPs may also stimulate bone formation by activating endothelial cells to promote angiogenesis (40,41).

1.2.2 Fibroblast Growth Factors (FGFs)

The fibroblast growth factors (FGFs) are a family of structurally related polypeptides that are known to have a crucial role in angiogenesis and mesenchymal cell mitogenesis (42-44). The most abundant FGFs in normal adult tissue are acidic fibroblast growth factor (FGF-1 or α-FGF) and basic fibroblast growth factor (FGF-2 or β-FGF). Both α-FGF and β-FGF promote growth and differentiation in many cells such as fibroblasts, myocytes, osteoblasts, and chondrocytes. The mitogenic effects of α-FGF have been associated with chondrocyte proliferation (45,46), while β-FGF is expressed by osteoblasts and is typically more potent (43,47,48).

The FGF family transduces signals by a group of four receptors that contain distinct membrane-spanning tyrosine-kinase domains (47,49). Mutations in the FGF receptors have been associated with abnormalities in intramembranous and endochondral ossification resulting in several skeletal dysplasias, including achrondroplasia, thanatophoric displasia, and hypochondroplasia (50,51).

1.2.3 Platelet-Derived Growth Factors (PDGFs)

Platelet-derived growth factor (PDGF) is a homo or heterodimeric polypeptide that has A and B poly-peptide chains (PDGF AA, PDGF BB and PFGD AB) (52-54). The effects of PDGF are exerted through receptors that have tyrosine kinase activity and is synthesized by platelets, macrophages, endothelial

cells, monocytes and osteoblasts and is a strong mitogen for mesenchymal cells (55).

PDGF is released by platelets during the early stages of fracture healing (56) and is stimulated by arachidonic acid (the precursor for prostaglandins) (57). PDGF has a major proliferative and migratory stimulus for MSCs and osteoblasts and a strong chemotactic stimulator for inflammatory cells (31). Interleukin-1 (IL-1), tumor necrosis factor-alpha (TNF-α), and TGF-β effect how PDGF binds to tyrosine kinase activity receptors (28,52).

1.2.4 Insulin–Like Growth Factors (IGFs)

Osteoblasts, endothelial cells and chondrocytes are the source for insulin growth factor-I (IGF-I, somatomedin-C) and II (IGF-II, skeletal growth factor) (28,31). IGF-I promotes bone matrix formation by fully differentiated osteoblasts (58). IGF-II acts during the later stages of endochondral bone formation and stimulates type 1 collagen production, cellular proliferation and cartilage matrix synthesis (59). Although IGF-2 is the most abundant growth factor in bone, IGF-1 has been found to be more potent (31) and has been localized in the healing fractures of rats and humans (60,61).

1.2.5 Pro-Inflammatory Cytokines

Pro-inflammatory cytokines, including interleukin-1 (IL-1), interleukin-6 (IL-6), and tumor necrosis factor alpha (TNF-α) have been shown to play a role in initiating the repair cascade or are expressed in the early stages of fracture repair

(12,62). While macrophages and inflammatory cells are responsible for secreting these cytokines, they are also secreted by cells of mesenchymal origin located in the periosteum (63). These cytokines recruit other inflammatory cells by chemotaxis, they enhance extracellular matrix synthesis and stimulate angiogenesis while recruiting endogenous fibrogenic cells to the injury site (63). Their peak expression is during the first 24 hours post-fracture, then is lowered during cartilage formation and finally rise again during remodeling (62,63).

Cytokines are also responsible for regulating endochondral bone formation and remodeling (20). While TNF-α promotes recruitment of mesenchymal stem cells, it also induces apoptosis of hypertrophic chondrocytes during endochondral ossification and stimulates osteoclastic functions. Loss of TNF-α results in a delay in the resorption of mineralized cartilage, leading to the prohibition of new bone formation, resulting in an inhibition of fracture healing (62).

1.2.6 Angiogenic and Metalloproteinase Factors

Matrix metalloproteinases (MMPs) are an enzyme family of more than 20 zinc-dependent proteases that are largely responsible for the degradation of extra-cellular matrix and are therefore required for extra-cellular matrix remodeling (64-66). During the last stages of endochondral ossification and remodeling, matrix metalloproteinases degrade the cartilage and bone and allows the infiltration of new blood vessels (27). During fracture healing, MMPs

2, 9, 13, and 14 are quantitatively expressed at the highest levels while lower levels of MMP 16, 19, 23, and 24 expression are observed (67).

As stated earlier, angiogenesis that results in adequate blood supply to the fracture site is essential for bone regeneration. There are two separate pathways that are believed to help regulate angiogenesis. The first pathway is a vascular-endothelial growth factor (VEGF) dependent pathway. The second is the angiopoietin-dependent pathway (27). Both pathways are most likely functional during fracture repair, with VEGF being essential in mediating new angiogenesis and endothelial-cell mitogens (68) and angiopoietin 1 and 2 being responsible for regulating vascular morphogenetic molecules responsible for forming larger blood vessels and developing branches off of existing vessels (27).

1.3.0 Bone Mineral Density, Bone Quality and Fracture Risk

Osteoporosis is a debilitating disease characterized by low bone mass and structural deterioration of bone. This leads to bone fragility and an increased risk of fracture (69). Fracture resistance is determined by the strength of the bone, which is dependent on the geometric properties, the activities of cells in the bone tissue, and the material properties of the bone tissue (70-72). However, unlike fragility, which can only be measured by destructive means, bone mineral density is readily accessible by non-invasive measures of bone mineral content. Therefore, the most commonly used clinical indication of osteoporosis and fracture risk is by measuring bone mineral density (73). Evidence suggests that

over 70% of peak bone mass is determined genetically in humans (74-80) and studies have begun to investigate the genes that may be responsible for acquiring adult peak bone density. In one report, it was suggested that vitamin D receptor (VDR) alleles can be associated with, and possibly responsible for, genetic variations in bone density (81). However, translating this data to human populations has provided various results (82-84). These conflicting results are thought to be attributed to the genetic heterogeneity of the human population along with environmental differences in the studied populations.

In contrast, inbred mice possess identical genetic backgrounds and therefore provide excellent animals to study the involvement of genetic factors including bone mineral density. Inbred strains of mice were developed by repeated matings between siblings for at least 20 consecutive generations (85). This resulted in nearly 100% homozygosity at all alleles across the mouse genome. This process was continued through the 60^{th} generation, allowing inbred mice to become 100% homozygous at all loci (except for any spontaneous mutations which arose), thereby providing genetically identical mice. Because every inbred strain is genetically different from every other inbred strain, planned matings to study the segregation of genes essential for bone density is possible (86).

A number of laboratories have used quantitative trait loci (QTL) methods to scan the mouse genome to identify candidate genetic loci, and ultimately the genes that affect bone properties (87-92). Mineral content also has been correlated with a variety of whole bone properties (including stiffness, strain and

ultimate load) (93,94). Moreover, studies have also shown that bone becomes more brittle when the mineral content exceeds a critical value (95) and less able to bear load when mineral content is too low (96). This indicates that having a high bone mineral density may help prevent a bone fracture. However, no data exists suggesting that having high mineral bone density will result in faster healing if a fracture was sustained.

1.4.0 Arachidonic Acid Metabolism

Because the inflammation stage is an important part of the repair process in the normal response to infection or injury, it is important to study the pathways that help mediate these responses. One important pathway is the arachidonic acid pathway (Figure 1.1).

Figure 1.1. Arachidonic Acid Metabolism and Signaling (from J.P. O'Connor).

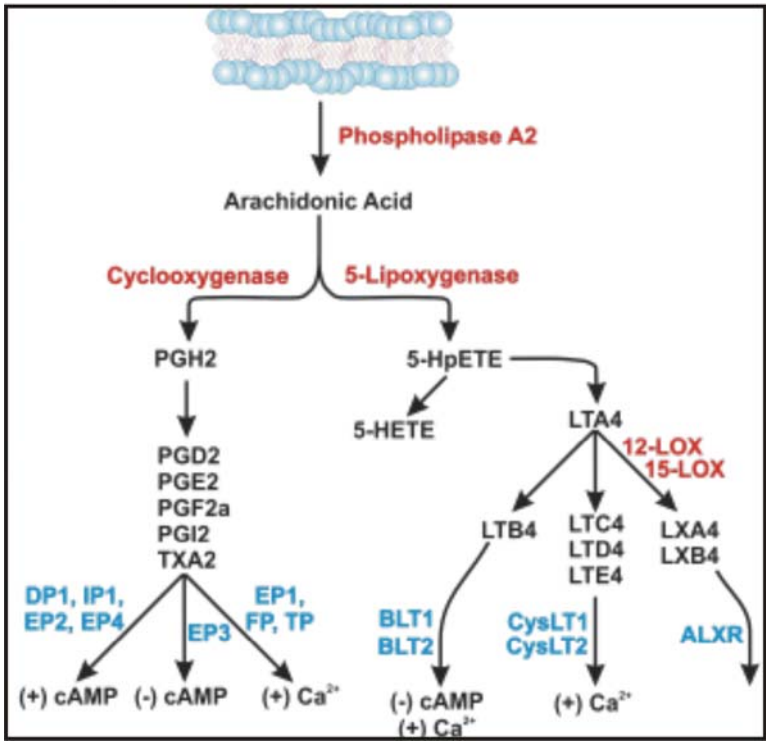

Arachidonic acid is an ω-6 polyunsaturated fatty acid that is converted into biologically active lipid compounds termed eicosanoids (97). Eicosanoids comprise a large family of biologically active lipid mediators that are produced by two enzyme classes, cyclooxygenase (COX) and 5-lipoxygenase (LOX), which then produce prostaglandins and leukotrienes, respectively (98-103). Prostaglandins and leukotrienes are involved in diverse biological functions, including cell proliferation (104,105), cell survival (106-108), modulate cell adhesion and motility (105,106), angiogenesis (108,109), increased vascular permeability (110,111), and inflammation (97,112),

1.4.1 Prostaglandin Biosynthesis

Prostaglandins are made by most cells of the body and act locally as autocrine and paracrine lipid mediators (113). Osteoblasts synthesize prostaglandins to stimulate bone formation and aid in bone resorption (114). Prostaglandins are not stored, but are synthesized from membrane-released arachidonic acid when cells are stimulated by mechanical trauma or by a specific growth factor or cytokine. This signaling ultimately affects intracellular cAMP and calcium levels by a specific receptor or group of receptors (97,115).

As seen on the left side of Figure 1.1, after stimulation, phosholipase A2 causes the hydrolysis of arachidonic acid from the glycerophospholipids of the cell membrane (116-118). The COX enzyme converts the released arachidonic acid into prostaglandin G2 (PGG_2) by adding two oxygen molecules (119). Additional peroxidase activity reduces this PGG_2 to its 15-hydroxy analog,

prostaglandin H_2 (PGH_2) (113,120-122). Isomerases further convert PGH_2 into prostaglandin E_2, prostaglandin D_2, prostaglandin F_2, prostaglandin I_2 and thromboxane A_2 (113,120,121,123).

There are two main isoforms of the COX enzyme, prostaglandin endoperoxide H synthases-1 and 2 (PGHS-1 and PGHS-2). These are more commonly called cyclooxygenase-1 (COX-1) and cyclooxygenase-2 (COX-2). COX-1 is always present in tissues, while COX-2 is induced by appropriate physiological stimuli, such as cytokines, tumor promoters, and growth factors (124,125). The genes for these two enzymes are about 65% homologous in their coding regions and each have a molecular weight of approximately 70kD (126,127). COX-1 and COX-2 are products of distinct, single-copy genes located on different chromosomes (128-134). The promoter region of the COX-2 gene (or *Ptgs2*) contains a TATA sequence, but the COX-1 gene (or *Ptgs1*) promoter lacks a TATA box (116). Through crystallographic analysis, an important difference between COX-1 and COX-2 was observed. The long hydrophobic channel running from the membrane-binding surface of the enzyme to the active site was somewhat larger in COX-2. Also, COX-2 had a small side pocket pointing away from the catalytic site (116,119). While there are differences between the two genes, the enzymatic activities and substrate specificities are similar (116,135).

1.4.1.1 Homeostatic versus Pro-Inflammatory Actions of COX-1 and COX-2

COX-1 is the only cyclooxygenase isoform expressed in normal gastric mucosa and is the only cyclooxygenase found in platelets (123). In the gastric antrum (or the distal part of the stomach before the outlet lined with mucosa not involved in acid production), PGE_2 and PGI_2, which are synthesized as a result of COX-1 activity, promote vasodilation that maintains mucosal integrity (136). In the kidney, COX-1 generates the vasodilatory prostaglandins PGE_2 and PGI_2 that helps maintain blood flow and glomerular filtration rates (137,138). In platelets, COX-1 is essential for production of thromboxane A_2 (TBA_2), which is necessary for platelet aggregation (139). Therefore, it is suggested that the main function of COX-1 is to maintain homeostasis and promote specific physiological activities.

Unlike COX-1, COX-2 is not detectable in most normal tissues, (113,120-122,140). However, when macrophages and endothelial cells were challenged with inflammatory mediators, COX-2 mRNA and COX-2 protein were up-regulated at the sites of inflammation and detectable before the increase in local prostaglandin production (141). While COX-1 was present in both macrophages and endothelial cells, it was not upregulated after challenged with inflammatory mediators. This suggested that COX-2 is an inducible enzyme that accounts for the local increase in production of arachidonic acid metabolites at the sites of inflammation. These metabolites are responsible for edema, vasodilation and pain, all clinical signs of inflammation (141).

Recent investigations have shown that these are only generalizations of the roles COX-1 and COX-2 play. Animal studies have shown that COX-2 also

plays a homeostatic role, as it is constitutively expressed in the kidney (142,143) and brain (144,145). Furthermore, while it is induced by inflammatory responses, it is also induced by physiological stimuli in the ovary (146), uterus (147,148), kidney (142), brain (149), cartilage (150), and bone (151,152). In addition, COX-1 has been shown to be inducible and not solely homeostatic. After radiation injury, it is present in the crypt cells of the small intestine (153). It also may play a role and contribute to inflammation (154). All of these findings indicate that the individual roles of COX-1 and COX-2 need further investigation.

1.4.2 Leukotriene Biosynthesis

Leukotrienes are mainly made by inflammatory cells, such as polymorphonuclear leukocytes, macrophages, and mast cells. Leukotrienes are lipid mediators that are integral in immune responses and maintaining tissue homeostasis (97). Synthesis of leukotrienes may be divided into two pathways, one to create the slow reacting substances of anaphylaxis [(SRS-A) or cysteinyl leukotrines (CysLTs)] and the other to create leukotriene B_4 (LTB_4) (155).

5-lipoxygenase (5-LO) is the key enzyme responsible in synthesizing leukotrienes and is located in the nucleus and cytosol of different cell types (156). This enzyme is a 72 to 80 kD monomeric soluble protein that contains a nonheme iron believed to be necessary for catalysis (157). Furthermore, 5-LO requires Ca^{2++} and is stimulated by ATP, membranes, phosphatidylcholine, and lipid hydroperoxides (158).

Following cellular stimulation, arachidonic acid is released by phospholipase A2 (Figure 1.1). Subsequently, 5-LO catalyzes the oxidation of arachidonic acid at the five-position to produce 5-hydroperoxy eicosatetraenoic acid (5-HpETE), which is dehydrated to produce the epoxide, leukotriene A_4 (LTA_4). LTA_4 is the critical intermediate in the synthesis of inflammatory and anaphylactic mediators. Depending on the cellular circumstance, LTA_4 has three possible fates: hydrolysis, conjugation with glutathione, or transcellular metabolism to generate bioactive lipid mediators (159). In the neutrophil and monocyte, LTA_4 is mainly converted to the chemoattractant LTB_4 by LTA_4 hydrolase (160). In human eosinophils, mast cells and basophils, LTA_4 is conjugated with reduced glutathione by LTC_4 synthase to form LTC_4 (161). Further enzymatic activity on LTC_4 can subsequently generate the extracellular metabolites, LTD_4 and LTE_4. LTC_4, LTD_4 and LTE_4 make up the CysLTs, a group of slow-reacting substances of anaphylaxis that sustain smooth muscle contraction (99).

Lipoxins (lipoxygenase interaction products or LXs) are also generated through the sequential lipoxygenation of arachidonic acid by 15- and 5-lipoxygenase to yield an unstable epoxide intermediate, 5(6)epoxytetraene (101,162). This intermediate may then be converted to the major bioactive lipoxins, LXA_4 and LXB_4 through reactions catalyzed by LXA_4 and LXB_4 hydrolases (101,162). Lipoxin biosynthesis is greatly changed through transcellular pathways if granulocytes are activated during co-incubation with platelets (163-168). Platelets cannot generate lipoxins from arachidonic acid.

During transcellular interactions, however, platelets convert neutrophil-derived LTA_4 to 5(6)epoxytetraene through the action of platelet 12-lipoxygenase (12-LO) (163-168). This same enzyme functions as 15-lipoxygenase (15-LO) when its substrate is LTA_4. Therefore, within the multicellular inflammatory environment, LTA_4 can serve as a crucial intermediate for both leukotriene and lipoxin formation.

Leukotriene action requires G-protein-coupled receptors. These receptors are members of the rhodopsin-like receptor superfamily (169,170). LTB_4 signals through either the BLT_1 or BLT_2 receptors which ultimately affect intracellular cAMP or calcium levels (102,171-174). The CysLTs signal through the $CysLT_1$ or $CysLT_2$ receptors to affect intracellular calcium (175-177).

Similar to prostaglandins, the functions of all leukotrienes are not known and their functions may possibly be cell-specific.

Additionally, 5-lipoxygenase activity is dependent on a protein cofactor, 5-lipoxygenase activating protein, or FLAP. FLAP is an 18 kD membrane associated arachidonic acid binding protein whose function is to optimally present substrate to 5-LO (178).

1.4.3 Drugs Affecting Prostaglandin and Leukotriene Formation and Action

Nonsteroidal anti-inflammatory drugs (NSAIDs) function by inhibiting cyclooxygenase activity. Traditionally, NSAIDs have inhibited COX-1 activity as much or more than COX-2. For example, indomethacin acts primarily on COX-1, while ibuprofen affects COX-1 and COX-2 equally (179). This activity resulted in

the desired outcome of decreased inflammation by inhibiting COX-2; however, it also inhibited the prostaglandin production by COX-1, which is necessary for normal cell function. Consequentially, this lead to multiple negative side effects, such as gastric bleeding and ulceration (136,180-182). Estimates indicate that about 25% of patients using traditional NSAIDs experience some side effects, with about 2% developing serious health issues (183-185). In response to these problems, drugs were developed that target the COX-2 enzyme more specifically (COXIBs). The goal of this was to interfere with the production of prostaglandins manufactured though the COX-2 pathway while simultaneously sparing the prostaglandins produced by COX-1 that are necessary for normal tissue function (179,186)

Leukotriene action may be blocked by inhibiting leukotriene production or by inhibiting leukotrienes from binding to their cellular receptors (187). Because leukotrienes work to contract smooth muscle, increase vascular permeability increase mucus secretion and attract and activate inflammatory cells, most leukotriene inhibitors were developed for patients with asthma (188). Zileuton, a specific inhibitor of 5-LO, inhibits the production of leukotrienes, especially LTB_4, LTC_4, LTD_4 and LTE_4. Zafirlukast and montelukast are both selective and competitive leukotriene receptor antagonists of LTD_4 and LTE_4 (189,190).

1.5.0 Evaluation of Experimental Fracture Healing

1.5.1 Radiography

Radiography is one of the more useful diagnostic tools in assessing fracture healing and is essential for identifying and defining a fracture (191). Radiography provides a minimally invasive way to visualize callus formation after mineralization (192,193). With the aid of anesthesia, animals may be serially radiographed to allow assessment of fracture healing over time without sacrifice.

While many fractures are visible as an abnormal radiolucent line, some fractures have no visible line, particularly those due to compression or other pathological process. Since standard radiography only generates a two-dimensional image, a minimum of two views is usually necessary. The views are usually perpendicular to each other in order to adequately assess the fracture and subsequent healing process (191).

High resolution radiography is useful by magnifying information not easily detected using standard radiography. Magnifying a film is achieved by one of two ways: by either optically enlarging the image using fine grain film or by increased the distance between the specimen and the film. With a small x-ray focal spot and an air gap to decrease scatter, a two to fourfold geometric enlargement may be obtained (194,195).

In fracture healing animal studies, radiographs are typically taken immediately after surgery to examine the location of the fracture and the quality of the fixation. Additionally, post-sacrifice radiographs are also generally taken and may be used for a variety of measurements, such as bone density or bone

dimensions. For long bone fractures, various healing parameters, such as periosteal reaction (callus formation), quality of union and bone remodeling, may be quantified on radiographs by using different scoring systems.

1.5.2 Histology and Histomorphometry

Histology is another basic parameter for assessing fracture healing in animal models. Common histological parameters, including callus formation, bone union, marrow changes and cortex remodeling, may be examined by using stained calcified or decalcified sections cut through the fracture callus and surrounding area (196,197).

Histomorphometry is another useful tool in evaluating fracture healing. Slides prepared for histological examination may be used to calculate multiple parameters, including specific cell counts, bone length and callus area. However, unlike histology, which presents a qualitative assessment of fracture healing, histomorphometry allows for quantitative assessment (198).

1.5.3 Mechanical Testing

Since one goal of fracture healing is to restore the mechanical integrity of the bone, the mechanical properties of the healing fracture callus are important to investigate. In order to evaluate the mechanical properties at the structural (whole bone) or material (bone tissue) level, mechanical testing of the fractured and contralateral control limb is frequently performed. Cross-sectional geometry is determined from the measurement of the bone before testing or from

measuring the contralateral control bone. Structural properties (for example, peak torque and rigidity) may then be measured or calculated from torsion or bending tests. Material properties (shear stress and shear modulus) may also be estimated by using the measured geometric and structural properties along with appropriate engineering equations. Three types of tests are most commonly used in estimating the mechanical properties of whole or fractured bone: three-point bending, four-point bending and torsional testing (199).

1.5.3.1 Three-Point Bending

Standard three-point bending is performed by placing the specimen on two supports. A center load is then placed equidistant between the supports to equally distribute the force across the two supports (Figure 1.2, panels A and B). The force generated by the center load that is required to bend the bone a specific distance or break the bone is measured. In addition, the distance the center load travels is also measured. The force generated from the center load creates compressive and tensile forces on the specimen on opposite sides. Due to its simplistic nature, many whole-bone studies implement the use of a three-point bending model. However, this model is considered inadequate for fracture healing studies since this type of bending test places a large center load on the fracture site, leading to high shear stresses and inconsistent movement near the midsection of the bone and distortion of the fracture callus during testing (Figure 1.2, Panel C) (200).

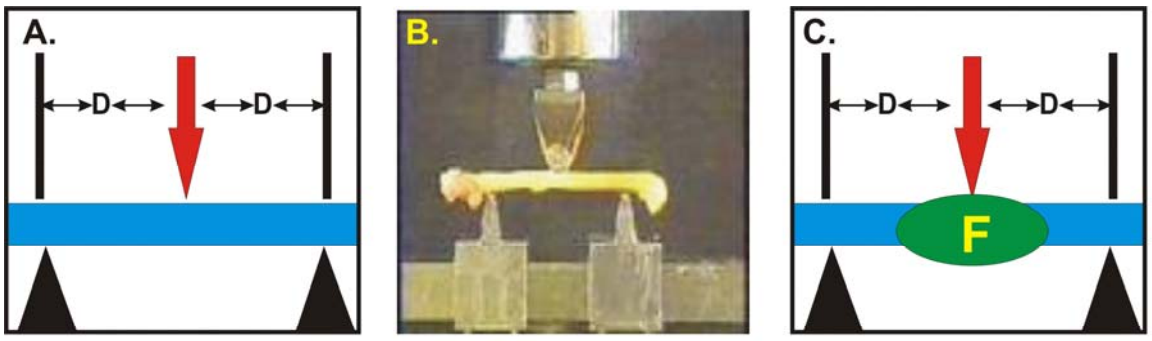

Figure 1.2. Three-Point Bending Mechanical Testing Schematic. D=distance between the load and the support; F= fracture site. (Panel A) Schematic representation of three-point bending showing the placement of a center load between two end supports. (Panel B) Laboratory representation of an intact rat femora in a three-point bending configuration (http://obl.caregroup.harvard.edu/images/3ptbend.gif). (Panel C) Schematic representation of a sample with a fracture. As shown, the fracture site is directly in line with the location of the load causing distortion of the fracture callus.

1.5.3.2 Four-Point Bending

A four-point bending mechanical test is another common protocol used in many animal studies. Four-point bending is designed with the specimen placed on two end supports. Two center loads are placed a uniform distance from the two supports (Figure 1.3, Panels A and B) and the force generated by these two loads that is required to bend the bone a specific distance or break the bone is measured. The force generated from the center loads creates compressive and tensile forces on the specimen on opposite sides. Four-point loading produces pure bending between the upper two loading points. However, four-point bending requires that the force at each loading point be equivalent. This is hard to achieve when the material is irregularly shaped, such as with bone. Additionally, the span of the specimen that is loaded must be sufficiently long (usually sixteen times the thickness of the specimen) to reduce measurement errors (200). This is because if the working length is very short, most of the displacement induced by loading will be due to shear stresses and not bending.

To guarantee a length-to-width ratio of 16:1 in small animal models would be nearly impossible. Also, various locations and sizes of the newly formed fracture callus would further make consistent placement of the loads and supports more complicated (Figure 1.3, Panel C). Finally, any internal fracture stabilization would have to be removed prior to testing, potentially destroying the sample.

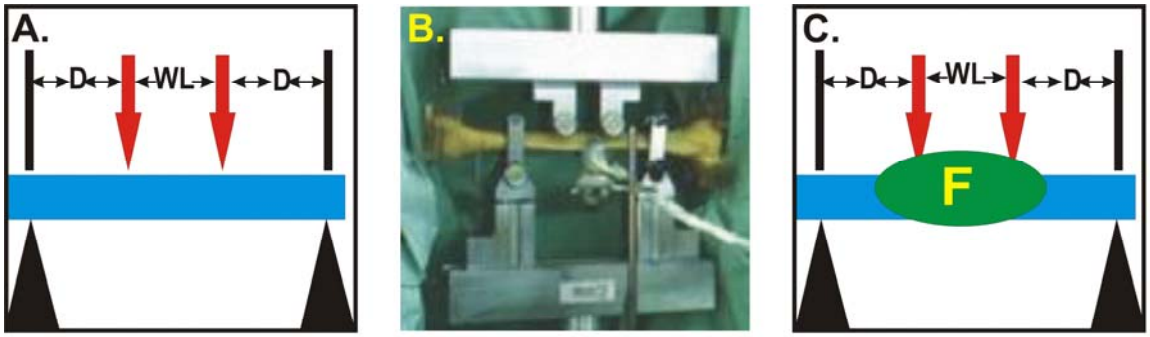

Figure 1.3. Four-Point Bending Mechanical Testing Schematic. D=distance between the load and the support; F= fracture site. (Panel A) Schematic representation of four-point bending showing the placement of two center loads between two end supports. The distance between the center loads is the working length (WL) of the specimen. (Panel B) Laboratory representation of an intact cadavaric femora in a four-point bending configuration. (Panel C) Schematic representation of a sample with a fracture. As shown, the fracture site is potentially underneath the center loads.

1.5.3.3 Torsional Mechanical Testing

Torsional mechanical tests are performed by rigidly securing ("potting") the two ends of the sample in place to prevent slipping, while the working length, or gage length (GL), remains exposed. This test is performed by twisting one end of the specimen while the other end is held fixed (Figure 1.4, Panels A and B). Parameters calculated from torsion tests, such as torsional rigidity, shear stress, and shear modulus are useful for determining the structural and material properties of the healing tissue. This type of mechanical test requires the specimen to be perpendicular to the potted ends and to be located on the neutral axis to ensure accuracy. Therefore, uniform samples are better suited for this type of mechanical testing. While the curved geometry of the tibia and the

confounding effect of the fibula make it unsuitable for torsional mechanical testing, the femur is a relatively straight long bone that should be more ideal for torsional testing. Furthermore, unlike bending tests, there is more flexibility as to the location and size of the fracture callus and to the size of the sample specimen (Figure 1.4, Panel C). Additionally, any internal fixation may remain during testing without compromising the results. This is because the stabilization should be located at the neutral axis and should not affect the testing (201). Therefore, smaller animals, like the mouse, may also be tested effectively.

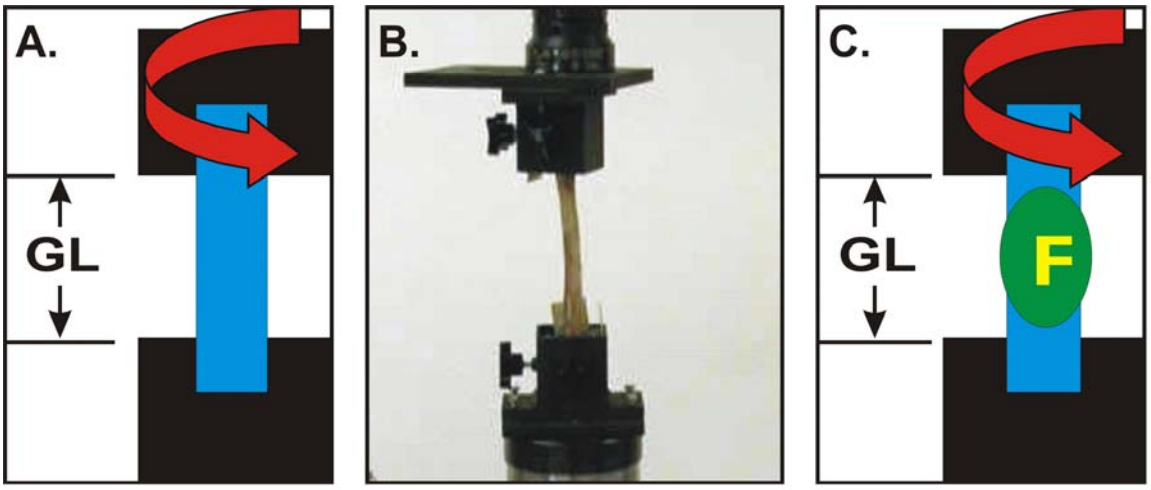

Figure 1.4. Torsional Mechanical Testing Schematic. GL = Gage Length of sample; F= fracture site. (Panel A) Schematic representation of torsional mechanical test. (Panel B) Laboratory representation of an intact rat femora in a torsional configuration (http://web.ecs.baylor.edu/faculty/Skurla/research.htm). (Panel C) Schematic representation of a sample with a fracture. As shown, the fracture site is placed between the two potted ends, allowing for variability between samples.

1.6.0 Models of Fracture Healing

Fracture healing has been evaluated using several animal models and various fracture types. The selection of the model type is dependent on the aims of the particular experiment. The challenges in experimental fracture models involve the stability of the fixation and the reproducibility in creating a natural fracture to give a valid representation of the fracture repair process (202,203). In

essence, a proper animal model must follow a highly reproducible order of events beginning with hematoma formation followed by inflammation, cell migration and proliferation, chondrocyte differentiation, endochondral ossification, and bone remodeling. Furthermore, animals used for biomechanical models should follow the four biomechanical stages of fracture healing as proposed by White *et al.* in 1977 (Table 1.1). These stages correlate with the progressive increases in the average force and energy absorption to failure as healing progresses (204).

Table 1.1. The Four Biomechanical Stages of Fracture Healing (204).

Stage	Description
I	Bone fails through original fracture site. Low-stiffness with rubbery pattern.
II	Bone fails through original fracture site. High-stiffness with hard-tissue pattern
III	Bone fails partially through original fracture and partially through intact bone. High-stiffness with hard-tissue pattern.
IV	Bone fails through intact bone. High-stiffness with hard-tissue pattern.

Animals most commonly used for fracture models are mice, rats, rabbits, dogs, sheep and goats (203,205-207). Large animal models, like dogs, closely resemble human bone and are valuable in orthopaedic studies (202). However, the ultimate cost of using these models may be restricting. Some animal fracture models (for example, the mouse and rat) differ physiologically from human cortical bone by lacking normal haversian remodeling. Rodent cortical bone remodeling occurs primarily along endosteal and periosteal surfaces (208). This is a particularly important difference during remodeling. In spite of this, rodents are widely used in orthopaedic research. While the rat has been extensively used in fracture studies (209-215), recent literature suggests that *in vivo* murine

models are becoming increasingly important in bone research. Using the mouse model allows investigators to examine the interactions between the mechanical, metabolic and functional characterizations of bone in animals with targeted genetic alterations.

Previous fracture models in the mouse have used the mandible, ribs, tibia, and femur as the fracture site to study bone healing. Studies including the distraction osteogenesis model for the mouse (216) and mandibular osteotomy murine model (217) were used to explore intramembranous ossification in genetically altered mice. Therefore, using these models is not suitable for exploring the endochondral ossification response associated with fracture healing. The mouse rib was fractured to study the expression of metalloproteinase-13 during fracture healing (218). Unfortunately, mechanically testing this type of bone using any method is difficult and inconsistent. Two investigators have reported on the development of a tibial fracture model, both non-stabilized (219) and stabilized (220). This tibial fracture model was subsequently applied to study both the histological and gene expression patterns during fracture healing in the mouse tibia (221-224). Lastly, the murine femoral model has also been used to study genetic expression (225-233) and mechanical properties (234-237) of fracture healing. However, in none of these studies were the radiographic, histological, and mechanical testing analyses extensively used to characterize the fracture healing pathway and none of the reports described the torsional mechanical properties of the fractured limbs.

2.0.0 Rationale and Hypothesis

With the development of mice with targeted genetic mutations, *in vivo* murine models are becoming increasing valuable in the field of orthopaedics. Additionally, evaluating the healing tissues using a torsional testing protocol better estimates the biomechanical properties and is more reproducible than using other mechanical testing protocols, especially involving smaller specimens. The development of a reproducible femur fracture model in the mouse suitable for torsional mechanical testing would be important in the study of complex genes and phenotypes associated with bone diseases.

While previous investigators have used the mouse as a fracture model, none of these studies extensively explored the radiographic, histological, and mechanical testing analyses used to characterize the fracture healing pathway. Furthermore, none of the reports described the torsional mechanical properties of the fractured limbs. Consequently, the first phase of this study was to develop a murine femoral fracture model capable of torsional mechanical testing in an outbred mouse strain. The parameters investigated in this study were chosen due to their relevance to previous fracture model literature, and included radiographical, early histological, late histological, early biomechanical and late biomechanical analyses.

After fully characterizing and validating the mouse fracture model and torsional testing protocol, the next phase of this study was to explore a complex phenotype that may affect bone healing. Bone mineral density has received much attention because of its connection with osteoporotic fracture risk. While it

is well-established that low bone mineral density is valuable in predicting bone fracture risk, no data exists to suggest that a high bone mineral density would be useful once a fracture is sustained. The second phase of this study focused on examining the role bone mineral density plays in fracture healing success. To that end, fracture healing was examined in three inbred mouse strains specifically chosen based on previously published bone mineral density data. Radiographic, histological, histomorphometric and biomechanical analyses were used to evaluate fracture healing in these inbred mouse strains to better understand the role bone mineral density plays in fracture healing.

The final phase of this work focused on how altering a single pathway affects fracture healing. Leukotrienes and prostaglandins are produced by the activity of three enzymes, namely 5-lipoxygenase, cyclooxygenase-1, and cyclooxygenase-2, as part of the arachidonic acid pathway. The arachidonic acid pathway, its products and the enzymes mediating their formation, play a crucial role in multiple aspects of human physiology, including vascular homeostasis, gastric protection, renal homeostasis, bone formation, and inflammation. Because inflammation is also a vital stage in the fracture healing cascade, the potential blocking of the arachidonic acid pathway may lead to deleterious results in fracture healing. Additionally, manipulating the arachidonic acid pathway may promote fracture healing. To explore how manipulating arachidonic acid metabolism affected fracture healing, fractures in genetically modified mice were assessed using the fracture model, torsional testing protocol, and parameters as described above. Lastly, fracture callus eicosanoid levels were measured to

determine if the arachidonic acid cascade reroutes itself under genetic conditions.

The hypothesis of this work was that the mouse is an exceptionally valuable tool in studying various orthopaedic conditions that involve genetics and complex phenotypes. Further, biomechanical testing provides a better understanding of healing bone properties. Developing a useful mouse model in conjunction with a suitable testing protocol will better estimate key properties to assess fracture healing success. Understanding the mechanisms which cause the fracture healing pathway to be inhibited or enhanced will provide potential future treatments for fracture healing patients, as well as the normal mechanisms needed for fracture healing success.

3.0.0 Materials and Methods

3.1.0 Mouse Strain Models

The experiments completed for this dissertation involved outbred, inbred and knock-out mouse strains and phenotypes. Table 3.1 is a summary of all animals bred and purchased for all experiments.

3.1.1 Outbred Strains

The mouse strain used to develop the fracture model and as a source of controls was the ICR. The ICR mouse was chosen because it is a commercially available, resilient, outbred stock. The ICR mouse was developed for its good reproductive performance and fast growth rate. The ICR line is typically a docile strain and produces large litter sizes (Taconic website). While relatively healthy, ICR mice do carry a recessive gene, *Pde6b*^{rdl}. This mutation is known to cause retinal degeneration (Taconic Website).

3.1.2 Inbred Strains

To examine the relationship between bone mineral density and fracture healing, female C3H, DBA/2, and C57BL/6 inbred mouse strains were chosen based on previously published bone mineral density data (C3H= 0.83 g/cm^2; DBA/2= 0.58 g/cm^2; C57BL/6= 0.45 g/cm^2) (238) Mice of an inbred strain are as genetically alike as possible, being homozygous at virtually all of their loci (85). While some traits may be influenced by diet and environment, many traits do not vary from generation to generation. Furthermore, all inbred strains have a

unique set of characteristics that set them apart from all other inbred strain (85). The three strains selected are widely used in genetic studies. Similar to the ICR, the C3H also carried the recessive gene for *Pde6b*^{rd1}, which causes retinal degeneration (Taconic website).

3.1.3 Gene-Deficient (Knock-Out) Strains

Three knock-out mouse models were utilized to examine how the regulation of arachidonic acid metabolism alters fracture repair. These are the *Ptgs1* deficient mouse, the *Ptgs2* deficient mouse and the *Alox5* deficient mouse. All three of these mouse lines were developed to study inflammation and a detailed description of each is found below.

3.1.3.1 Description of Cyclooxygenase-1 Deficient Mice

To study the physiological role of cyclooxygenase-1 (COX-1), the *Ptgs1* gene that encodes COX-1 was disrupted to create the cyclooxygenase-1 deficient (Cox-1KO) mouse (154). The disruption of the gene before exon 11 was chosen based on literature that showed aspirin inactivates COX-1 by acetylating Ser-530 (239-241). The targeting vector for disrupting COX-1 was designed to replace approximately 1 kb of intron 10, the intron 10: exon 11 splice junction and first 44 bp of exon 11 with the neomycin resistant (*Neo*) gene (154). Any protein made from this resultant disrupted gene would lack the carboxy-terminal 120 amino acids, which includes Ser-530 in the active site of the enzymes. Splicing that resulted in the elimination of the *Neo* cassette would

result in the elimination of 14 amino acids and the loss of the proper reading frame. Thus, this targeting should produce a null allele of COX-1. The targeting vector was electroporated into E14TG2a embryonic stem cells. Positive stem cells were injected into C57BL/6J blastocysts to generate mice with the COX-1 null allele.

Western blot analysis done by Langenbach *et al.* further showed that the normal 70 kDa COX-1 protein was readily detectable in the kidney, stomach and colon microsomes of wild-type F2 *Ptgs1*^{tm1Unc} mice (154). However, normal-sized or smaller COX-1 proteins fragments were detected in the same tissues from homozygous *Ptgs1*^{tm1Unc} mice. Further evaluation showed that the COX-1 protein levels were not significantly altered by lipopolysaccharide (LPS) in macrophages from wild-type mice and was not detected in the homozygous mutant mice. LPS did induce the COX-2 protein, COX-2 mRNA and PGE_2, similarly in peritoneal macrophages from wild-type and homozygous *Ptgs1*^{tm1Unc} mutant mice. These results show that the disruption on *Ptgs1* prevents the constitutive synthesis of COX-1, but does not alter *Ptgs2* inducibility in macrophages.

3.1.3.2 Description of Cyclooxygenase-2 Deficient Mice

To study the physiological role of the cyclooxygenase 2 (COX-2) isoform, the *Ptgs2* gene that encodes COX-2 was disrupted to create the cyclooxygenase-2 deficient (Cox-2KO) mouse (242,243). The targeting vector used to disrupt COX-2 introduces an insertion in exon 8 of *Ptgs2* and

simultaneously deletes 104 bp from exon 8. This creates a null COX-2 allele. The targeting vector was electroporated into E14TG2a embryonic stem cells. Positive stem cells were injected into C57BL/6J blastocysts to generate mice with the COX-2 null allele.

3.1.3.3 Description of 5-Lipoxygenase Deficient Mice

To study the physiological importance of leukotrienes, the 5-lipoxygenase (5-LO) gene was disrupted by homologous recombination in embryonic stem cells (244). The targeting vector was made by inserting a 1.7 kb PGK1neo cassette into a Scal site in exon 6. The thymidine kinase gene was added to the end of the targeting vector for negative selection using gancyclovir. The targeting vector was electroporated into D3H-ES cells (245). Positive embryonic stem cells were injected into C57BL/6J blastocytes and chimaeric offspring males were mated with C57BL/6J females to pass this allele to future offspring.

Strain	Source	Name	Description	Purpose
ICR	Harlan Sprague Dawley	Hsd:ICR (CD-1)	Outbred Mouse Strain	Development of torsion mouse fracture model
ICR	Taconic Farms	IcrTac:ICR	Outbred Mouse Strain	Controls for bone mineral density and fracture healing
C3H	Taconic Farms	C3H/HeNTac-MTV	Inbred Mouse Strain	Bone mineral density and fracture healing
DBA/2	Taconic Farms	DBA/2NTac	Inbred Mouse Strain	Bone mineral density and fracture healing
C57BL/6	Taconic Farms	C57BL/6NTac	Inbred Mouse Strain	Bone mineral density and fracture healing
WT	Jackson Laboratories	C57BL/6J	Inbred Mouse Strain	Controls for *Alox5*$^{-/-}$ Arachidonic Acid Metabolism in Fracture Healing
Cox1-KO	Taconic Farms and Bred in house	B6;129P2-Ptgs1^{tm1Unc}	Cox1$^{-/-}$; *Ptgs1* knock-out mouse	Arachidonic Acid Metabolism in Fracture Healing
Cox1-HET	Taconic Farms and Bred in House		Cox1$^{+/-}$; *Ptgs1* heterozygous mouse	Arachidonic Acid Metabolism in Fracture Healing
Cox1-WT	Bred in house		Cox1$^{+/+}$; *Ptgs1* wild-type mouse	Arachidonic Acid Metabolism in Fracture Healing
Cox2-KO	Taconic Farms and Bred in House	B6;129P2- Ptgs2^{tm1Smi}	Cox2$^{-/-}$; *Ptgs2* knock-out mouse	Arachidonic Acid Metabolism in Fracture Healing
Cox2-HET	Taconic Farms and Bred in house		Cox2$^{+/-}$; *Ptgs2* heterozygous mouse	Arachidonic Acid Metabolism in Fracture Healing
Cox2-WT	Bred in house and Bred in house		Cox2$^{+/+}$; *Ptgs2* wild-type mouse	Arachidonic Acid Metabolism in Fracture Healing
5-LOKO	Jackson Laboratories and Bred in House	*B6;129S2-Alox5^{tm1Fun}/J	Alox5$^{-/-}$; *Alox5* knock-out mouse	Arachidonic Acid Metabolism in Fracture Healing

Table 3.1. Strain Descriptions and Nomenclature Used in This Dissertation. *This strain originated on a B6;129S2 background and has been backcrossed into the C57BL/6J background.

3.2.0 General Health, Breeding and Maintenance of Animals

3.2.1 Cyclooxygenase-1 Deficient Mice

The COX-1 deficient mouse develops normally and appears healthy. Previously published necropsy and microscopic examination of selected tissues, such as the heart, liver, and spleen showed no significant pathology (154). However, there was a minimal difference noticed in the kidneys, mainly characterized by one or two foci per section of basophilic, immature tubules in the Cox-1KO mice (154).

Cox-1KO females and males are fertile. However, crosses between Cox-1KO males and females result in smaller litter sizes (154). For these experiments, initial matings involved a Cox-1KO male with a Cox-1HET female to produce both Cox-1KO and Cox-1HET offspring. Preliminary data including the Cox-1HET showed no significant differences when compared to the Cox-1KO animals (data not shown). Thus, the mating scheme was altered to solely be Cox-1KO males mating with Cox-1KO females to produce all Cox-1KO offspring, as the Cox-1HET group was eliminated from future experiments.

3.2.2 Cyclooxygenase-2 Deficient Mice

The COX-2 deficient mouse was previously found to have specific peri-natal kidney pathologies that lead to increased mortality among Cox-2KO mice (242,243). Because of the high death incidence of Cox-2KO animals at about 8 weeks, Morham *et al.* examined Cox-2WT, Cox-2HET and Cox-2KO for any pathological disorders in several tissues, including brain, heart, liver, spleen, and

kidney (242). While no noticeable physiological issues were reported with either the Cox-2HET or Cox-2WT mice, these investigations showed that the Cox-2KO mouse kidney had several significant and consistent genotype-related abnormalities. Cox-2KO animals had kidney lesions ranging from mild to extremely severe that were characterized by abnormal subcapsular parenchyma with small immature glomeruli and tubules. These findings were consistent with nephron hypoplasia. Other cases involved a thinned renal cortex, with reduced numbers of glomeruli as compared to the wild-type kidneys. Glomeruli not in the hypoplastic region were often enlarged. Other findings included cortical areas with tubular atrophy and regeneration, tubular dilation, interstitial inflammation and fibrosis, and papillary mineralization. These symptoms were more pronounced in the male than the female. Furthermore, these abnormalities were not present in Cox-2KO mice sacrificed at three days, suggesting that the kidney problems observed are a postnatal developmental that increase in severity with increasing age (242).

Other health problems observed by Morham *et al.* in the Cox-2KO animals were cases of suppurative peritonitis in two-thirds of the examined animals at 8 weeks of age (242). While no abnormalities were observed in the Cox-2WT animals, the male Cox-2KO mouse examined had acute suppurative peritonitis and the female Cox-2KO mouse had chronic suppurative peritonitis. The Cox-2KO female mouse had multiple adhesions around the abdominal organs. These adhesions corresponded to abscesses and chronic inflammatory tissue bridged the lobes of the liver and loops of the bowel. This peritonitis affected multiple

abdominal organs and was characterized by serosal exudation and focal necrotizing inflammation penetrating into the superficial tissues of the viscera and retroperitoneum (242).

While the experiments here did not specifically address a single organ or organ system, differences among Cox-2KO animals compared to Cox-2HET and Cox-2WT included a lower weight at surgery (Table 4.6), a higher death rate associated with anesthesia (Table 4.5) and a higher instance of dying before reaching the appropriate time point, as 8 out of 14 animals lost before reaching a time point were Cox-2KO animals.

Cox-2KO male mice are fertile, but female Cox-2KO mice are infertile (246). Therefore, Cox-2KO male mice were mated to Cox-2HET female mice. Based upon Mendelian genetics, half of the offspring should be Cox-2KOs and half should be Cox-2HETs. However, the number of Cox-2KO mice that were weaned was approximately 25% of every litter, due to Cox-2KO pups having a higher mortality rate than their control littermates. This was also shown by Morham *et al.* and Dinchuk *et al.*, who also found abnormal Mendelian ratios for Cox-2KO mice that reached weaning (approximately 20 days old) (242,246). Cox-2WT animals were produced by mating Cox-2HET males with Cox-2HET females to produce the initial offspring. This mating scheme should theoretically result in 25% of every litter being Cox-2WT, 50% Cox-2HET and 25% Cox-2KO. However, in practice this resulted in approximately 40% Cox-2WT, 50% Cox-2HET and 10% Cox-2KO. Subsequent Cox-2WT animals were produced by

mating male Cox-2WT animals with female Cox-2WT animals, resulting in an all Cox-2WT population.

3.2.3 5-Lipoxygenase Deficient Mice

Previous studies found no physiological abnormalities 5-LOKO mice up to ten months of age (244). The only noticeable difference was in the spleen being statistically smaller ($p<0.05$) when compared to 5-LOWT animals (244). Examination of total blood cell populations, differential cell counts and analysis of bone marrow showed no evidence of abnormal precursor cells of any lineage in either 5-LOKO or 5-LOWT animals (244). This indicated that 5-Lipoxygenase products are not required for normal development and is not necessary in the mouse under normal physiological conditions (244).

Male and female 5-LOKO animals are fertile. Therefore, 5-LOKO males were mated to 5-LOKO females to produce all 5-LOKO offspring. Genotyping of random 5-LOKO offspring was checked periodically to insure that mice being produced were in fact 5-LOKO animals.

Matings to produce wild-type control animals for experiments using 5-LOKO animals was not necessary, as the appropriate identical genetic background control animals used in these experiments (C57BL/6, WT) were commercially available and purchased from Jackson Laboratories (Bar Harbor, ME).

3.3.0 Tail Biopsy and Genotyping of Mice

At weaning (approximately 28 days), a one to two centimeter section of tail was clipped from each animal. Lysis and purification of the mouse tail DNA was performed using a Qiagen DNeasy kit (Qiagen Inc., Valencia, CA) as per the manufacturer's specifications for purification of total DNA from rodent tails. To obtain optimum DNA yield and quality, only a 0.4 to 0.6 cm sample of tail was used for purification to prevent overloading of the DNeasy spin columns. The expected yield of genomic DNA was between 10 and 40 μg per tail biopsy. However, DNA yield was dependent on the strain, biopsy length and mouse age.

Briefly, samples were first lysed using proteinase K. The buffering conditions are then adjusted to provide optimal DNA-binding conditions and the lysate is loaded onto the DNeasy Mini spin column. After a brief centrifugation, DNA is selectively bound to the DNeasy membrane as contaminants pass through. Any remaining contaminants and enzyme inhibitors are then removed in two steps. Finally, the DNA is eluted in either water or TE buffer and is ready for analysis.

Polymerase chain reaction (PCR) was performed with the tail biopsy DNA to determine mouse genotype. The 10μl reaction volume consisted of 1μl of dNTP mix, 1μl of Pyrococcus woesei (*Pwo*) polymerase, 1μl of 10X *Pwo* buffer, 1μl of primer solution, 0.4μl of genomic DNA solution and 5.6μl of distilled water. Primers were purchase from Integrated DNA Technologies Inc. (Coralville, IA). The primer solution consisted of 5mM of the forward primer and 5 mM of the

reverse primer. The 10X *Pwo* buffer contained 100 mM Tris-Cl (pH 8.8), 500 mM KCl, 25 mM $MgCL_2$ and 1% Triton X-100.

Optimal thermocycler parameters were empirically determined for each primer set. It was found that primers sets used to genotype Cox-1KO, Cox1-WT, 5-LOKO and 5-LOWT produced optimal results using Program 1 (see below) while primer sets for Cox-2KO and Cox-2WT produced optimal results using Program 2 (see below).

Primers used in these studies are listed in Table 3.2. In the primer sequences: C represents cytosine, G represents guanosine, T represents thymidine and A represents adenosine.

Program 1:
Step 1: 95 ºC for two minutes
Step 2: 95 ºC for fifteen seconds
Step 3: 55 ºC for thirty seconds
Step 4: 72 ºC for one minute
Step 5: Repeat steps 2-4, 34 times
Step 6: Hold at 15 ºC

Program 2:
Step 1: 95 ºC for two minutes
Step 2: 95 ºC for fifteen seconds
Step 3: 60 ºC for thirty seconds
Step 4: 72 ºC for one minute
Step 5: Repeat steps 2-4, 39 times
Step 6: Hold at 15ºC

The resultant PCR product obtained after amplification was separated by electrophoresis in a 2% agarose gel using 1X Tris-Borate EDTA (TBE) buffer (pH 8.3, 89 mM Tris, 89 mM boric acid and 2 mM EDTA). The gel was stained with

ethidium bromide and photographed using an instant camera (FR-PDC-34, Fisher Scientific, Springfield, NJ) and Polaroid film (Type 667, Polaroid Corp., Waltham, MA). The genotype of each animal was based upon the base pair sizes of the PCR product as indicated in Table 3.2.

Table 3.2. Mouse Primer Sequences and Amplification Sizes for PCR Genotyping of Mice Used in These Studies.

Gene	Approximate Product Size (bp)	Forward Primer 5' to 3'	Reverse Primer 5' to 3'	Reference
Cox1-KO	600	GCA GCC TCT GTT CCA CAT ACA C	AAT CTG ACT TTC TGA AGT TGC C	Forward: (247); Reverse: This Study
Cox1-WT	700	AGG AGA TGG CTG CTG AGT TGG	AAT CTG ACT TTC TGA AGT TGC C	Forward: (247); Reverse: This Study
Cox2-KO	950	ACG CGT CAC CTT AAT ATG CG	TCC CTT CAC TAA ATG CCC TC	Forward and Reverse:(247)
Cox2-WT	800	CCG ACA CCT TCA ACA TTG AAG ACC AGG	TCC CTT CAC TAA ATG CCC TC	Forward: This Study; Reverse:(247)
5LO-KO	600	ATC GCC TTC TTG ACG AGT TC	GCA GGA AGT GGC TAC TGT GGA	Forward and Reverse: (248)
5LO-WT	164	TGC AAC CCA GTA CTC ATC AAG	GCA GGA AGT GGC TAC TGT GGA	Forward and Reverse:(248)

3.4.0 Surgical Procedure and Fracture Model for Mice

Mice were anesthetized by an intraperitoneal injection (0.01 ml/g body weight) of 10% ketamine and 5% xylazine. The right leg was scrubbed with a 10% povidone-iodine solution in preparation of surgery. A three millimeter parapatellar incision was created and the patella was dislocated laterally to expose the femoral condyles. A hole was drilled into the femoral intramedullary canal at the intracondylar notch using a thirty-gauge needle (Becton Dickinson

Co., Franklin Lakes, NJ). The medullary canal was further reamed to the proximal femur using a three-quarter inch, twenty-seven gauge needle (Becton Dickinson Co.). Next, a 0.01 inch diameter stainless steel wire (Small Parts Inc., Miami Lakes, FL) was inserted into the intramedullary canal to retain the impending fracture. A thirty-gauge two millimeter long wedge, taken from the tip of the thirty-gauge needle, was then lodged between the bone at the femoral condyles and the intramedullary pin to stabilize the pin in place. The wire extending past the femoral condyles was cut and discarded. The patella was repositioned and the incision was closed in two layers using 5-0 synthetic absorbable suture (Ethicon Inc., Somerville, NJ).

A closed diaphyseal fracture was produced in the right femur using a custom-made, three-point bending device (BBC Specialty Automotive Center, Linden, NJ), similar to the methods described by Bonnarens and Einhorn (209). The unfractured, left femur was used an internal control. The animals were allowed free, unrestricted weight bearing after recovery from anesthesia. The animals were sacrificed at the necessary time points using halothane gas (Sigma Chemical Co., St. Louis, MO.)

3.5.0 Radiography of Mouse Femur Fractures

Fracture healing was examined by dorsal-ventral radiographs of the mice. All animals were radiographed immediately post-fracture to verify that a mid-diaphyseal fracture had been produced and once again at sacrifice to check for pin slippage. A subset of animals in each experiment was serially radiographed

to assess fracture healing over the course of several weeks to months in the same animal. Radiographs were made using a Model 804 Faxitron (Field Emission Corp., McMinnville, OR) and Kodak Min-R 2000 mammography film (Eastman Kodak Co., Rochester, NY). Mice were either anesthetized or euthanized, as described above, prior to radiography.

3.6.0 Histology and Histomorphometry of Mouse Femur Fractures

3.6.1 Decalcified Histology of Fractured Femurs

Animals scheduled for decalcified histology had the fractured and contralateral control limbs harvested, cleaned of soft tissue without disturbing the callus and fixed in 10% buffered formalin (Fisher Scientific, Fair Lawn, NJ) or STF (Streck Laboratories Inc., La Vista, NE). The femora were decalcified using a 5% formic acid solution (Immunocal Decal Chemical Corp., Congers, NY), dehydrated through successive grades of ethanol, cleared using d-Limonene-based solvent (CitriSolve, Fisher Scientific) and paraffin embedded in Paraplast X-Tra Tissue embedding medium (Fisher Scientific). The complete decalcified embedding protocol is located in Appendix A.

The embedded femurs were then cut sagittally in the medio-lateral plane into six μm sections using a manual microtome, stained with Masson's trichrome and examined by light microscopy. The protocol for Masson's trichrome is located in Appendix A.

3.6.2 Calcified Histology of Fractured Femurs

Animals scheduled for calcified histology had the fractured and contralateral control limbs harvested, cleaned of soft tissue without disturbing the callus and fixed in 10% buffered formalin overnight. The femora were then dehydrated through successive grades of ethanol, cleared using a d-Limonene-based solvent (Citrisolve, Fisher Scientific) and embedded in polymethylmethacrylate (PMMA) (249). The complete calcified embedding protocol is located in Appendix A.

A medio-lateral sagittal section was cut from each femur sample using a low-speed saw (Isomet 11-1180, Buehler, Ltd., Evanston, IL). The cut section was than polished on one side and glued onto a plexiglass slide. Samples were allowed to adhere overnight and then ground down through four successively finer grits of Carbimet sandpaper (Buehler, Ltd.). After approaching a thickness of approximately 100 μm, samples were polished using a Mastertex 8 inch cloth (Buehler, Ltd.) and 1 μm and 0.05 μm deagglomerated alpha alumina micropolish (Buehler, Ltd.). Samples were then stained with Stevenel's Blue, counterstained with Van Gieson's Picrofuchsin and examined by light microscopy (250). The protocol for Stevenel's Blue and Van Gieson's Picrofuchsin is located in Appendix A.

3.6.3 Histomorphometry of Fractured Femurs

3.6.3.1 Acquisition of Histological Images

Histomorphometrical measurements were made using ImageProPlus software (v. 5.0.1.11, Media Cybernetics Inc., Silver Spring, MD). Histomorphometric data was collected from digital microscopic images captured using a Nikon DXM1200F camera, the Nikon ACT-1 software package (version 2.63, Nikon Co, Japan) and an Olympus BH2-RFCA light microscope (Olympus America Inc, Center Valley, PA). Histomorphometric measurements were made to calculate the total fracture area (TA), amount of cartilage (CA), fibrous granulation tissue (GT), mineralized tissue (MA) and original femur bone (B) in each fracture callus. Callus area (CALLUS) was calculated by subtracting the original femur bone from the total fracture area (TA-B=CALLUS). Due to callus sizes varying by the size of the femur and location of the sagittal section, further analysis was done involving the amount of MA, CA and GT as a percentage of callus area (%MA, %CA, %GT).

3.6.3.2 Statistical Analysis of Histomorphometrical Data

Means and standard deviations were calculated and statistical analysis of the data was performed using an analysis of variance (ANOVA) with appropriate post-hoc tests, as required. Differences were considered to be significant at $p < 0.05$. Statistical analysis was performed using SigmaStat 3.0 software (SPSS Inc., Chicago, IL).

3.7.0 Mechanical Testing of Intact and Fractured Mouse Femurs

3.7.1 Preparation of Mouse Femurs for Mechanical Testing

Both the fractured and contralateral femurs were harvested and cleaned of soft tissue without disturbing the callus. Femur length and the maximum anteroposterior and mediolateral dimensions of the external fracture callus were measured using electronic calipers (Mitutoyo Corp., Japan). Similar measurements were made of the contralateral femurs. To minimize the disturbance to the fracture callus, the pin was left in the femur during torsional testing. Since the pin is the axis of rotation of the bone during torsional mechanical testing, it should have theoretically no effect on the torsional mechanical testing results (201).

3.7.2 Torsional Testing Protocol for Mouse Femurs

The distal and proximal ends of the femurs were cemented vertically in 0.25 inch hexagon acorn nuts (Small Parts Inc.) with cyanoacrylate glue (Electron Microscopy Sciences, Hatfield, PA). The acorn nuts were then filled with a self-curing acrylic powder and liquid system (Seta-Tray, Accurate Set, Inc., Newark, NJ) to only expose the mid-diaphyseal region of the femur. The self-curing acrylic was prepared by mixing 10 grams of power with 10 milliliters of liquid. The powder and liquid were mixed thoroughly for 20 seconds and allowed to set until the composition has a paste-like consistency. Specimens were rehydrated after the potting process by allowing the potted femurs to soak in 0.9% saline for one hour prior to testing.

Torsional testing was conducted on a servohydraulic testing machine (MTS Corp., Minneapolis, MN, U.S.A.) using a 20 Nm reaction torque load cell (Interface, Scottsdale, AZ). Because bone is anisotropic, femurs were internally rotated to failure at an angular rotation rate of 1°/sec. The peak torque and angular rotation at failure were measured from the torque-angle deflection curves. From the callus dimensions, the polar moment of inertia (J) was calculated based upon a hollow ellipse model (251,252). In contrast, cross sectional area (A) of the fracture site was based on a solid ellipse model. Shear stress (τ) and shear modulus (G) were also calculated (253). The wall-thickness (t) value used in all equations was taken by averaging wall thickness measurements of ten randomly chosen intact femurs from every strain and phenotype. Left intact femurs were embedded as described above for calcified histology. Transverse sections were cut from the resulting blocks. Wall thickness was measured in four places from every slide and then averaged for each animal for all ten animals in every group to obtain the average wall thickness. All mechanical testing equations used are described in Appendix B.

3.7.3 Statistical Analysis of Torsional Mechanical Testing Data

Only femurs harvested and tested without an adverse incident were used in the final calculations. Means and standard deviations were calculated and statistical analysis of the data was performed. Unpaired two-tailed Student's t-tests were used when comparing only two groups or the same group but at different time points. Paired two-tailed Student's t-tests were used when

comparing the fractured and control limb of the same animal. Analysis involving multiple groups or time points was performed using ANOVA with appropriate post-hoc tests, as required. Differences were considered to be significant at $p < 0.05$.

3.8.0 Eicosanoids Levels in Fracture Callus

3.8.1 Fracture Callus Preparation

Closed femur fractures were produced in 5-LOKO, Cox-2KO, Cox-2HET, Cox-2WT, Cox-1KO and C57BL/6 (WT) mice as described above. In addition, a subset of the Cox-2KO mice and Cox-1KO mice were treated with either the COX-1 selective inhibitor, SC-560 (Cayman Chemical Co. Ann Arbor, MI), or the COX-2 selective inhibitor, rofecoxib (Vioxx, Merck, West Point, PA) at a dose of 30 mg/kg by oral gavage, 2 hours prior to sacrifice, respectively. All mice were sacrificed at four days after fracture. The fracture callus with surrounding muscle was quickly resected and flash frozen in liquid nitrogen. The callus was weighed and pulverized using a mortar and pestle. The pulverized callus was extracted into 5 volumes of M-PER buffer reagent (Pierce Biotechnology, Inc., Rockford, IL) that was supplemented with protease inhibitors (Sigma Aldrich, St. Louis, MO). The samples were placed on a mixer at 4°C for 30 minutes. The extract was clarified by centrifugation at 10,000 rpm for 10 minutes at 4°C. The supernatant was collected and stored at -80°C. An aliquot of the clarified extract from the fracture callus was used to partially purify eicosanoids.

3.8.2 Purification Technique of Fracture Callus Eicosanoids

Two milliliters of ethanol was added to 0.5 milliliters of clarified extract and the precipitate proteins were removed by centrifugation at 3000 x g for 10 minutes. The supernatant was dried in vacuo, resuspended in 1 M citrate buffer, pH 4, and applied to a 500 mg C_{18} column (Waters Sep-Pak) that had been pre-activated by methanol and water washes. The columns were washed with water and hexane. Eicosanoids were eluted from the C_{18} resin using 5 milliliters of ethyl acetate containing 1% methanol. The eluate was dried in vacuo to remove all organic materials and resuspended in EIA buffer (0.4 M sodium chloride; 0.1 M sodium phosphate, pH 7.4; 1 mM ethylene-diamine-tetra-acetic acid; and 0.1% bovine serum albumin).

3.8.3 Quantification of Fracture Callus Eicosanoids

PGE_2, $PGF_{2\alpha}$, and LTB_4 were measured using enzyme-linked immunoassays as described by the manufacturer (Cayman Chemical, Ann Arbor, MI). To ensure eicosanoid levels were in the proper range of the standard curve, dilutions for each assay were made using EIA buffer. The PGE_2, $PGF_{2\alpha}$, and LTB_4 concentrations were normalized to total protein concentration measured using bicinchoninic acid (BCA Protein Assay, Pierce Biotechnology, Inc., Rockford, IL) (254).

3.8.4 Statistical Analysis of Fracture Callus Eicosanoids

PGE_2, $PGF_{2\alpha}$ and LTB_4 levels were normalized to soluble protein concentration and levels were compared between mouse genotypes and treatment groups using ANOVA and post-hoc Holm-Sidak tests using SigmaStat software (SPSS). Differences were considered to be significant at $p < 0.05$.

4.0.0 RESULTS

4.1.0 Characterization of a Closed Murine Femoral Fracture Model

4.1.1 Disposition of ICR Mice Used in This Study

Female ICR mice (Harlan Sprague Dawley, Indianapolis, IN) weighing 30.8 ± 3.2 grams (mean ± standard deviation) were used in this experiment. All animals were 10 to 12 weeks old at the beginning of the study. All experimental procedures were approved by the New Jersey Medical School Institutional Animal Care and Use Committee. Of the 246 mice used as part of this study, 185 were ultimately included in the radiographic, histologic, and mechanical analyses. This resulted in an overall success rate of 75.2%. A more detailed disposition of the mice used in this study may be found in Table 4.1.

Table 4.1. Disposition of the 246 ICR Mice Used in the Study.

	Surgical Errors			Mechanical Testing			Histology
	Anesthesia Death	Fracture Destabilization	Poor Fracture	Potting Errors	User Errors	Total Analyzed	Total Used
Number	8	6	8	35	4	68	117
Percentage	3.3	2.4	3.3	14.2	1.6	27.6	47.6

*** An average of 9.75 femurs (range 4-14) was examined for each of the 12 histology time points.**

4.1.2 Surgical Procedure for ICR Mice

The surgical procedure to produce the mouse femur fractures was easily accomplished. One problem that arose while defining the overall surgical procedure was the loss of fracture fixation by slippage of the pin from the intramedullary canal. Several methods were explored to stop the pin from slipping, and it was found that staking the pin in place using a 2-mm wedge from

the tip of a 30-gauge needle provided the most dependable fixation. This wedge stabilization was subsequently used for all future experiments described.

Femoral fracture production was also easily achieved. Fractures were consistently transverse or slightly oblique with minimal comminutions. Only 3.3% of the fractures were eliminated from the study due to poor fracture quality (Table 4.1). The animals began to bear weight on their hind legs within a few hours after the surgical procedure. A slight decrease in weight was observed between 2 days and 10 days post-surgery and a weight gain was seen from 14 days to 84 days post-fracture (Table 4.2).

Table 4.2. Average Pre-Surgical and Post-Sacrifice Weights of ICR Mice.

Time Point	n	Pre-Surgical Weight in Grams (Mean ± SD)	Post-Sacrifice Weight in Grams (Mean ± SD)
6 Hours	7	34.0 ± 1.6	34.0 ± 1.6
2 Days	11	30.7 ± 1.6	30.6 ± 1.8
4 Days	12	31.5 ± 0.9	31.0 ± 1.0
7 Days	16	30.9 ± 1.0	29.9 ± 1.5
10 Days	17	30.1 ± 1.7	28.8 ± 1.2
14 Days	13	29.7 ± 1.6	30.2 ± 1.3
21 Days	33	31.2 ± 2.4	32.5 ± 1.4
28 Days	44	31.8 ± 3.0	32.6 ± 2.8
42 Days	39	28.9 ± 1.3	32.2 ± 2.3
84 Days	32	30.8 ± 2.1	37.2 ± 3.2

4.1.3 Radiography of ICR Mouse Femurs

Fracture healing was assessed by serial radiography at 7, 10, 14, 21, 28, and 42 days post-fracture using a representative group of animals. This allowed for visual assessment of the healing process and was an indication of the

reproducibility of fracture healing between animals. Figure 4.1 shows the timeline of fracture healing in two representative ICR mice.

Analysis of the radiographs showed anatomical reduction at the fracture with periosteal lifting around the callus site visible at 7 days. A radiolucent zone at the fracture line was still apparent at 14 and 21 days after fracture. Bridging of the peripheral callus was apparent by 21 days post-fracture. By 28 days, the fracture was fully bridged with new bone and the external callus appeared ossified. Remodeling appeared to begin by 21 days after fracture, as the callus size visually appeared to be decreasing. Remodeling continued through 42 days post fracture when the external callus appeared almost completely resorbed (Figures 4.1 and 4.2). Maximum callus area peaked between 10 and 14 days and then began to decrease (Figure 4.2).

4.1.4 Decalcified Histology of ICR Mouse Femurs

Murine femoral fracture healing was observed to undergo the key regenerative processes of inflammation, callus formation, endochondral ossification, and remodeling that are indicative of the fracture healing process established in other models (219,220). Figure 4.3 shows the early events in murine fracture healing using decalcified samples stained with Masson's trichrome. Hematoma formation was apparent six hours after fracture. By two days after fracture, inflammation was seen at the fracture site. Additionally, the surrounding soft-tissue appeared swollen based on the increased distance between muscle fibers. Four days after fracture, large numbers of new cells

were present within the intramedullary canal at the fracture site and in the external callus area. By seven days post-fracture, the callus had clearly defined borders. Neither edema nor muscle fiber degeneration were evident at seven days post-fracture. However, new bone formation was evident at the periphery of the fracture callus at this time. While chondrocytes were present within the external fracture callus at seven days post-fracture, the majority of the callus was still populated with mesenchymal cells. By ten days post-fracture, chondrocytes were abundantly present within the external callus between new bone at the periphery of the external callus and mesenchymal cells at the center of the callus. The histological appearance of the newly formed bone at the cartilage interface within the external callus was consistent with endochondral ossification. The fracture callus size appeared to peak at ten days post-fracture (see also Figure 4.2). Fourteen days after fracture, endochondral ossification was clearly evident in the fracture callus and the center of the external callus was no longer populated with mesenchymal cells but completely with chondrocytes.

4.1.5 Calcified Histology of ICR Mouse Femurs

The calcified histology confirmed that endochondral ossification had begun by 7 days post-fracture. Figure 4.4 shows regions of calcified cartilage in the external fracture callus seven days after fracture. By 10 days post-fracture, the amount of calcified cartilage had increased and was closer to the fracture site. The center of the callus was filled with apparently undifferentiated mesenchymal cells. However, undifferentiated mesenchymal cells were not

observable in the seven or ten day histology of the decalcified specimens (Figure 4.3). Fourteen days after fracture, the callus was filled with calcified cartilage between new bone at the periphery and chondrocytes at the center. All of the fractures were bridged with some new bone by 21 days post-fracture. Healing continued through 28 days after fracture, with an increase in the amount of new bone that occupied the fracture callus being observed. By 42 days post-fracture, remodeling of the fracture callus was clearly evident based upon the lamellar appearance of the bone spanning the fracture site.

4.1.6 Mechanical Testing of ICR Mouse Femurs

Fracture healing was also evaluated in the ICR mouse model using torsional mechanical testing. The testing procedure provided reproducible torque-angular displacement curves. Callus cross-sectional area (mm^2) was estimated based upon a solid elliptical geometry using the measured maximum and minimum diameters from each bone prior to mechanical testing (Table B1). The polar moment of inertia used to estimate shear modulus and shear stress was calculated based upon a hollow ellipse model as described in the Materials and Methods (Section 3.7.2). Similarly, the contralateral left femurs were also mechanically tested as the control group. The measured peak torque, angle at failure, working gauge length from the mechanical testing procedure, and the calculated polar moment of inertia were used to determine torsional rigidity (Nmm^2/rad), shear modulus (GPa), and shear stress (MPa). All mechanical testing parameters were analyzed at 21, 28, 42 and 84 days post-fracture for the

fractured limb and control femur. No statistical difference was observed when comparing the control femurs from any time point for the parameters of peak torque, rigidity, shear modulus, and shear stress (ANOVA p=0.204, p=0.576, p=0.051, p=0.053, respectively). It was then decided to pool these samples into one control group to be compared against all time points.

Figures 4.5, 4.6 and Table B1 summarize the mechanical testing results obtained. Peak torque increased rapidly during healing to reach values near 82% of the unfractured femur values by 21 days (Figure 4.5, Panel A). This large increase in torque can be accounted for by the structural changes in the fractured femur as its diameter dramatically increases at the fracture callus. In contrast, rigidity only showed a continual increase after 28 days of healing, which is consistent with the observed radiological and histological bridging of the fracture site with new bone occurring between 21 and 28 days after fracture (Figure 4.5, Panel B). Similar to rigidity, the material properties of the healing femur began to increase 28 days after healing. However, shear stress and shear modulus only obtained 35% and 29%, respectively, of the contralateral control femur even after 84 days of healing (Figure 4.5, Panels C-D). Additionally, while some bone bridging was seen in one-third of the fractured femurs tested at 21 days post-fracture, bone bridging was seen in 100 percent of the specimens tested at 28 days post-fracture.

Figure 4.6 shows the mechanical testing results after the fractured femur is normalized to its contralateral control femur. Normalized peak torque, (Panel A), normalized rigidity (Panel B), normalized modulus values (Panel C) and

normalized shear stress values (Panel D) at 21 and 28 days correspond to Stages I and II of the biomechanical stages proposed by White *et al.* (204), while Stage III and the beginning of Stage IV correspond to 42 and 84 days post-fracture. This correlation to White's stages validates the mouse femoral fracture as a valid biomechanical research model.

Figure 4.1. Radiographic Assessment of Femur Fracture Healing in ICR Mice. Serial radiographs of healing femur fractures from two representative mice are shown to illustrate the reproducibility of this fracture model (left and right columns, respectively). Dorsal-ventral radiographs of the healing femurs were taken at 7, 10, 14, 21, 28, and 42 days post-fracture. Note that a radio-opaque callus is first evident by 7 days post-fracture, that fracture bridging appears to occur approximately 21 days post-fracture, and that callus remodeling is evident by 28 days post-fracture.

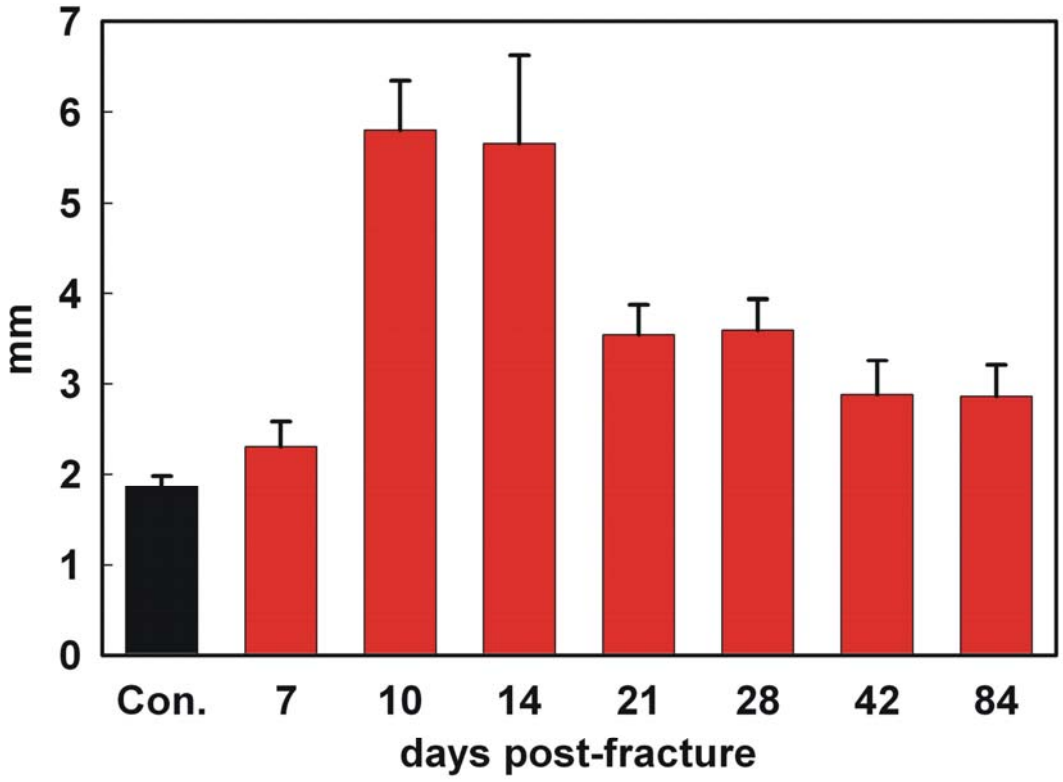

Figure 4.2. Fracture Callus Maximum Diameter Changes Over Time in ICR Mice. Maximum fracture callus diameters were measured from radiographs for the 7, 10 and 14 day time points or using electronic calipers for the contralateral left femur (Con.), 21, 28, 42 and 84 day time points. Maximum callus diameters peaked between ten and fourteen days post-fracture. Afterward, it began to decline. Sample sizes were 68, 11, 15, 18, 18, 18, 15, and 17 for control and successive time points, respectively. Error bars represent standard deviations. Diameters were statistically significant between all time points except 10 versus 14, 21 versus 28, and 42 versus 84 ($p < 0.05$; 2-tailed, unpaired t-test).

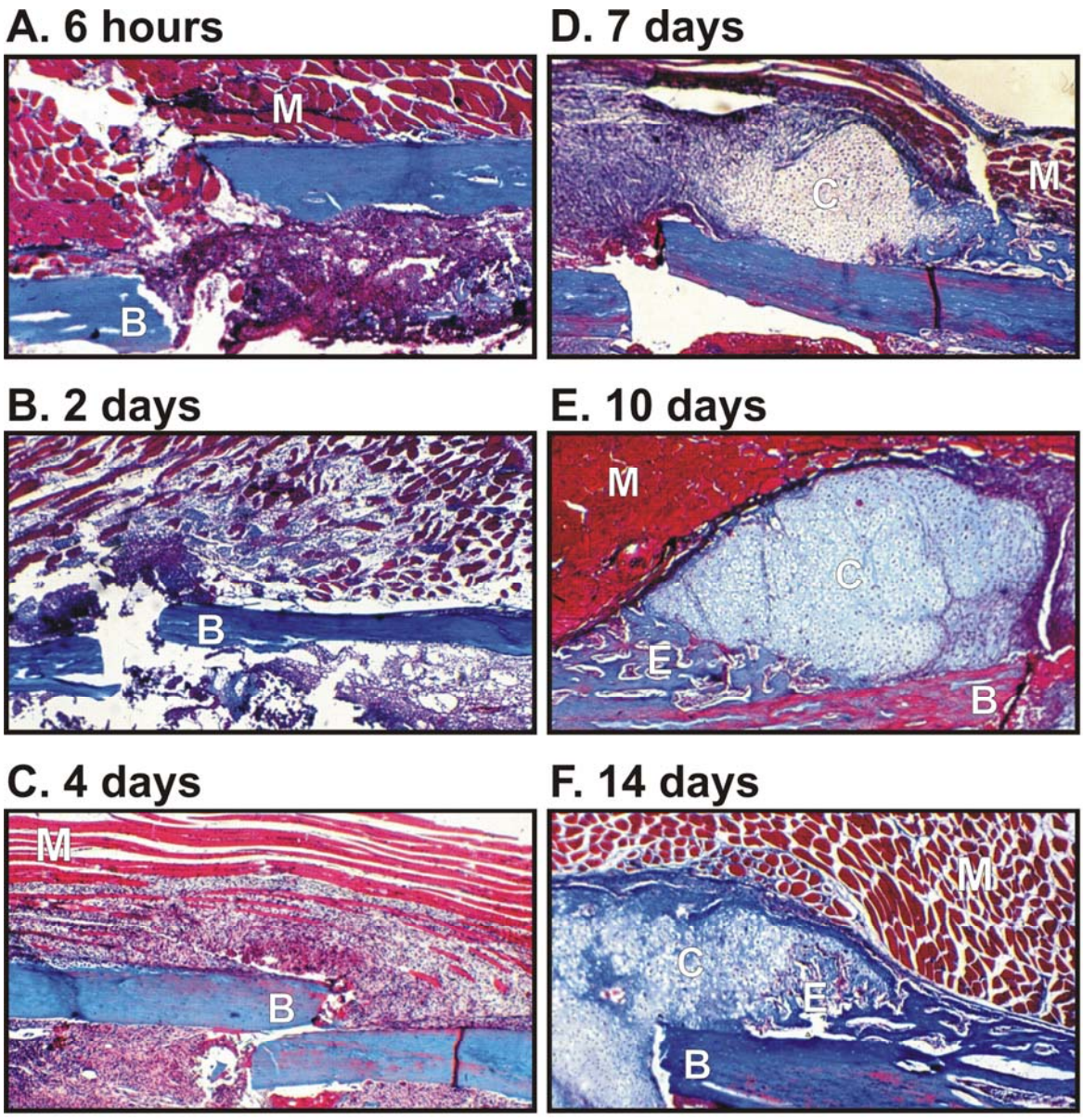

Figure 4.3. Early Histological Events of Femur Fracture Healing in ICR Mice. Fractured femurs were harvested at the indicated time points and processed for decalcified histology. Sections were stained with Masson's trichrome. (A) Hematoma formation but no apparent inflammation was evident by six hours post-fracture. (B) Inflammation, tissue swelling, and visible muscle fiber degeneration were evident by two days post-fracture. (C) Tissue swelling appeared to be reduced at four days post-fracture but a distinct callus filled with mesenchymal cells was also evident. (D) Chondrocytes and bone formation at the periphery of the fracture callus were seen by seven days post-fracture. (E) At ten days post-fracture, the callus appeared to reach maximum volume and was filled with chondrocytes, but still had some mesenchymal cells located in the callus middle, with new bone forming at the callus periphery. (F) Distinct areas of endochondral ossification were evident by fourteen days post-fracture. Symbols: B = bone; C = cartilage and chondrocytes; E = endochondral ossification; and M = muscle.

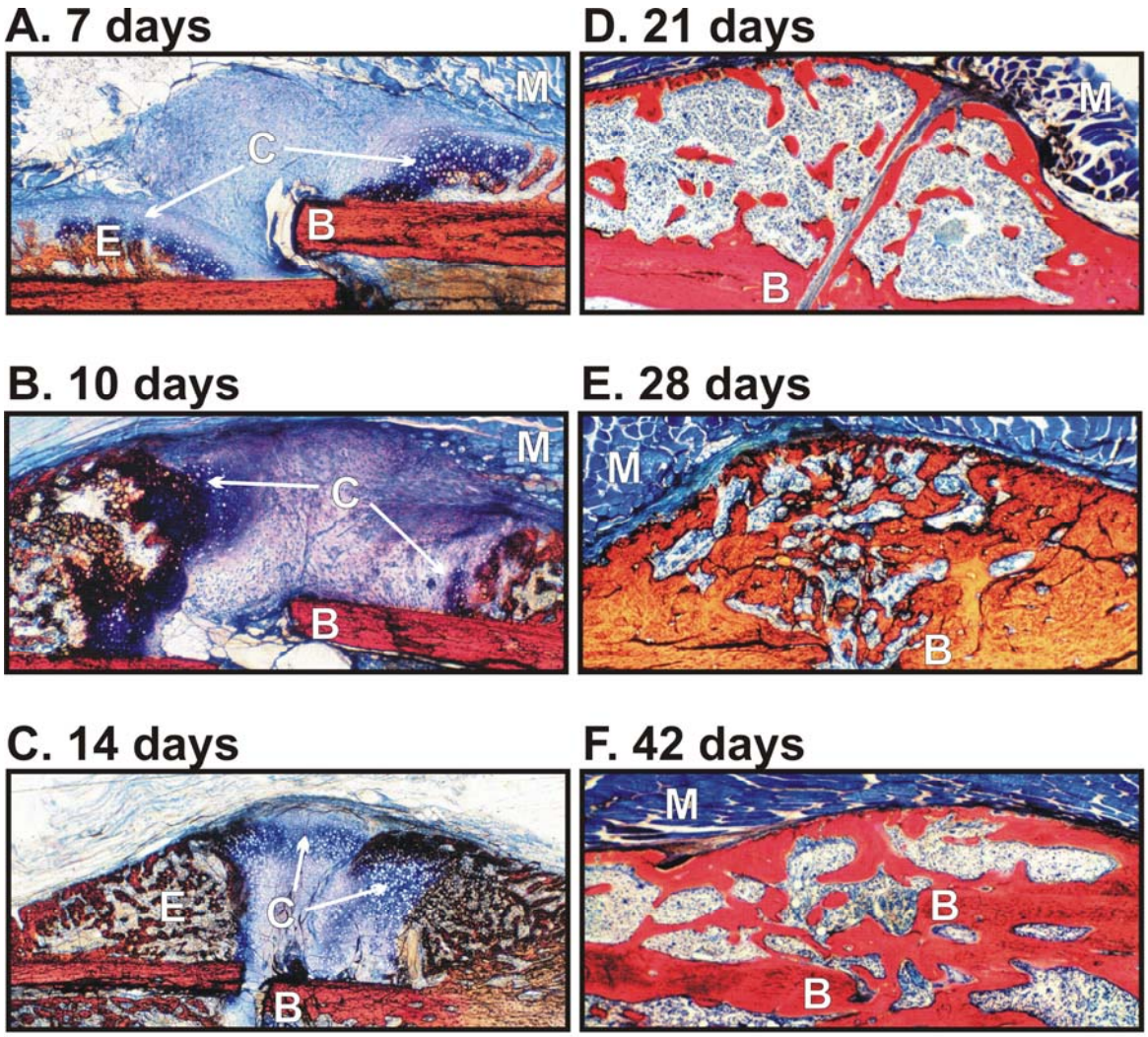

Figure 4.4. Late Histological Events of Femur Fracture Healing in ICR Mice. Fractured femurs were harvested at the indicated time points and processed for calcified histology. Sections were stained with Stevenel's blue and counterstained with van Gieson's picrofuchsin (bone is red; calcified cartilage is orange to red; cartilage is deep blue to purple; soft tissues are lighter shades of blue). (A) After 7 days, calcified cartilage and endochondral ossification were evident in the fracture callus. (B) By 10 days post-fracture, continued endochondral ossification was evident. (C) The callus appeared bridged with cartilage by 14 days post-fracture with extensive areas of new bone formation and endochondral ossification towards the callus periphery. (D) The fracture appeared bridged with bone by 21 days post-fracture. (E) The callus appeared more consolidated with bone remodeling evident by 28 days post-fracture. (F) Remodeled, lamellar bone bridged the fracture site by forty-two days post-fracture. Symbols: B = bone; C = cartilage; E = endochondral ossification; and M = muscle.

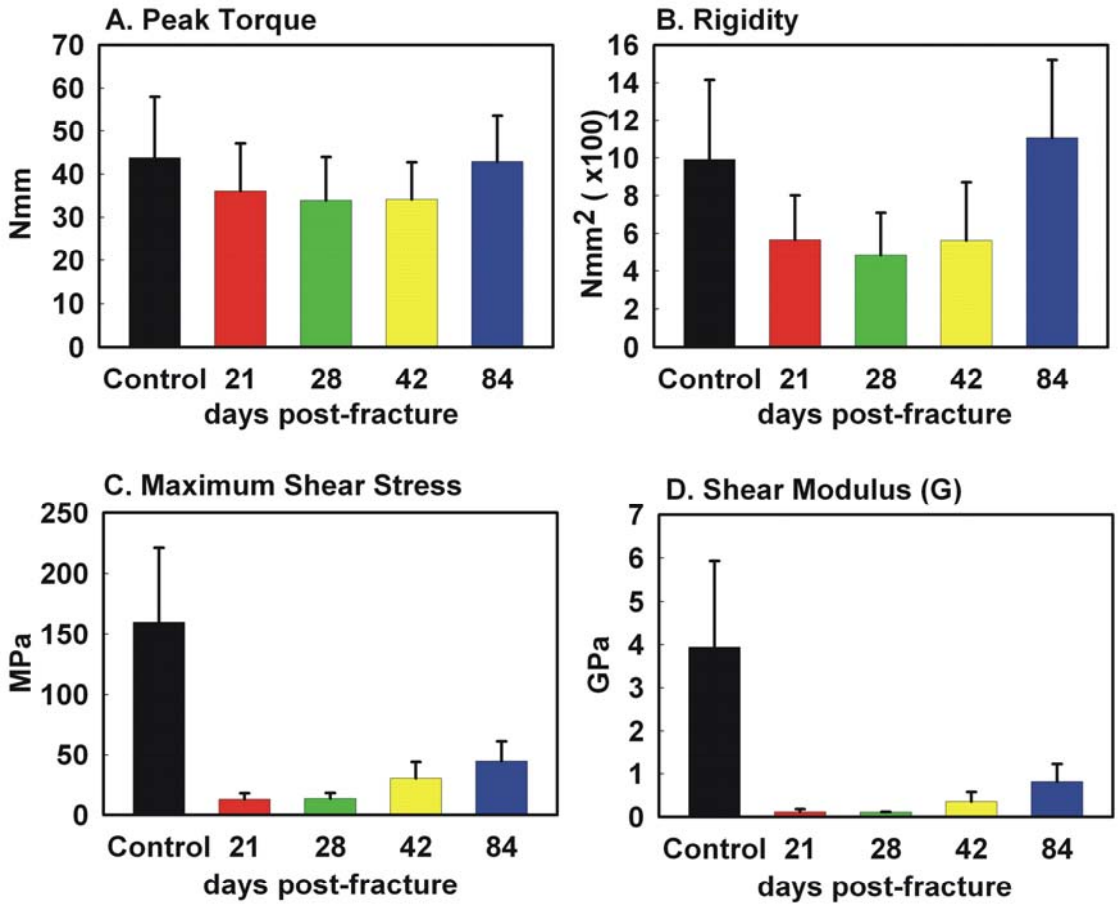

Figure 4.5. The Mechanical Properties of ICR Mouse Fractured Femurs. Peak torque (A), rigidity (B), maximum shear stress (C), and shear modulus (D) were measured or calculated from bone dimensions, peak torque, and angular displacement at failure at the time points indicated. Error bars represent standard deviations. The structural properties (torque and rigidity) of the fractured femurs were never less than 48% of the contralateral femur after 21 days of healing and were equivalent to the contralateral femurs by 84 days post-fracture. Relative to the contralateral femurs, the intrinsic material properties (maximum shear stress and shear modulus) of the fractured femurs were less than those for the structural properties at each time point and remained relatively low even after 84 days of healing. There were no statistically significant differences when the mechanical values obtained between the 21 and 28 day fractured femurs were compared. Between 28 and 42 days post-fracture, the were no statistical differences in the structural properties (peak torque and rigidity) of the fractured femurs but the material properties (maximum shear stress and shear modulus) of the 28 day fractured femurs were significantly less than the 42 day fractured femurs. All the mechanical values were significantly less for the 28 day and 42 day fractured femurs as compared to the 84 day fractured femurs ($p < 0.05$, two-tailed, unpaired t-tests).

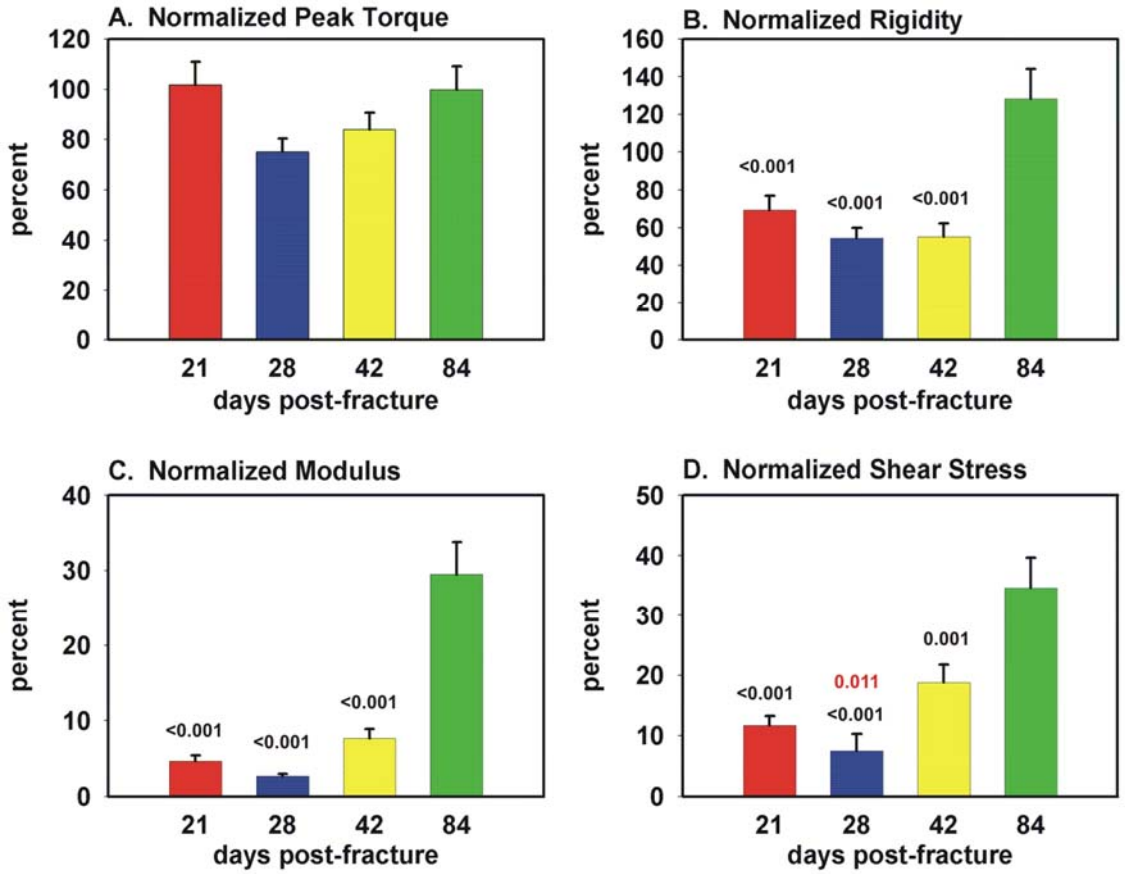

Figure 4.6. Normalized Mechanical Properties of ICR Mouse Fractured Femurs. Fractured and contralateral femurs from ICR mice were mechanically tested to failure in torsion from 21 to 84 days post fracture. Normalized peak torque (A), normalized rigidity (B), normalized maximum shear stress (C), and normalized shear modulus (D) were measured or calculated from bone dimensions, peak torque, and angular displacement at failure at the time points indicated. Fractured femur values were normalized to the values obtained from the contralateral femur of that mouse as a percentage. Bars represent avg ± SEM. Black statistical values show comparisons between 21, 28, and 42 days versus 84 days. Red statistical values show comparisons between 28 days versus 42 days. Structural properties (normalized peak torque (A) and normalized rigidity (B)) shows initially large percentages at 21 days when normalized to their contralateral control femur. This is indicative of the large callus still present at the fracture site. As callus size diminishes from 21 to 28 days, so does the normalized peak torque and rigidity values obtained, as structurally, the fractured bone is very weak. Mineralized tissues begins to replace the fibrous callus, resulting in increases in both normalized peak torque and rigidity by 42 days. By 84 days, normalized structural values are at or passed 100 percent of the control values and are significantly higher than the values obtained at the other time points. Material properties (normalized shear modulus (C) and shear stress (D))show similar trends as the structural properties, but with much lower percentages. This indicates immature bone at the fracture site at 21 and 28 days. Normalized shear modulus and shear stress values increase at 42 days and reach a maximum at 84 days. However, these values only reach 29 and 35 percent respectively after 3 months of healing indicating the material present is still vary immature.

4.2.0 The Effect of Genetic Background on Fracture Repair

4.2.1 Disposition of Inbred Animals Used in This Study

Female C3H, DBA/2, C57BL/6 and ICR mice (Taconic Farms, Germantown, NY) weighing 30.4 ± 3.0, 28.2 ± 2.9, 30.1 ± 3.1, and 40.5 ± 3.8 grams, respectively, were used in this experiment. All animals were purchased as retired breeders and were approximately 6 to 9 months old at the beginning of the study. All experimental procedures were approved by the New Jersey Medical School Institutional Animal Care and Use Committee. Of the 306 mice used in this phase of the study, 165 were ultimately included in the radiographic, histologic, histomorphometric, and mechanical analyses. A more detailed disposition of the mice used in this study may be found in Table 4.3.

Table 4.3. Disposition of the 306 Inbred Mice Used in the Study.

	Surgical Errors			Mechanical Testing			Histology	
	Anesthesia Death	Fracture Destabilization	Poor Fracture	Potting Errors	User Errors	Total Analyzed	Poor Slide	Total Analyzed
ICR	0	4	3	6	4	13	3	25
C3H	3	5	3	11	8	11	6	34
DBA/2	1	7	0	9	7	11	7	27
C57BL/6	4	9	14	10	8	11	9	33

It was observed that a high number of C57BL/6 mice had comminutions from the surgical and fracture procedure, which resulted in poor or unstable fractures and were ultimately excluded from the final analysis. This was largely due to the quality of bone in this particular strain and not because of the fracture procedure. Animals in all strains were able to bear weight on their hind legs

within a few hours after surgery and no significant decrease in weight over time was noted (Table 4.4).

Table 4.4. Average Pre-Surgical and Post-Sacrifice Weights of Inbred Mice.

Strain	Time Point	n	Pre-Surgical Weight in Grams (Mean ± SD)	Post-Sacrifice Weight in Grams (Mean ± SD)
ICR	7 Days	6	43.7 ± 5.9	43.0 ± 6.5
	10 Days	4	41.0 ± 1.2	41.0 ± 1.2
	14 Days	6	41.7 ± 2.7	41.3 ± 2.7
	21 Days	6	37.0 ± 7.1	36.0 ± 2.8
	28 Days	25	40.0 ± 3.4	37.2 ± 6.7
	42 Days	4	39.5 ± 3.0	40.5 ± 1.9
C3H	7 Days	4	34.0 ± 1.6	34.0 ± 1.6
	10 Days	4	32.0 ± 3.3	32.5 ± 2.5
	14 Days	7	33.1 ± 1.1	33.4 ± 1.0
	21 Days	7	30.0 ± 2.3	29.4 ± 2.2
	28 Days	38	30.2 ± 2.9	28.7 ± 2.3
	42 Days	10	27.8 ± 2.2	27.4 ± 2.3
DBA/2	7 Days	4	28.5 ± 3.4	28.5 ± 3.4
	10 Days	4	29.5 ± 1.9	29.5 ± 1.9
	14 Days	4	30.0 ± 4.3	30.0 ± 4.3
	21 Days	6	25.7 ± 2.7	25.7 ± 2.7
	28 Days	31	28.7 ± 2.8	26.6 ± 2.1
	42 Days	12	27.2 ± 2.2	25.3 ± 2.6
C57BL/6	7 Days	6	30.0 ± 1.3	30.0 ± 1.3
	10 Days	5	32.8 ± 2.7	32.4 ± 3.6
	14 Days	14	30.3 ± 3.1	30.7 ± 2.7
	21 Days	6	26.7 ± 2.4	27.3 ± 3.0
	28 Days	23	30.2 ± 2.7	29.7 ± 2.5
	42 Days	17	30.2 ± 3.2	29.4 ± 2.4

4.2.2 Radiography of Inbred Mice

All animals were radiographed immediately post-fracture to ensure the placement of a mid-diaphyseal fracture and post-sacrifice to confirm pin

stabilization. In addition, a subset of animals was serially radiographed at 7, 10, 14, 21, 28 and 42 days post-fracture to establish a typical pattern of fracture healing for each of the experimental strains (Figure 4.6). At 7 days post-fracture, all fours strains appear to have a mid-diaphyseal femur fracture, but no periosteal lifting is detected. By 10 days, periosteal lifting and a defined callus border are apparent in the C3H and DBA/2 fracture calluses. However, the ICR and C57BL/6 fractures show very little callus formation at this time point. By 21 days, it visually appears that the C3H and DBA/2 fracture calluses were bridged, while the ICR and C57BL/6 still have a radiolucent zone in the center of their callus indicating bridging has not yet occurred. By 28 days, the fractures in all four strains appear bridged. Furthermore, the C3H and DBA/2 fractures look like they have begun to remodel. Remodeling appears to continue through 42 days post-fracture in all four strains as callus size visually appears smaller compared to 28 days.

4.2.3 Calcified Histology of Inbred Mouse Femurs

Animals used for histology were sacrificed at 7, 10, 14, 21, 28 or 42 days post-fracture. The histological assessment showed different results than the radiographical analysis first indicated.

As seen in Figure 4.7, at 7 days post-fracture, the fracture calluses have definitive borders and infiltration of multiple cell types is apparent in the fractures from all four strains. By 10 days post-fracture, a large mass of chondrocytes is evident in the DBA/2 and C57BL/6 calluses, while only a small amount of

cartilage was present in either the ICR or the C3H calluses. However, all three inbred strains visually appear to have extremely similar cartilage and mineralized areas by 14 days post-fracture, while the ICR mice continued to lag behind. By 21 days post-fracture, all cartilage in each of the inbred strains fractures seemed to be replaced by mineralized tissue. However, the ICR mice still had a slight amount of visible cartilage present. All cartilage was replaced by bone at approximately 28 days in all strains. Remodeling of the fracture calluses had occurred by 42 days, as was evident by the decrease in callus size and reshaping of the callus toward the original femur dimensions.

4.2.4 Histomorphometry of Inbred Mouse Femurs

Histomorphometric measurements confirmed what was seen visually in the histology (Figure 4.8). In order to reduce variability between sample cuts and sample sizes, mineralized area, cartilage area and granulation tissue area were normalized to the callus area for that specific sample.

C57BL/6 has the highest percentage of mineralized area (%MA) at 7 days while C3H had the largest percentage of cartilage area (%CA) with respect to the total callus area (CALLUS). The largest percentage of any parameter measured at this time point in all strains was that of granulation tissue (%GT), which filled between 46 to 70% of the callus area. At 10 days post-fracture, C57BL/6 had a significantly greater %MA than C3H ($p<0.001$), DBA/2 ($p<0.001$), and ICR ($p=0.002$). No measurable mineralized areas were detected in either the DBA/2 or C3H fractures. Both C3H and DBA/2 had significantly greater %CA than the

fracture calluses from the ICR (p= 0.009 and p= 0.004, respectively) or C57BL/6 mice (p= 0.048 and p= 0.021, respectively). All strains also showed a decrease in %GT measured in the callus at 10 days post-fracture. At 14 days post-fracture, over half of the C57BL/6 callus was filled with mineralized tissue and DBA/2 and C3H both had significantly larger increases in %MA compared to their own values at 10 days. By 21 days post-fracture, all strains had the majority of their calluses filled with newly mineralized tissue. Percent cartilage area and percent granulation tissue also had begun to decrease in the fracture calluses of all strains, with only a slight amount of either remaining. By 28 days post-fracture, no slide examined had any remaining measured granulation tissue or cartilage present. All strains showed extensively mineralization covering between 80 to 85% of the callus area. At 42 days post-fracture, %MA decreased. This signaled that remodeling of the newly mineralized bone had taken place and the bone was returning to its original shape. A summary table and statistical analysis for all histomorphometrical parameters may be found in Appendix B.

4.2.5 Mechanical Testing of Inbred Mouse Femurs

To assess how bone mineral density affects mechanical testing properties of healing bone, the fractured (right) and contralateral control (left) femurs of the mice were torsionally tested at 28 days post-fracture. When comparing the control left femurs' structural properties, peak torque and rigidity, the ICR and C3H mice have significantly greater values than either DBA/2 or C57BL/6 mice.

Additionally, the material properties, shear modulus and shear stress, of the C3H animals were far superior to all other experimental groups. This was expected, as C3H animals having the highest published bone mineral density values (Figure 4.9).

Assessment of the mechanical testing data for the right fractured femur showed very different results. Peak torque and rigidity values were significantly higher in the ICR and C57BL/6 animals than in either C3H or DBA/2 (Figure 4.9). However, ICR values declined when analyzing the material properties. In contrast, DBA/2 had significantly higher values compared to ICR and C3H and comparable values to C57BL/6, suggesting more mature bone had developed in this strain by 28 days post-fracture compared to ICR or C3H. Of surprise was how well the C57BL/6 had healed. While this strain has the lowest bone mineral density, both structural and material properties were significantly greater than C3H animals. Tables summarizing the mechanical testing data and statistical analyses are located in Appendix B.

One method used to minimize variability among the different strains is to normalize the fractured data with some type of control. Because these four strains had multiple variable parameters, several different normalization methods were utilized. The first method was to normalize the fractured femur by its contralateral control femur value for all parameters. These results are shown as a percentage (Figure 4.10 and Table B4). This data had trends similar to the data shown in Figure 4.9. While C57BL/6 has the lowest published bone mineral density values, it has significantly higher values for all parameters when

compared to DBA/2 and C3H. Additionally, DBA/2 had significantly greater shear stress values than C3H. This suggests that bone mineral density is inversely proportional to fracture healing rate.

Due to a significant difference in the weights between strains, one question that needed to be addressed was whether or not animal weight influenced the mechanical testing outcomes. Since mechanical testing parameters are based on cross-sectional area and various other geometric measurements of the bone, variations in mouse strain body weight need to be considered as a factor in the mechanical testing outcomes. After normalizing to the animal's body weight, different results were in fact observed, predominately in the material properties of the fracture callus (Figure 4.11 and Table B6). For the left femur, C3H had far superior shear modulus and shear stress compared to all other strains. However, this changed when comparing the fractured femur. DBA/2 and C3H had similar values of peak torque and rigidity. On a per gram basis, the DBA/2 had a higher shear modulus value than all strains and a comparable shear stress value to the C57BL/6.

It was observed that the cross-sectional areas of all strains were also statistically different (Figure 4.12 and Table B4). Therefore, cross-sectional area was another parameter used to normalize the data. The results obtained were similar to those when normalizing to weight (Figure 4.13 and Table B8). This was expected since there is a correlation between weight and bone size.

The last normalization method used was to normalize by the previously published average values of bone mineral density (238). Because ICR did not

have published values, only C3H, DBA/2 and C57BL/6 were evaluated. When looking at peak torque and rigidity values for the left femur, C57BL/6 had significantly higher values than either C3H or DBA/2 (Figure 4.14 and Table B10). Additionally, C3H and DBA/2 had similar values for the structural properties examined. Upon investigating the fractured femur, similar results as shown in Figure 4.9 were observed. Statistical analysis for all normalization parameters is located in Appendix B.

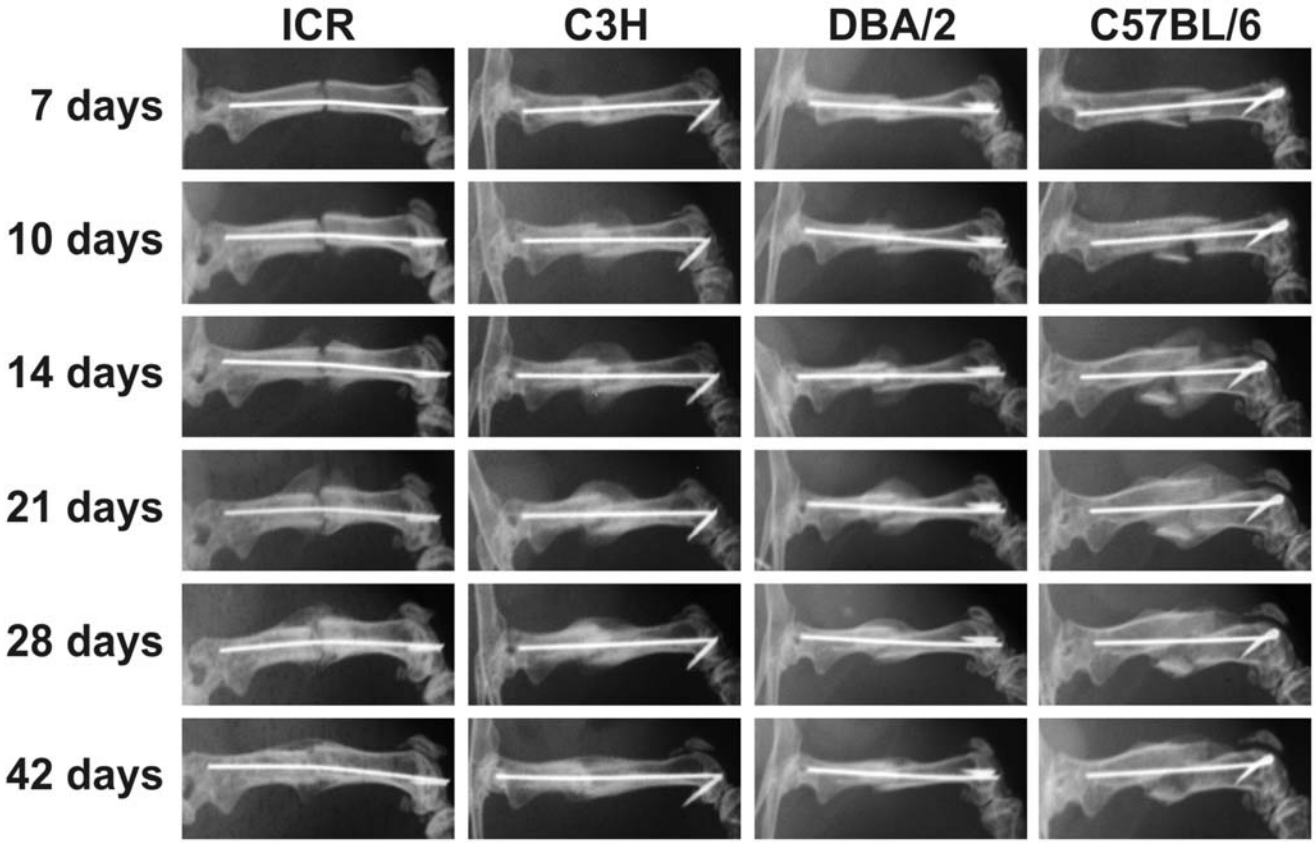

Figure 4.7. Radiographic Assessment of Fracture Healing in Inbred Mice. Serial radiographs of healing femur fractures from a representative mouse from each strain is shown to illustrate healing. Dorsal-ventral radiographs of the healing femurs were taken at 7, 10, 14, 21, 28 and 42 days post-fracture. (7 days) All 4 strains appeared to have a mid-diaphyseal fracture, but periosteal lifting was not detected. (10 days) A well-defined callus was visible in the C3H strain while periosteal lifting at the fracture periphery was detected in the DBA/2 and C57BL/6 mouse fractures. (14 days) The callus volume of the three inbred strains appeared to be at a maximum after fourteen days post-fracture. However, the outbred ICR strain continued to lag behind. (21 days) All three inbred strains appeared to have bridged their fractures by twenty-one days post-fracture. (28 days) Callus dimensions have visuallly decreased by twenty-eight days post-fracture, signaling the start of remodeling. (42 days) Fracture calluses continued to remodel through forty-two days post-fracture in all four strains.

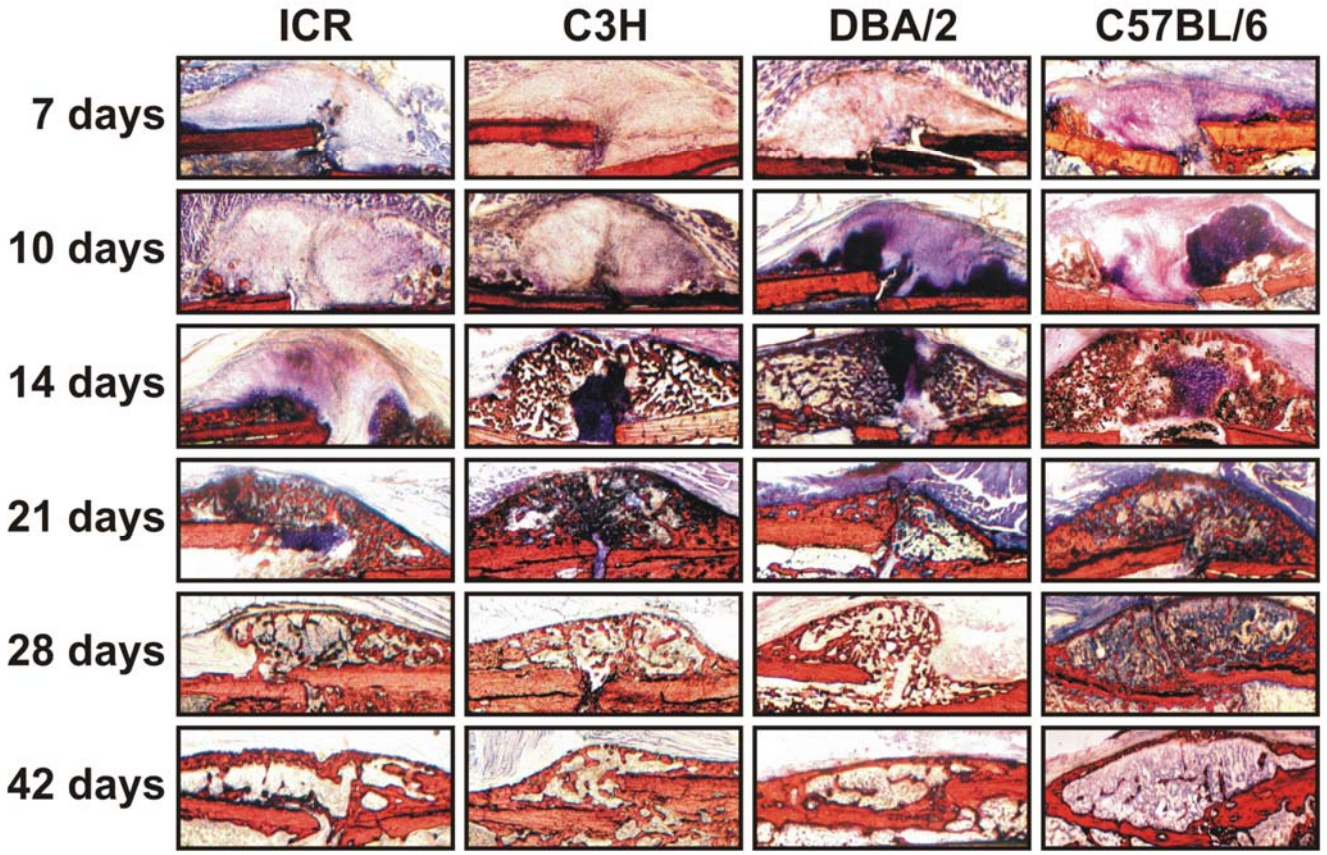

Figure 4.8. Histological Events of Fracture Healing in Inbred Mice. Fractured femurs were harvested at indicated time points and processed for calcified histology. Sections were stained with Stevenel's Blue and counter-stained with van Geison's Picro-fuchsin (bone is red; calcified cartilage is orange to red; cartilage is deep blue; soft tissues are lighter shades of blue. (7 days) A clearly defined callus was visual after seven days post-fracture. (10 days) By 10 days post-fracture, a large cartilage population was detected in all four mouse strains. (14 days) Calcified cartilage and endochondral ossification was evident in all three inbred strains, with C3H and C57BL/6 appeared to be bridged with new bone. However, the outbred ICR strain continued to lag behind. (21 days) The callus appeared bridged with bone in all four strains. Only the ICR strain appeared to still have a large population of cartilage. (28 days) Callus remodeling had begun by 28 days post-fracture in all four strains. (42 days) Remodeling continued through 42 days, with lamellar bone bridging the fracture site.

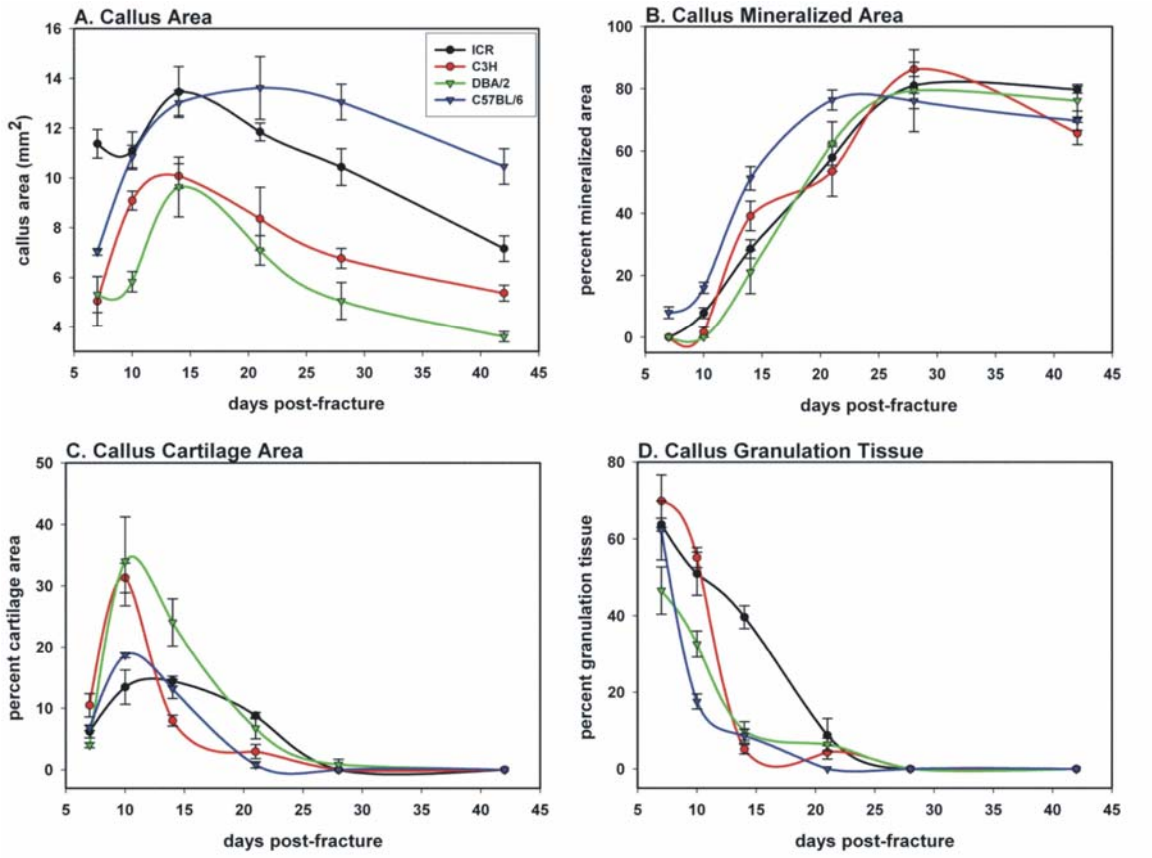

Figure 4.9. Histomorphometrical Measurements of Femur Fracture Healing in Different Inbred Mouse Strains. Callus area (A), percent callus mineralized area (B), percent callus cartilage area (C), and percent callus granulation tissue (D) were measured using samples prepared for histological analysis. Error bars represent standard errors. (A) Total callus area peaked at 14 days for the ICR, C3H and DBA/2 strains. Callus area peaked at 21 days for C57BL/6. Additionally, ICR and C57BL/6 had significantly greater areas at 14 days than either C3H ($p=0.006$ and $p=0.043$) or DBA/2 ($p=0.002$ and $p=0.012$). By 28 days, callus area had begun to decrease in size in all strains, suggesting remodeling had begun or was continuing. (B) At 7 days post-fracture, C57BL/6 had statistically greater values for mineralized tissue when compared against all other strains ($p < 0.001$). ICR and C3H had some mineralized tissue by 10 days. However, DBA/2 showed no measureable mineralized tissue until 14 days post-fracture. (C) Both C3H and DBA/2 had significantly more percent cartilage at 10 days post-fracture than either ICR ($p=0.009$ and $p =0.0021$) or C57BL/6 ($p<0.001$ and $p =0.013$). DBA/2 continued to have significantly greater cartilage values after 14 days post-fracture($p < 0.001$). (D) Granulation tissue was visible in all four strains between 7 to 14 days post-fracture. By 21 days post-fracture, C57BL/6 showed no further granulation tissue, while the other three strains still had some measurable values.

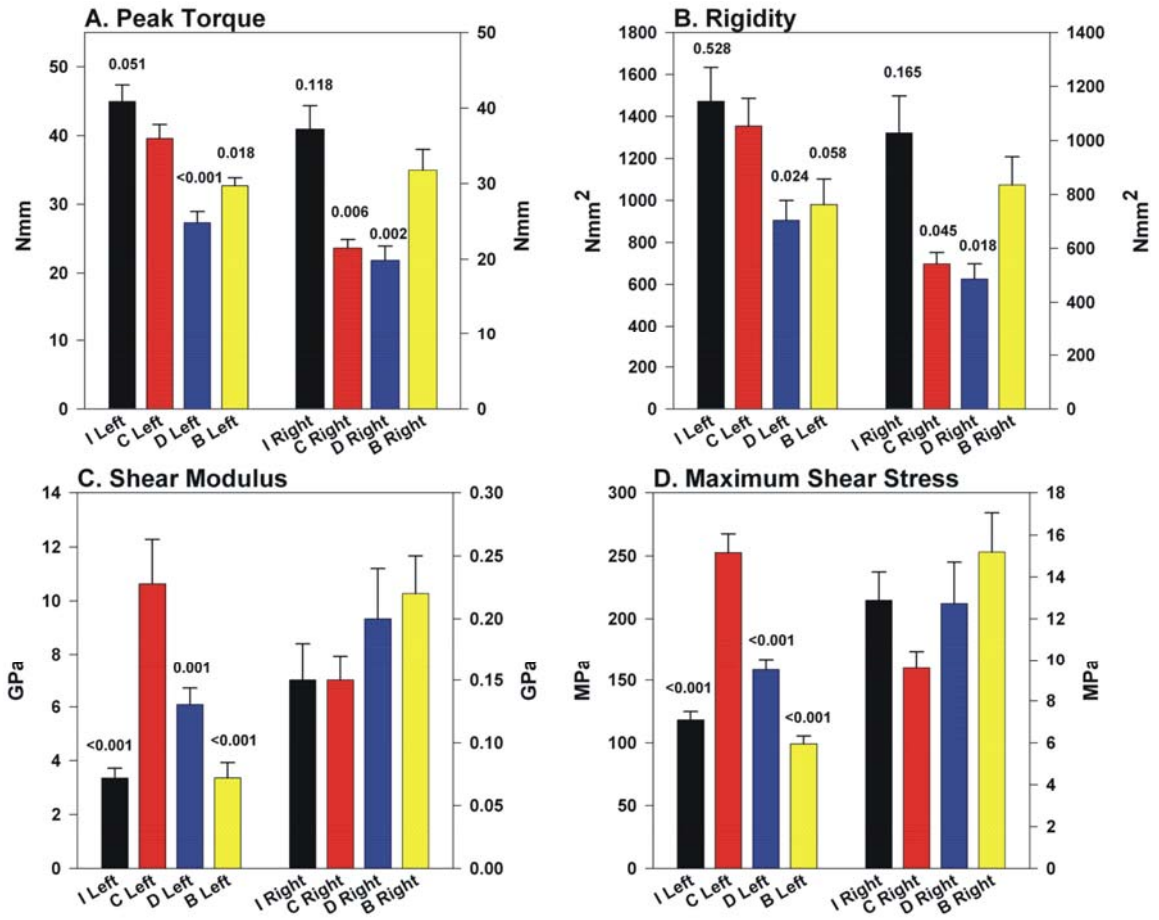

Figure 4.10. The Effects of Different Mouse Genetic Backgrounds on the Torsional Mechanical Testing Properties of Healing Femurs at 28 Days Post-Fracture. Fractured and contralateral femurs from ICR (n=13), C3H (n=11), DBA/2 (n=11) and C57BL/6 (n=11) mice were mechanically tested to failure in torsion after 28 days of healing. I=ICR; C= C3H; D= DBA/2; B= C57BL/6. Peak torque (A), rigidity (B), shear modulus (C), and maximum shear stress (D) were measured or calculated from bone dimensions, peak torque and angular displacement at failure at 28 days post-fracture for both the control (left) and fractured (right) femurs. Bars represent avg ± SEM. The structural properties (torque and rigidity) and material properties (shear modulus and shear stress) for the left femur show that a high bone mineral density results in significantly higher peak torque, rigidity, shear modulus and shear stress values. However, when comparing the right femur, the results suggest an inverse correlation, implying that having too high bone mineral density results in impaired fracture healing success.

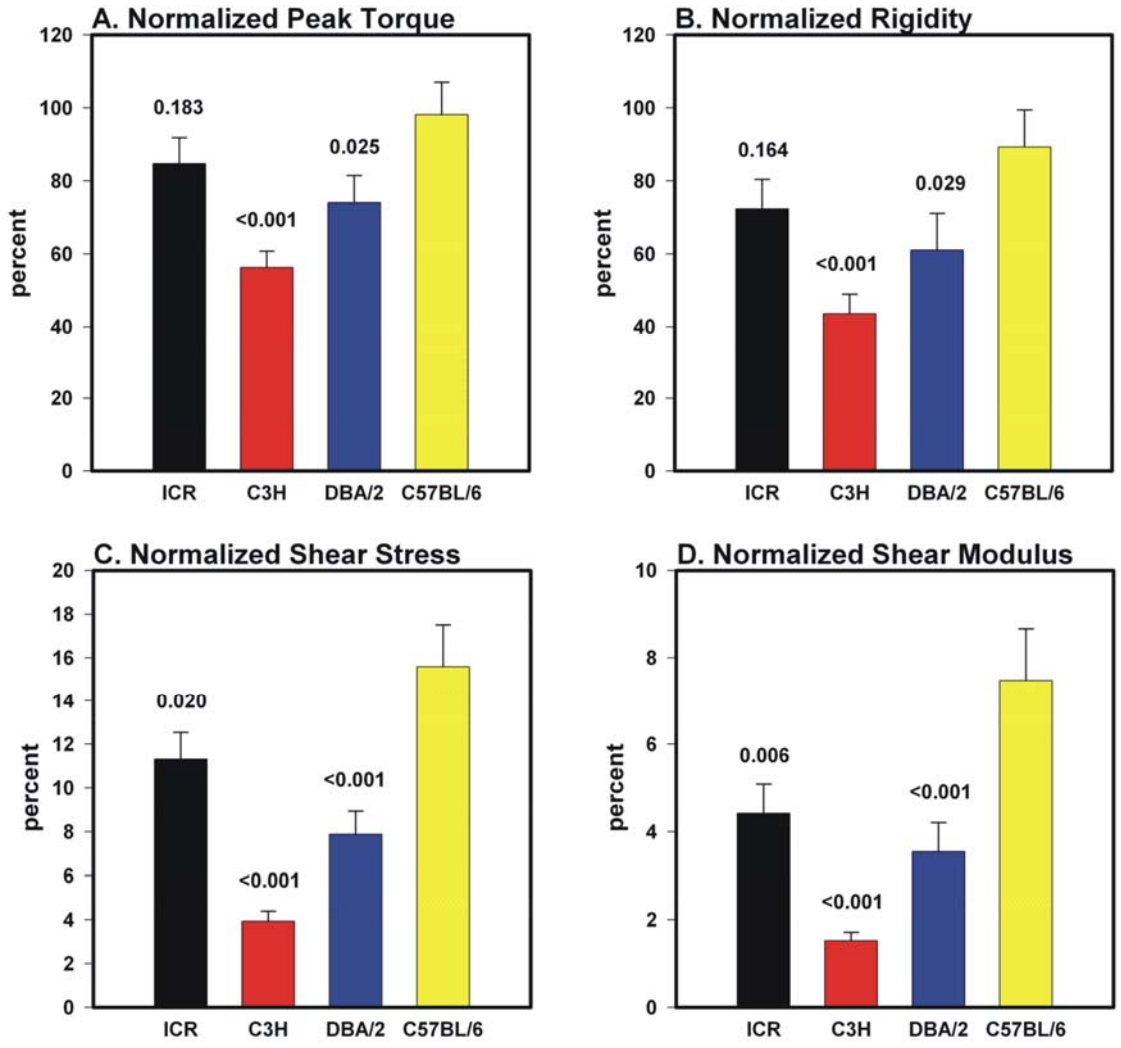

Figure 4.11. Mechanical Testing Properties of Healing Femurs from Different Strains of Inbred Mice at 28 Days After Fracture Normalized to Contralateral Control Femurs. Fractured and contralateral femurs from ICR (n=13), C3H (n=11), DBA/2 (n=11) and C57BL/6 (n=11) mice were mechanically tested to failure in torsion after 28 days of healing. I=ICR; C= C3H; D= DBA/2; B= C57BL/6. Peak torque (A), rigidity (B), shear modulus (C), and maximum shear stress (D) were measured or calculated from the peak torque and angular displacement curves generated during the testing procedure and the callus dimensions. Fractured femur values were normalized to the values from the contralateral femur of that mouse as a percentage. Bars represent avg ± SEM. Normalized values were compared between all strains at 28 days. All parameters were significantly higher in the C57BL/6 mice than either the DBA/2 or C3H mice after 28 days of healing.

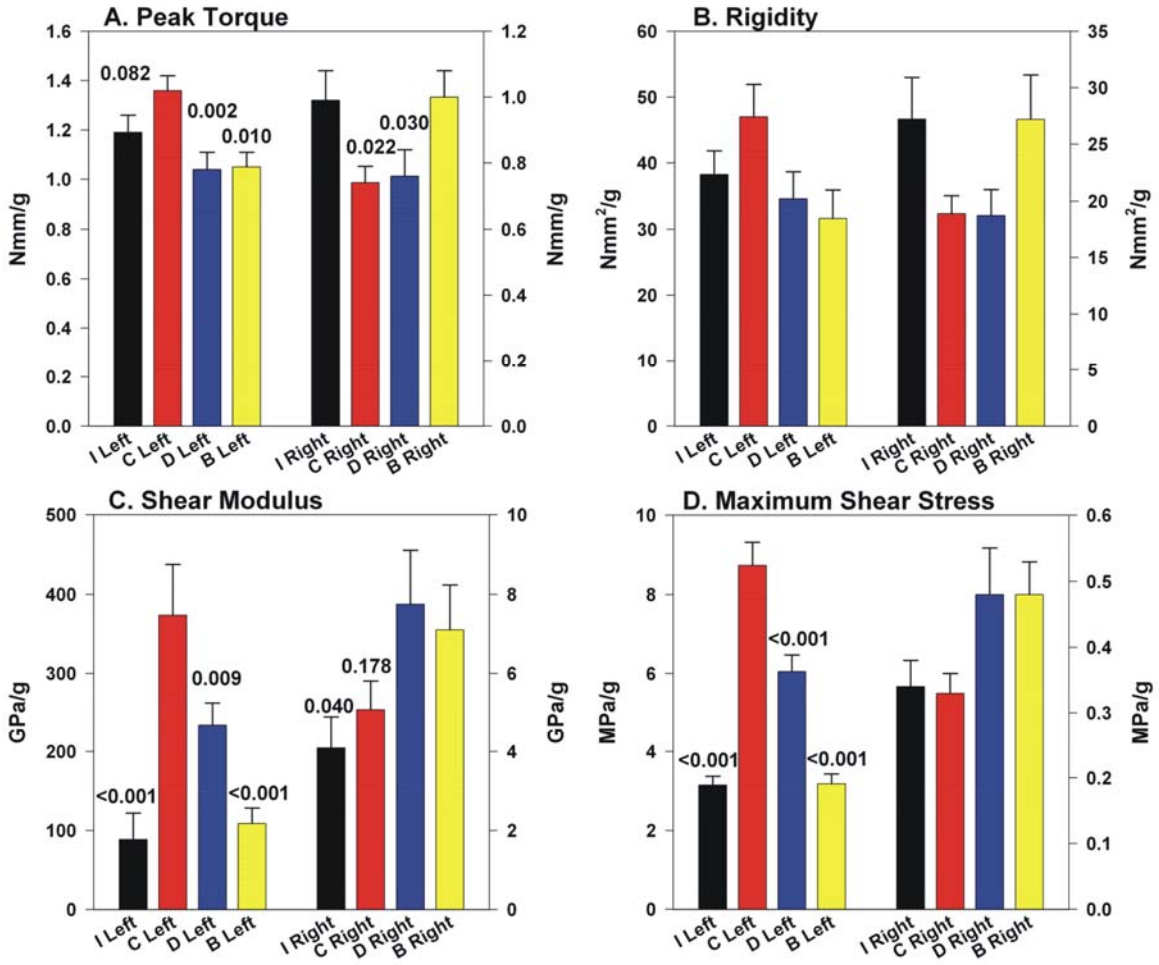

Figure 4.12. Mechanical Testing Properties of Healing Femurs from Different Strains of Inbred Mice at 28 Days After Fracture Normalized to Body Weight. Fractured and contralateral femurs from ICR (n=13), C3H (n=11), DBA/2 (n=11) and C57BL/6 (n=11) mice were mechanically tested to failure in torsion after 28 days of healing. I=ICR; C= C3H; D= DBA/2; B= C57BL/6. Peak torque (A), rigidity (B), shear modulus (C), and maximum shear stress (D) were measured or calculated from the peak torque and angular displacement curves generated during the testing procedure and the callus dimensions. Fractured femur values were normalized to the values from the weight (grams) of that mouse as a percentage. Bars represent avg ± SEM. Normalized values were compared between all strains at 28 days. C3H has significantly higher values when comparing the torsional properties of the left femur. This suggests that having a high bone mineral density results in higher mechanical properties for the left (control) femur for all parameters at 28 days. In contrast, comparing the right (fractured) femur among strains results in C57BL/6 having significantly higher structural properties than either C3H or DBA/2. Additional, the material properties of the DBA/2 show that, on a per gram basis, the DBA/2 mouse has significantly higher shear modulus values than C3H and comparable values to C57BL/6.

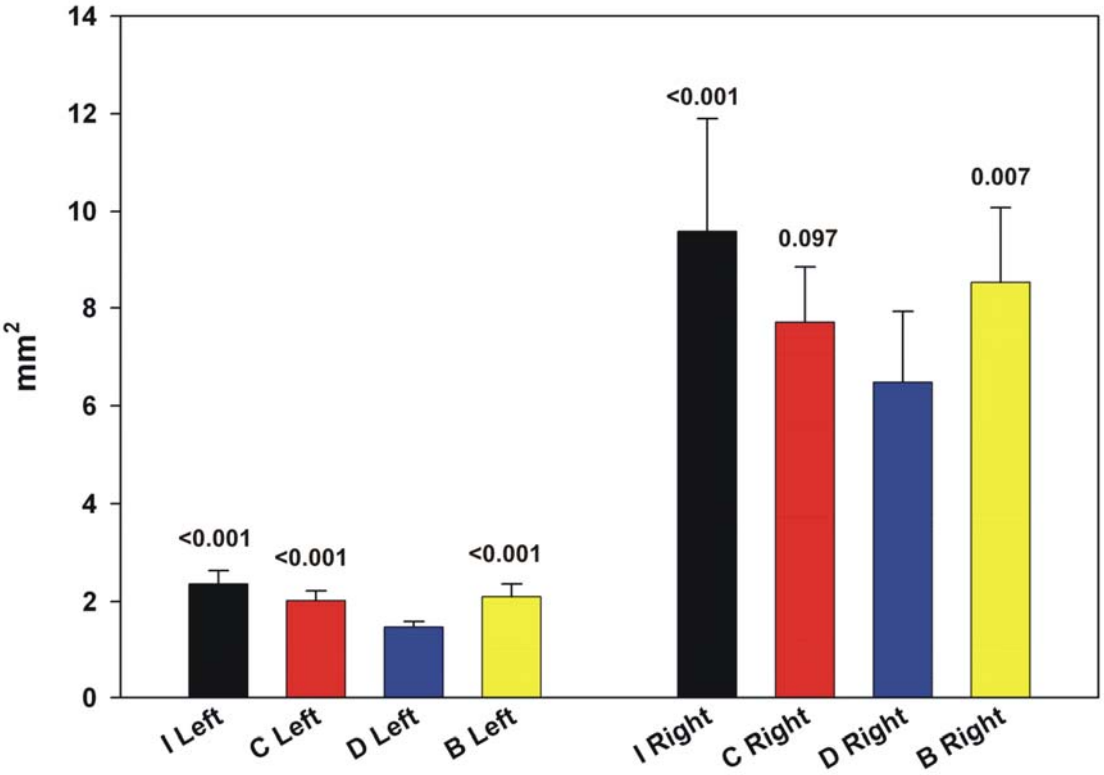

Figure 4.13. Cross-Sectional Area of the Contralateral (Left) and Fractured (Right) Femurs from Different Strains of Inbred Mice. Maximum and minimum cross-sectional dimensions were measured using electronic calipers and area was based on the solid ellipse model. I=ICR; C= C3H; D= DBA/2; B= C57BL/6. Bars represent avg ± SD. DBA/2 has a significantly less cross-sectional area than all other strains for control (left) femur and has a significantly less cross-sectional area than ICR or C57BL/6 fractured (right) femurs.

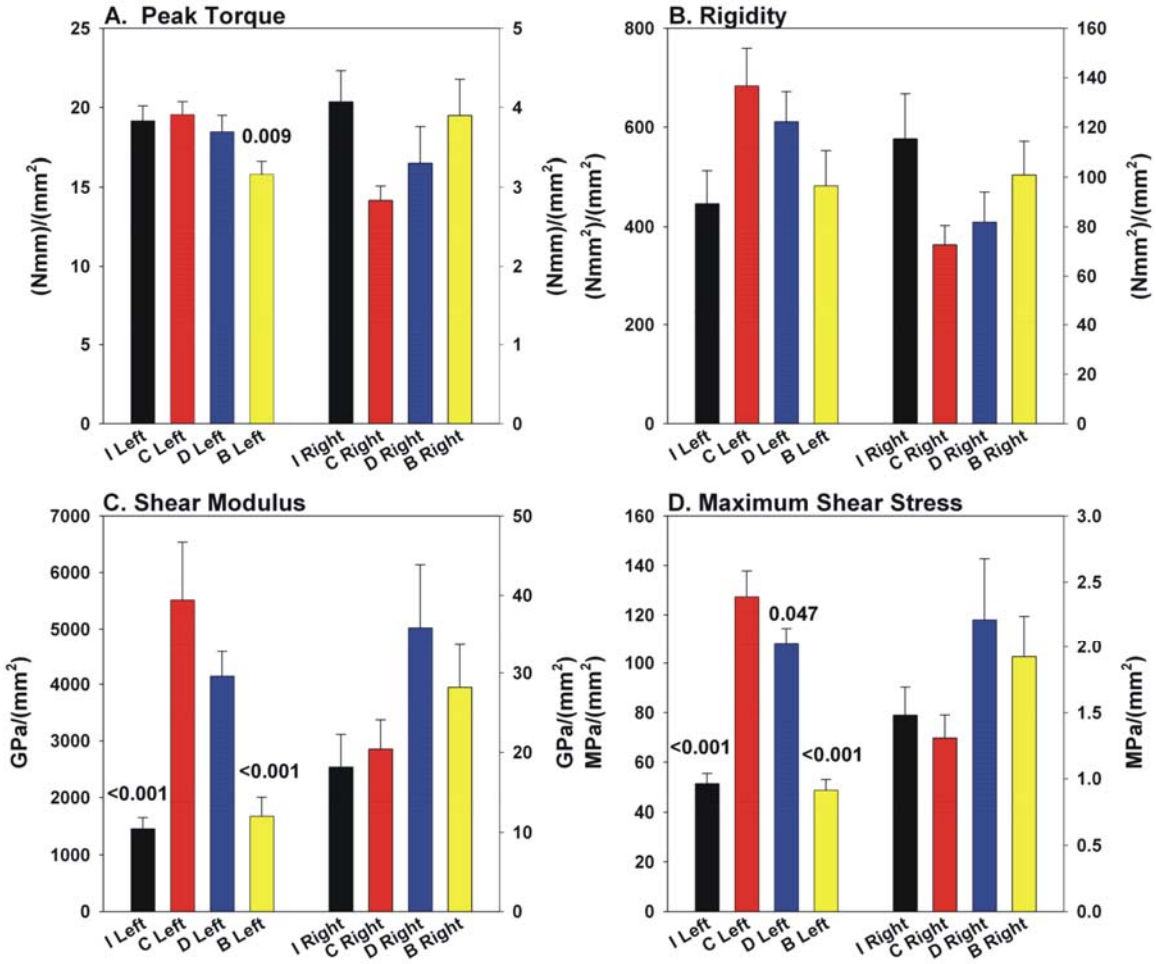

Figure 4.14. Mechanical Testing Properties of Healing Femurs from Different Strains of Inbred Mice at 28 Days After Fracture Normalized to Cross-Sectional Area. Fractured and contralateral femurs from ICR (n=13), C3H (n=11), DBA/2 (n=11) and C57BL/6 (n=11) mice were mechanically tested to failure in torsion after 28 days of healing. I=ICR; C= C3H; D= DBA/2; B= C57BL/6. Peak torque (A), rigidity (B), shear modulus (C), and maximum shear stress (D) were measured or calculated from the peak torque and angular displacement curves generated during the testing procedure and the callus dimensions. Fractured femur values were normalized to the values from the left or right femur cross-sectional area of that mouse as a percentage. Bars represent avg ± SEM.

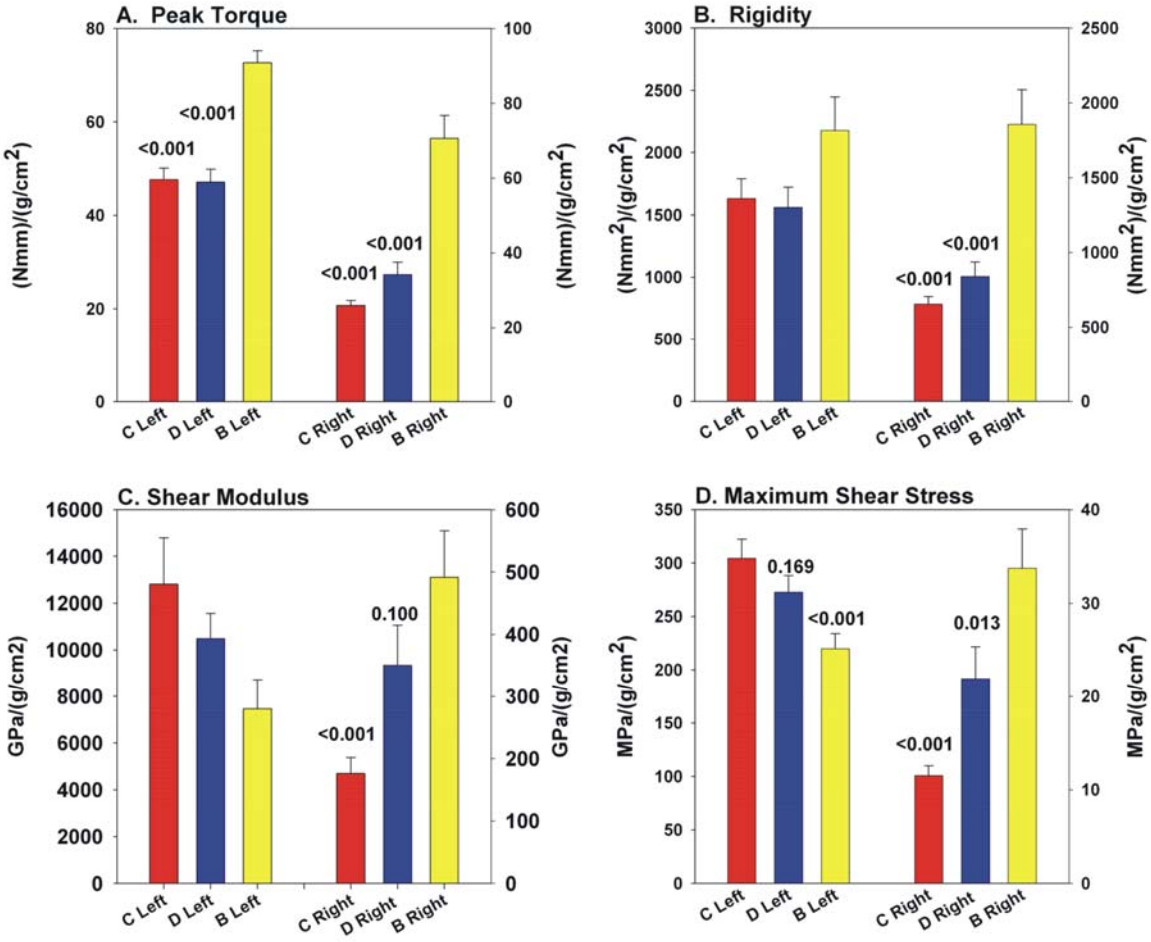

Figure 4.15. Mechanical Testing Properties of Healing Femurs from Different Strains of Inbred Mice at 28 Days After Fracture Normalized to Bone Mineral Density. Bone mineral density was used as the normalization parameter in analyzing peak torque, rigidity, shear modulus and shear stress. Bars represent avg ± SEM. Bone mineral density values used were from previously published work (Beamer *et al*., Bone 1996). C= C3H; D= DBA/2; B= C57BL/6. (Panel A) Normalized peak torque values for the three inbred strains show that C57BL/6 has significantly greater values than both DBA/2 and C3H for the left and right femur. (Panel B) Normalized rigidity values are also significantly higher in the C57BL/6 than in the DBA/2 or C3H. This is consistent with the larger geometric properties seen in the C57BL/6 femurs. (Panels C and D) The material properties, shear modulus and shear stress, are shown to be directly proportional to the bone mineral density levels in the unfractured left femur. However, these values become inversely proportional in the fractured leg. This suggests that having a high bone mineral density inhibits fracture healing.

4.3.0 The Role of Cyclooxygenase in Fracture Healing

4.3.1 Disposition of COX Deficient Mice Used in This Study

Female Cox2-KO, Cox-2HET, Cox-2WT and Cox-1KO mice weighing 21.7 ± 2.2, 24.7 ± 2.9, 22.4 ± 2.2 and 23.6 ± 3.2 grams, respectively, were used in this experiment. All animals used in these experiments were bred and maintained in the Center for Comparative Medicine Resources at UMDNJ. All animals were 10-12 weeks old at the beginning of the study. All experimental procedures were approved by the New Jersey Medical School Institutional Animal Care and Use Committee. Of the 312 mice used in this study, 204 were ultimately included in the radiographic, histologic, histomorphometric, and mechanical analyses. A more detailed disposition of the mice used in this study may be found in Table 4.5.

Table 4.5. Disposition of the 312 COX Deficient and Wild-Type Mice Used in This Study.

	Surgical Errors			Other		Mechanical Testing			Histology	
	Anesthesia Death	Fracture Destabilization	Poor Fracture	Non-Unions	Died Prematurely	Potting Errors	User Errors	Total Analyzed	Poor Slide	Total Used
Cox-1KO	2	0	1	3	4	8	1	24	8	26
Cox-2KO	7	1	0	0	8	0	0	17	6	27
Cox-2HET	6	1	3	0	1	12	2	24	19	38
Cox-2WT	3	0	1	0	1	3	0	19	7	29

Additionally, 3 Cox1-KO animals could not be mechanically tested because they were non-unions at harvest and could not be potted. A total of 14 animals died before reaching a time point (Cox-2KO:8; Cox-2HET:1; Cox-2WT:1;

Cox-1KO:4). Therefore, these animals could not be used in any analysis for these experiments. Animals were able to bear weight on their hind legs within a few hours after surgery and no significant decrease in weight over time was noted (Table 4.6).

Table 4.6. Average Pre-Surgical and Post-Sacrifice Weights of COX Deficient and Wild-Type Mice.

Strain	Time Point	n	Pre-Surgical Weight in Grams (Mean ± SD)	Post-Sacrifice Weight in Grams (Mean ± SD)
Cox-1KO	7 Days	4	24.5 ± 1.0	24.5 ± 1.0
	10 Days	4	23.0 ± 1.2	24.0 ± 0.0
	14 Days	9	22.9 ± 2.7	23.1 ± 2.3
	21 Days	4	19.5 ± 1.0	20.5 ± 1.0
	28 Days	20	24.6 ± 3.6	26.3 ± 4.0
	42 Days	4	26.5 ± 1.0	28.5 ± 1.0
	84 Days	22	24.5 ± 1.8	26.9 ± 2.0
Cox-2WT	7 Days	6	24.4 ± 1.7	24.4 ± 1.7
	10 Days	3	24.0 ± 0.0	24.7 ± 1.2
	14 Days	8	21.5 ± 2.6	22.0 ± 2.8
	21 Days	4	21.0 ± 1.2	22.0 ± 1.6
	28 Days	16	22.4 ± 2.0	24.6 ± 1.7
	42 Days	4	21.5 ± 1.9	22.0 ± 2.3
	84 Days	15	22.7 ± 2.4	24.9 ± 2.5
Cox-2HET	7 Days	6	23.7 ± 1.5	24.0 ± 1.3
	10 Days	7	23.0 ± 1.2	23.0 ± 1.2
	14 Days	18	21.8 ± 1.8	22.3 ± 1.7
	21 Days	4	24.5 ± 1.0	25.5 ± 1.0
	28 Days	26	24.0 ± 2.7	24.8 ± 3.2
	42 Days	6	22.3 ± 2.3	24.0 ± 2.2
	84 Days	43	24.7 ± 2.9	26.2 ± 2.3
Cox-2KO	7 Days	5	21.2 ± 2.3	21.2 ± 2.3
	10 Days	5	20.8 ± 1.1	21.2 ± 1.1
	14 Days	5	21.6 ± 0.9	22.0 ± 0.0
	21 Days	4	20.7 ± 2.3	21.3 ± 1.2
	28 Days	13	21.2 ± 2.1	21.8 ± 1.7
	42 Days	4	22.5 ± 1.9	24.0 ± 1.6
	84 Days	16	22.5 ± 2.8	23.8 ± 2.2

4.3.2 Radiography of COX Deficient Mice

All animals were radiographed immediately post-fracture to verify the placement of a mid-diaphyseal fracture and post-sacrifice to confirm constant pin stabilization. In addition, a subset of animals from each strain was radiographed at 7, 10, 14, 21, 28, and 84 days post-fracture for serial radiographical comparison of fracture healing. Radiography clearly showed the importance of COX-2 on fracture healing. While Cox-1KO, Cox-2HET and Cox-2WT all showed a similar temporal pattern of healing from 7 to 84 days, fracture healing in Cox-2KO mice appeared to severely lag behind (Figure 4.15). At 7 days, all groups had similar radiographic findings of a clear transverse femoral fracture. After 10 days, the fractures in the Cox-1KO, Cox-2HET and Cox-2WT animals showed signs of periosteal lifting around the fracture edges. However, the fractures in the Cox-2KO animals showed little callus formation by this time. Robust callus was detected in the Cox-1KO, Cox-2HET and Cox-2WT at 14 days, but the Cox-2KO still showed very little callus formation. By 21 days post-fracture, the fractures in the Cox-1KO, Cox-2HET and Cox-2WT mice appeared fully bridged. Initial observations of the Cox-2KO fracture callus would suggest that these calluses were also bridged. However, upon closer inspection, a faint radio-opaque line down the center of the callus was detected. This line represents the front edge and back edge of the callus overlapping. Remodeling of the fracture callus was evident in all mouse genotypes by 28 days after fracture. Remodeling continued through 84 days post-fracture when the experiment was terminated.

4.3.3 Calcified Histology of COX Deficient Mouse Femurs

Histological analysis was evaluated at 7, 10, 14, 21, 28, 42 and 84 days post-fracture (Figure 4.16). Fracture healing followed a similar histological pattern in the Cox-1KO, Cox-2HET and Cox-2WT mice. At 7 days, a definitive fracture callus was evident with cartilage and other cells invading the area. At 10 days, endochondral ossification was visible, along with continued cartilage formation. By 14 days, a small amount of cartilage remained in the fracture callus. However, mineralized cartilage was abundant. After 21 days of healing, any cartilage remaining was replaced completely by mineralized tissue. Furthermore, the femur fractures in all three of these strains were bridged by 21 days. By 28 days, remodeling of the fracture callus had begun in the Cox-1KO, Cox-2HET and Cox-2WT animals. Subsequent remodeling continued from 42 through 84 days post-fracture, as the fracture callus for these three strains began to reshape itself back to its original dimensions.

In contrast, the Cox-2KO fracture callus showed vastly different results (Figure 4.16). At 7 days, fracture callus borders were clearly defined, although it did appear smaller in size compared to the other three strains. By 10 days, only a small amount of cartilage that stained with Stevenel's Blue appeared on the periphery of the fracture callus along with an abundance of fibrous tissue in the center of the callus. By 14 days, cartilage formation appeared to have halted in this strain, leaving a fibrous mass in the center of the callus, surrounded by the beginning of mineralizing bone. This was further exaggerated by 21 days post-fracture, when a huge mass of fibrotic tissue was still clearly present in the center

of the callus. Without clearly bridging the fracture gap, the fracture callus appeared to begin remodeling at 28 days and continued through 84 days post-fracture.

4.3.4 Histomorphometry of COX Deficient Mouse Femurs

The histomorphometry measurements confirmed the conclusions seen in the histological observations. Histology and histomorphometry clearly showed the importance of COX-2 on fracture repair. Callus area peaked at 14 days post-fracture for Cox-1KO and Cox-2WT mice and at 21 days for Cox-2Het and Cox-2KO mice (Figure 4.17-Panel A). At 7 days post-fracture, Cox1-KO, Cox2-HET and Cox-2WT fractures all had similar percentages of mineralized area, while Cox-2KO fractures had no measurable quantities (Figure 4.17-Panel B). Also, the Cox-2KO callus had very little cartilage present and a statistically greater percentage of granulation tissue (%GT) than Cox-1KO, Cox-2HET and Cox-2WT fractures. Cox-2HET fractures had the largest percentage of cartilage area, peaking at almost 22% of the callus area (Figure 4.17- Panel C).

At 10 days post-fracture, one Cox-2KO fracture slide had a measurable percentage of mineralized area and the percentage of cartilage area (%CA) increased from approximately 3% at 7 days to 11% at 10 days post-fracture in these animals. However, this was the highest the cartilage percentage ever reached and the majority of the callus area was still largely granulation tissue. In contrast, almost a quarter of the callus was filled with newly mineralized tissue in the Cox-1KO animals by 10 days post-fracture (Figure 4.17- Panel B). Cox-1KO

fracture calluses also saw the percentage of cartilage area increased from about 6.5% to almost 18% in three days. Additionally, the %GT decreased from 47% at 7 days to 31% at 10 days. The Cox-2Het and Cox-2WT animals also had significant increases in the percentage of mineralized tissue in their calluses from 7 to 10 days post fracture, going from 7% and 8% to about 18% and 21%, respectively. The percentage of cartilage area increased 50% or more from 7 to 10 days in the Cox-2Het and Cox-2WT animals (Figure 4.17-Panel C). Similar to Cox-1KO, granulation tissue in the Cox-2HET animals fractures were roughly one-third of the callus area. Cox-2WT animals had significantly less granulation tissue in their calluses at 10 days than all other strains (Figure 6.3, Panel B).

By 14 days post-fracture, Cox-2KO animals began to show significant increases in the percentage of new mineralized area, but was still significantly less than all other strains compared (Figure 4.17-Panel B). The fractures of Cox-1KO, Cox-2HET and Cox-2WT mice had %MA values from 40% to 50% compared to the fractures of Cox-2KO value of 27%. Also, a large portion of the Cox-2KO callus was still filled with granulation tissue, comprising roughly one-third of the callus. In contrast, the fractures of Cox-1KO, Cox2-Het and Cox-2WT %GT values had decreased to about 11%, 14% and 8%, respectively. The percentage of cartilage in the callus at 14 days was highest in the Cox-1KO animals at 15% (Figure 4.17- Panel C).

At 21 days post-fracture, Cox-1KO and Cox-2WT fractures no longer had measurable cartilage or granulation tissue in the fracture callus. Of the Cox-2HET specimens, one had some remaining granulation tissue in the callus,

however this was negligible. Cox-1KO, Cox-2HET and Cox-2WT animals had between 62 and 72% of the callus area filled with mineralized tissue compared to 49% for Cox-2KO. Cox-2KO still had almost 17% of the callus area filled with granulation tissue and a small amount of cartilage present (Figure 4.17- Panel D).

By 28 days post-fracture, the %MA in Cox-1KO, Cox-2HET and Cox-2WT fracture calluses decreased, signifying that remodeling had begun. In contrast, the Cox-2KO callus %MA was still increasing and filled with about 12% of granulation tissue. At 42 days, callus %MA still decreased in the Cox-1KO and Cox2-WT animals, while slightly increasing in both the Cox-2KO and Cox-2HET animals. Granulation tissue was still present in some of the Cox-2KO animal fractures. By 84 days post-fracture, only mineralized tissue was seen in the calluses of all strains. Similar to the histology examined, remodeling was present in all strains.

4.3.5 Mechanical Testing of COX Deficient Mouse Femurs

Mechanical properties were evaluated at two time points, 28 and 84 days post fracture. The results are summarized in Figure 4.18. As can be seen, the Cox-2KO mice had significantly lower structural (peak torque, rigidity) and material properties (shear modulus and maximum shear stress) at 28 days than Cox-2HET, Cox-2WT and Cox-1KO mice. However, by 84 days post fracture, the Cox-2KO animals regain some structural properties compared to those values of the other groups. Material properties reflected similar results. Shear

modulus and maximum shear stress values were similar in the Cox-1KO, Cox-2HET and Cox-2WT animals at 28 days. However, the Cox-2KO mice showed significantly less material property values at this time point. After 84 days of healing, the material properties in all experimental strains and genotypes increased. However, Cox-2KO animals still had significantly less values when compared to the other three groups. This signifies an immaturity in the new bone's material properties of the Cox-2KO mouse.

Of interest was the high average shear modulus value the Cox-1KO mice reached. It should be addressed that ONLY femurs collected without incident were used and if the specimen could be successfully potted, it was torsionally tested. This may lead to skewing of the data as the Cox-1KO group had three animals out of a possible 36 animals excluded due to non-unions. In essence, only the best healed animals were tested for the Cox-1KO group which may have lead to uncharacteristically high values for the mechanical testing parameters obtained for this group.

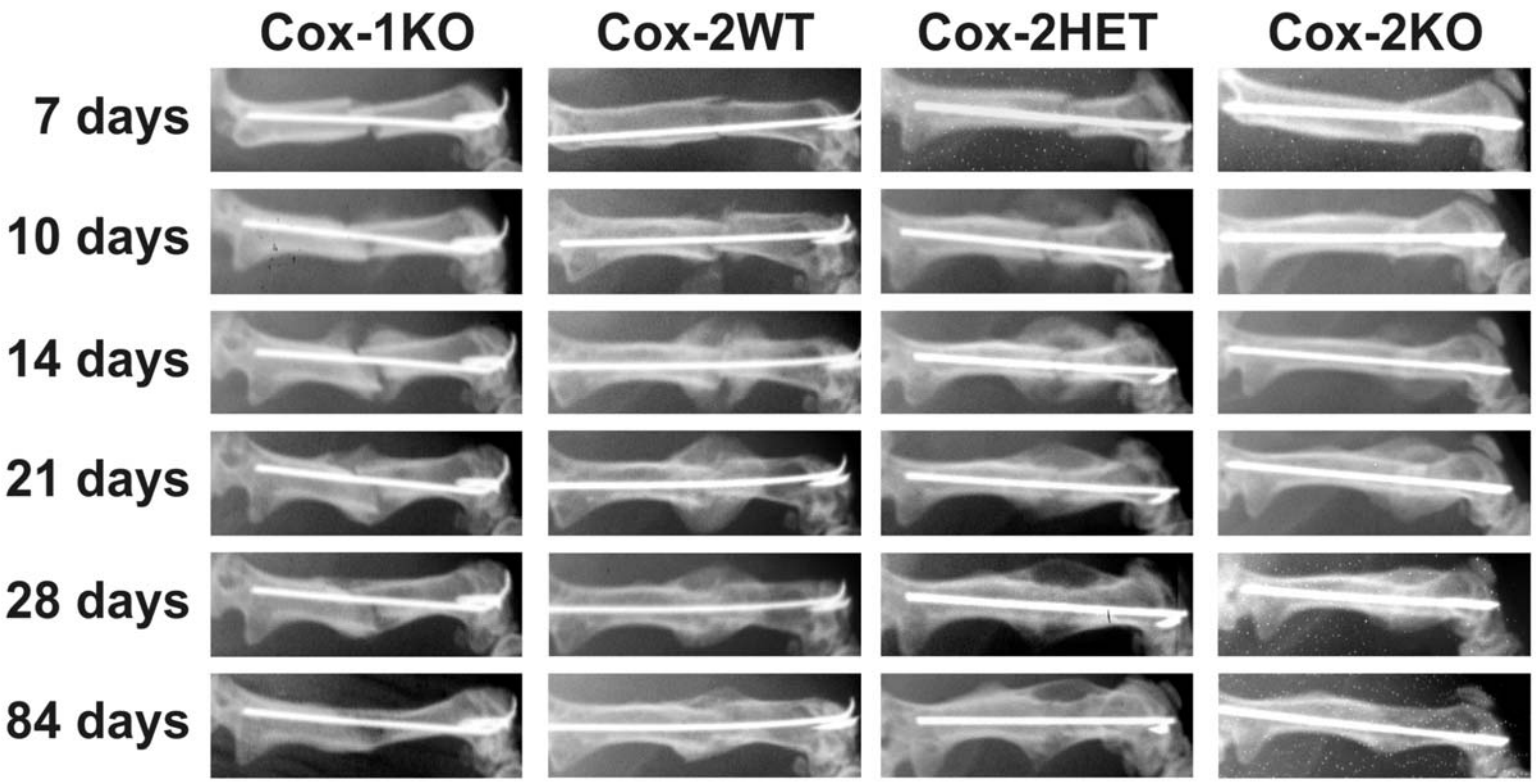

Figure 4.16. Radiographic Assessment of Fracture Repair in COX Deficient Mice. Serial radiographs of healing femur fractures from a representative mouse of each genotype are shown to illustrate healing. Dorsal-ventral radiographs of the fractured femurs were taken at 7, 10, 14, 21, 28, and 84 days post-fracture. (7 days) Mid-diaphyseal fractures were observed in all four genotypes. (10 days) Periosteal lifting was visible at the fracture site. (14 days) A clearly defined callus was observed in the Cox-1KO, Cox-2WT and Cox-2HET phenotypes. However, the Cox-2KO callus was less visible and appeared smaller. (21 days) Callus bridging occurred by 21 days post-fracture in the Cox-1KO, Cox-2WT and Cox-2HET. While initial inspection of radiography in the Cox-2KO callus suggested it was bridged, the radio-lucent line visible indicates invagination of fibrous tissue into the fracture callus. (28 days) Smaller fracture calluses were noted suggesting that remodeling of the fracture callus had begun. (84 days) Remodeling of the fracture callus continued in all genotypes.

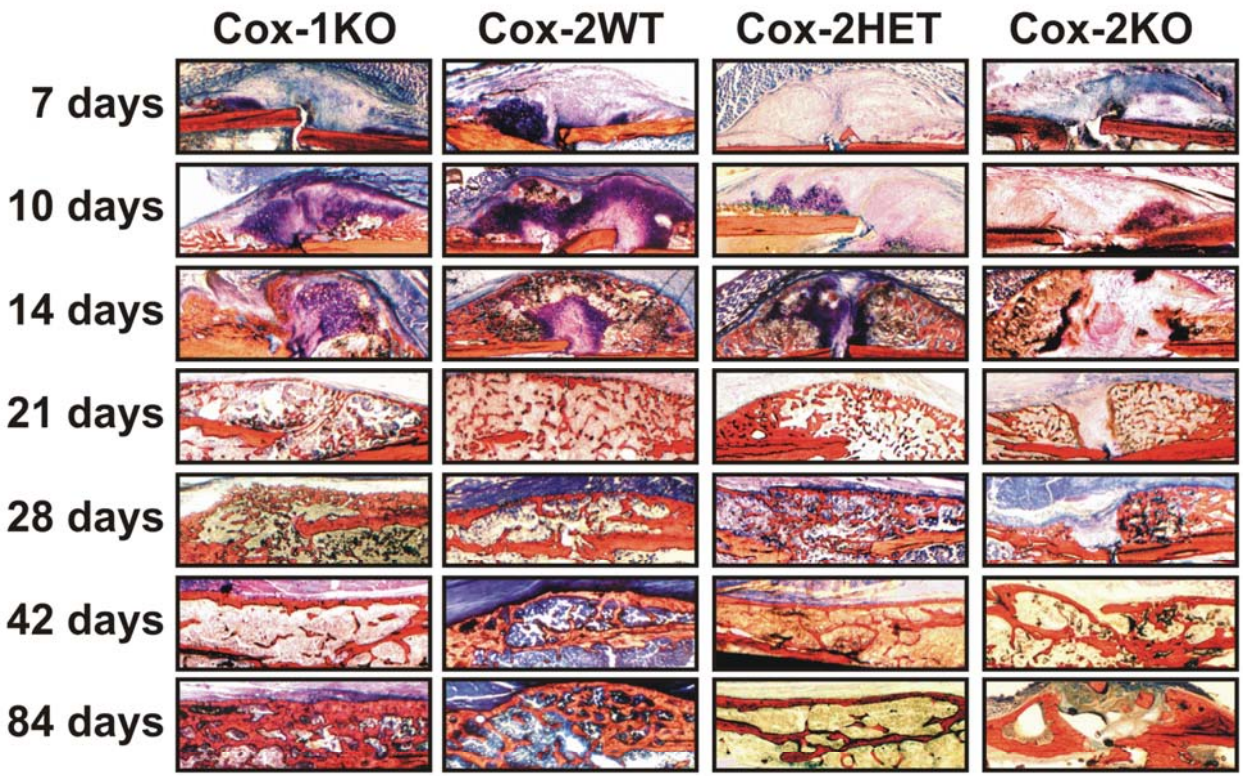

Figure 4.17. Histology of Fracture Healing in Cox Deficient Mice. Fractured femurs were harvested at indicated time points and processed for calcified histology. Sections were stained with Stevenel's blue and counter-stained with van Geison's picro-fuchsin (bone is red; calcified cartilage is orange to red; cartilage is deep blue; soft tissues are lighter shades of blue). A clearly defined callus is evident in all mouse strains. Visually, the Cox-2KO fracture callus appears smaller and a less defined than the Cox-1KO, Cox-2HET and Cox2-WT fractures. By 10 days post-fracture, cartilage had spread throughout the Cox-1KO and Cox-2WT fractures. Smaller amounts of cartilage were detected in the Cox-2HET and Cox-2KO fractures. Fracture callus bridging was seen by 14 days post-fracture in the Cox-1KO and Cox-2WT mice. Bridging was almost complete in the Cox-2HET callus, but was incomplete in the Cox-2KO fracture. Additionally, the Cox-2KO callus was still filled with large amounts of fibrotic tissue and immature chondrocytes. The calluses of the Cox-1KO, Cox-2WT and Cox-2HET had no visual cartilage left by 21 days post-fracture. In constrast, the Cox-2KO fractures were not bridged and contained a large mass of fibrous tissue. Remodeling had begun in the Cox-1KO, Cox-2WT and Cox-2HET fractures by 28 days and continued through 84 days. However, the Cox-2KO fractures began to collapse down and degrade before ever bridging the fracture site. This continued through 84 days post-fracture, when clear gaps of bone were present at the fracture site.

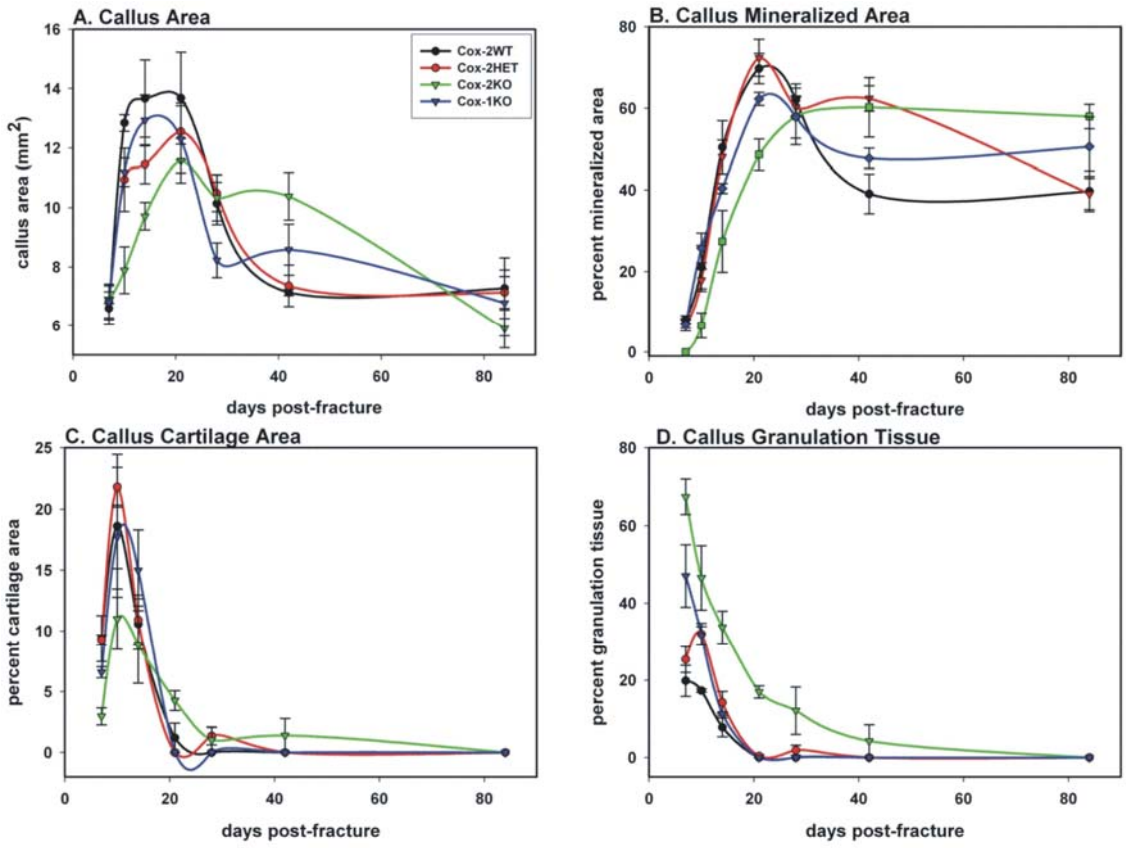

Figure 4.18. Histomorphometric Analysis of Fracture Healing in COX Deficient Mice. Callus area (A), percent mineralized area (B), percent cartilage area (C), and percent fibrous tissue (D) were measured from histological sections. While granulation tissue comprised the largest percentage of area in all four strains at 7 days, some cartilage was also present. Unlike Cox-1KO, Cox-2HET and Cox-2WT, mineralized tissue was not found in the calluses of Cox-2KO animals at 7 days. While cartilage and mineralized tissue had rapidly begun to replace granulation tissue in the COX-1KO, COX-2HET and COX-2WT fracture calluses at 10 days post-fracture, Cox-2KO fracture calluses still had the majority of their callus area as granulation tissue. By 14 days post-fracture, most of the Cox-1KO, Cox-2HET and Cox-2WT calluses were filled with mineralized tissue. However, the Cox-2KO fractures still had an abundance of granulation tissue present. By 21 days post-fracture, no granulation tissue was found in the Cox-1KO, Cox-2HET or Cox-2WT. However, the Cox-2KO still had almost 20% of its callus filled with granulation tissue. Trace cartilage levels were found in Cox-2HET and Cox-2WT, while approximately 5% of cartilage was found in Cox-2KO at this time point.

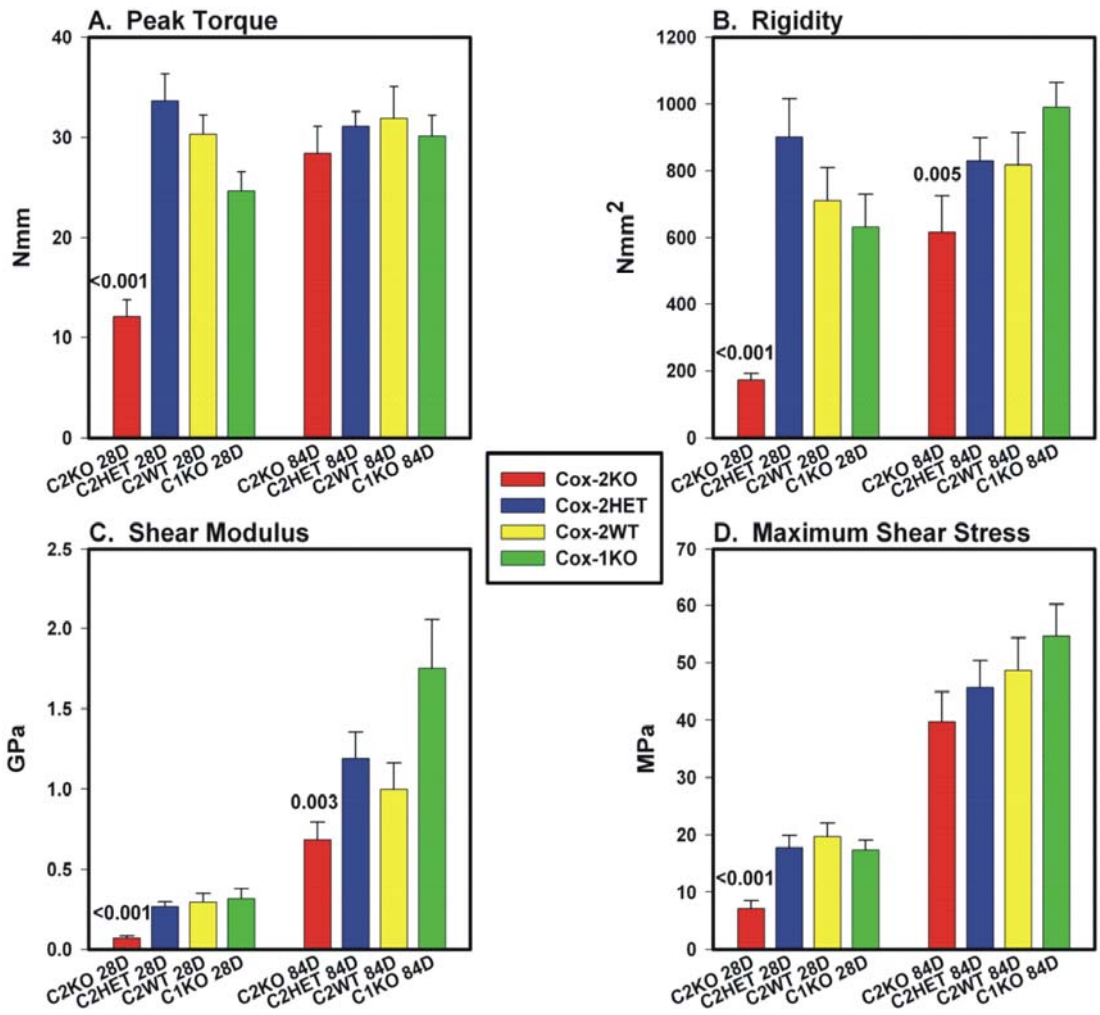

Figure 4.19. Mechanical Testing Properties of COX Deficient Mice at 28 and 84 Days Post-Fracture. Fractured and contralateral femurs from Cox-2KO (28 days n= 9, 84 days n= 8)Cox-2HET (28 days n=10, 84 days n=14), Cox-2WT (28 days n=9, 84 days n=10), and Cox-1KO (28 days n=11, 84 days n=13) were harvested and prepared for mechanical testing at 28 and 84 days post-fracture. Peak torque (A), rigidity (B), shear modulus (C), and maximum shear stress (D) were measured or calculated from bone dimensions, peak torque and angular displacement curves at 28 and 84 days post-fracture for the control and fractured femurs. Bars represent avg ± SEM. As shown, the structural properties, peak torque and rigidity, were significantly higher in Cox-2HET, Cox-2WT and Cox-1KO animals compared to Cox-2KO values at 28 days. While an increase in Cox-2KO structural values was found by 84 days, they were still significantly less than the other 3 strains. Similarly, the material properties of the Cox-1KO, Cox-2HET and Cox-2WT animals were all similar at 28 days, with Cox-2KO values significantly less. Increases of values were found in all strains at 84 days. However, Cox-2KO mice have a significantly less shear modulus and a decreased shear stress compared to the other groups. This is indicative of immature bone at the fracture site.

4.4.0 The Role of 5-Lipoxygenase (5-LO) in Fracture Healing

4.4.1 Disposition of 5-LO Deficient Mice Used in This Study

Female 5-LOKO (bred in house) and C57BL/6 (WT) animals (Jackson Laboratory, Bar Harbor, ME) weighing 20.0 ± 1.5, and 19.4 ± 1.3 grams, respectively, were used in this experiment. All animals were 10-12 weeks old at the beginning of the study. All experimental procedures were approved by the New Jersey Medical School Institutional Animal Care and Use Committee. Of the 168 mice used in this study, 140 were ultimately included in the radiographic, histologic, histomorphometric, eicosanoid and mechanical analyses. A more detailed disposition of the mice used in this study may be found in Table 4.7.

Table 4.7. Disposition of the 168 5-LO Deficient and Wild-Type Mice Used in the Study.

	Surgical Errors			Mechanical Testing			Histology		Eicos. Levels
	Anesthesia Death	Fracture Destabilization	Poor Fracture	Potting Errors	User Errors	Total Analyzed	Poor Slide	Total Used	Total Used
5-LOKO	5	0	0	3	1	19	6	23	6
WT	1	0	0	4	0	22	7	34	6
Cox-1KO	0	0	0	NA	NA	NA	NA	NA	4
Cox-1KO(Rx)[a]	1	0	0	NA	NA	NA	NA	NA	3
Cox-2WT	0	0	0	NA	NA	NA	NA	NA	6
Cox-2HET	0	0	0	NA	NA	NA	NA	NA	6
Cox-2KO	0	0	0	NA	NA	NA	NA	NA	6
Cox2-KO(Rx)[b]	0	0	0	NA	NA	NA	NA	NA	5

a = treated with 30 mg/kg of rofecoxib; b= treated with 30 mg/kg of SC-560

Animals were able to bear weight on their hind legs within a few hours after surgery and no significant decrease in weight over time was noted (Table 4.8).

Table 4.8. Average Pre-Surgical and Post-Sacrifice Weights of 5-LO and WT Mice.

Strain	Time Point	n	Pre-Surgical Weight in Grams (Mean ± SD)	Post-Sacrifice Weight in Grams (Mean ± SD)
5-LOKO	7 Days	7	20.6 ± 1.0	20.3 ± 0.8
	10 Days	12	20.7 ± 1.3	20.8 ± 1.3
	14 Days	7	21.1 ± 1.1	21.4 ± 1.5
	21 Days	5	21.2 ± 1.1	21.2 ± 1.1
	28 Days	13	18.8 ± 1.0	20.6 ± 2.2
	84 Days	8	18.9 ± 1.0	21.3 ± 1.0
WT	7 Days	6	21.0 ± 1.1	21.3 ± 1.0
	10 Days	7	18.6 ± 1.0	20.0 ± 0.0
	14 Days	21	19.2 ± 1.4	19.8 ± 0.9
	21 Days	8	20.5 ± 1.4	21.3 ± 1.0
	28 Days	12	18.8 ± 1.0	19.3 ± 1.0
	84 Days	14	19.3 ± 1.0	21.4 ± 1.2

4.4.2 Radiography of 5-LO Deficient Mice

All animals were radiographed immediately post-fracture to validate the placement of a mid-diaphyseal fracture and post-sacrifice to confirm pin stabilization. In addition, a subset of animals from each group was radiographed at 7, 10, 14, 21 and 28 days post-fracture for serial radiographical comparison of fracture healing (Figure 4.19). The 5-LOKO mouse showed a mineralized callus at the periphery of the fracture site by 7 days post fracture as compared to 10 days in the control mice. At 10 days post-fracture, a large mineralized callus was apparent in the 5-LOKO similar in appearance to the 14 day post-fracture callus

of the control mice. Fracture bridging with new bone was apparent by 14 days after fracture in the 5-LOKO mice but not until 21 days post-fracture in the control mice. After 28 days, the reduced size of the 5-LOKO callus suggested bone remodeling had occurred as compared to the equivalent time in the control fracture callus. This series of radiographs suggests that 5-LOKO mice have accelerated fracture healing.

4.4.3 Calcified Histology of 5-LO Deficient Mouse Femurs

Histological analysis further supports the radiographic findings, as the 5-LOKO fracture calluses appear to have more abundant cartilage formation at 7 days. Furthermore, there was visually more mineralized tissue by 10 days, callus bridging by 14 days and substantial remodeling by 21 days, as compared to the same time points in WT animals (Figure 4.20).

To see if this increased fracture healing was due to an increased response in the endochondral ossification process or by potentially a different mechanism; higher magnification histology at 7 days post-fracture was examined. As can be seen in Figure 4.21-Panel A, histology at 4X the magnification of the wild-type mouse fracture shows a cartilage region ahead of a slight amount of new mineralization. Increased magnification to 20X (Figure 4.21-Panel B) shows this cartilage becoming hypertrophic, with a slight amount of calcified cartilage at the zone separating cartilage and bone. However, at 4X magnification, the 5-LOKO mouse has a very visual robust cartilage area coupled with a strong endochondral bone zone (Figure 4.21-Panel C). Further magnification to 20X

reveals hypertrophic chondrocytes with extensive mineralized cartilage on top of a new bone layer (Figure 4.21-Panel D). This histology supports that the 5-LOKO mice have an accelerated endochondral ossification process.

4.4.4 Histomorphometry of 5-LO Deficient Mouse Femurs

Histomorphometric measurements showed a slight increase in total callus area (TA) and callus area (CALLUS) was observed in the 5-LOKO mice as compared to WT controls at 7 days post-fracture. Furthermore there was a significant increase in MA and CA and a significant decrease of GT in the 5-LOKO as compared to WT controls at the same time point. By 10 days, these effects seemed to have minimized, except the GT levels in the WT controls were still significantly greater.

However, it has been reported that 5-LOKO mice have increased cortical bone thickness (255). Since wall thickness directly affects the amount of original femur bone present, thereby affecting the results of the callus area, this information was taken into account. Therefore, a normalized percentage value of MA, CA and GT (%MA, %CA, %GT) as compared to the calculated callus area was used.

As seen in Figure 4.22, after taking the wall thickness into consideration, a more pronounced effect is seen. With only seven days of healing, the 5-LOKO shows a significantly greater percentage of mineralized and cartilage and a significantly less amount of fibrous tissue (Figure 4.22-Panel A). While these results are similar as before wall thickness was addressed, it is clearly more

apparent that the differences between these two groups are more definitive. At ten days post-fracture, %MA is still significantly greater in the 5-LOKO animals as compared to WT and %GT is still significantly less than WT (Figure 4.22-Panel B). However, no significant differences were seen in any parameter past 10 days (Figure 4.21-Panels C and D). This indicates that the accelerated fracture healing observed in the 5-LOKO mice occurs because of changes during the early stages of fracture healing.

4.4.5 Mechanical Testing of 5-LO Deficient Mouse Femurs

Since wall thickness is a main variable in the calculation of mechanical properties, the normalized values of fractured femur as a percentage of the unfractured contralateral were considered as a better representation of the data (Figure 4.23).

It was observed that the structural properties of peak torque and rigidity of the 5-LOKO fracture callus were approximately 20% and 40% higher for the 5-LOKO mice than the control mice after 28 days (Figure 4.23- Panels A and B). In addition, the material properties of maximum shear stress and shear modulus were approximately 40% and 70% higher after 28 days of healing in the 5-LOKO mice (Figure 4.23- Panels C and D). By 84 days, peak torque and maximum shear stress remained significantly higher in the 5-LOKO mouse fractures than in controls. This further demonstrates that the 5-LOKO fracture callus obtains better structural and material properties sooner than control fracture callus.

4.4.6 Eicosanoid Levels in Fracture Callus of 5-LO Deficient Mice

Fracture callus levels of PGE_2, $PGF_{2\alpha}$ and LTB_4 were assayed to validate the hypothesis that the elimination of the COX-2 pathway leads to excess arachidonic acid shunting into the 5-LO pathway resulting in excess leukotriene production, reduced prostaglandin production, and ultimately impaired healing. This was accomplished by measuring eicosanoid levels in extracts from 4-day post-fracture calluses from mice of different genotypes.

The PGE_2 levels did not appear to initially follow this hypothesis (Figure 4.24). Our hypothesis predicted elevated levels of PGE_2 would be found in the 5-LOKO mice, the values obtained seem to be similar to the values of the controls. However, elevated levels of PGE_2 were measured in the Cox-2KO and Cox-1KO animals. Subsequently, Cox-2KO (Cox-2KOTreated) animals received a 30 mg/kg treatment with SC-560 (a COX-1 inhibitory drug) and Cox-1KO animals (Cox-1KOTreated) received a 30 mg/kg treatment of rofecoxib (a COX-2 inhibitory drug), by oral gavage, two hours before sacrifice. Treatment with these drugs showed that the elevated PGE_2 levels observed in the COX-1KO or COX-2KO mice was COX-2 or COX-1 dependent respectively.

$PGF_{2\alpha}$ levels also were measured in the 4-day post-fracture callus extracts (Figure 4.25). However, the results here were somewhat different. The 5-LOKO mice again did not see an elevation of $PGF_{2\alpha}$, suggestion that pure shunting was not occurring. Cox-1KO fractures showed significantly decreased $PGF_{2\alpha}$ values when compared to the 5-LOKO ($p= 0.004$), Cox2-HET ($p= 0.003$) and Cox2-WT fractures ($p= 0.003$), but significantly increased values when compared to Cox-

2KO fractures (p= 0.005). However, Cox-1KO mice treated with rofecoxib had further reduced $PGF_{2\alpha}$ levels (p= 0.006) compared to the untreated Cox-1KO animals. Unlike the PGE_2 assay, which showed elevation of PGE_2 in the Cox-2KO, the levels of $PGF_{2\alpha}$ in fracture callus extracts from the non-treated Cox-2KO animals were very low. This suggests that $PGF_{2\alpha}$ synthesis in the fracture callus, but not PGE_2 synthesis, is primarily dependent on COX-2 activity.

As expected, LTB_4 levels were very low in the fracture callus extracts from the 5-LOKO mice (Figure 4.26). However, shunting into the 5-LO pathway was observed in the Cox-2KO mouse fracture callus. Treating animals with SC-560 resulted in the LTB_4 levels decreasing back to normal values.

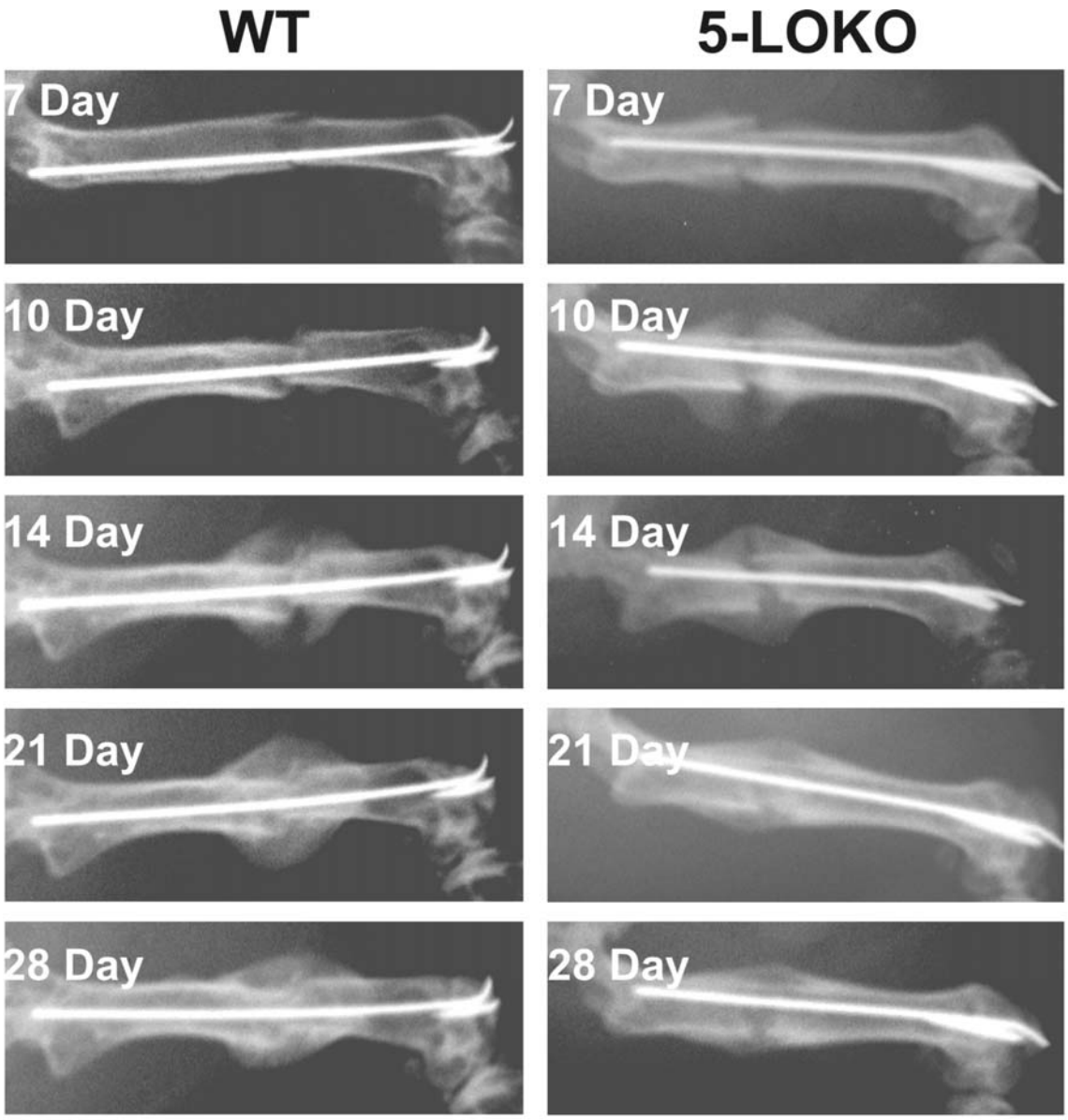

Figure 4.20. Radiographic Examination of Fracture Healing in 5-LOWT and 5-LOKO Mice. Shown are serial dorsal-ventral radiographs made from a wild-type mouse (WT) and a 5-LOKO mouse at 7, 10, 14, 21, and 28 days after fracture as indicated. The pelvis is to the left in each image. The intramedullary pin, fracture site, and resulting x-ray dense fracture callus are evident in each panel. The results shown are representative of those observed in other mice of identical genotype.

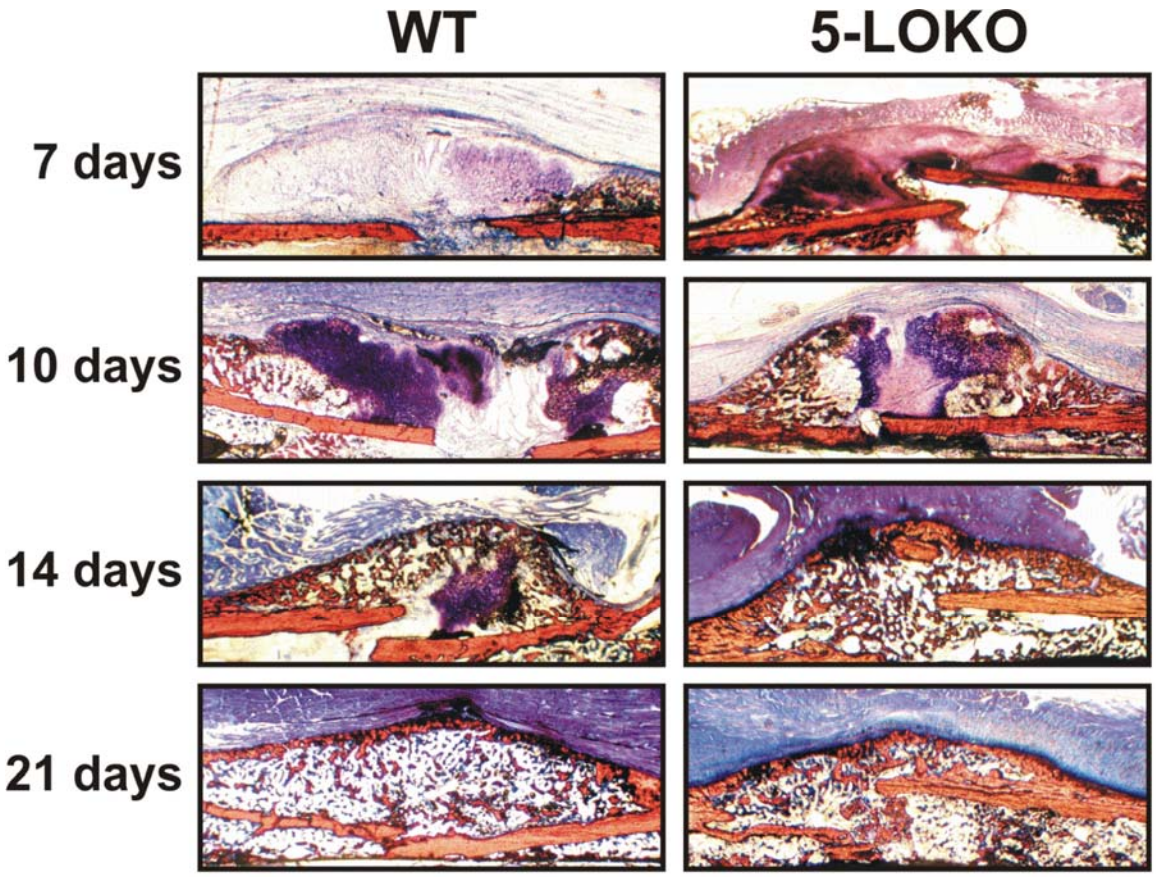

Figure 4.21. Accelerated Fracture Repair in 5-LOKO Mice is Observed in Histological Sections From 7 to 21 Days Post-Fracture. Healing femurs were fixed and embedded in polymethylmethacrylate. Longitudinal sections were stained with van Geison's picro-fuchsin (mineralized tissue is stained orange to red) and Stevenel's blue (cartilage is stained deep blue). At 7 days post-fracture, the WT fracture has some stained cartilage near the fracture ends and distinct callus borders. However, the 5-LOKO fracture callus is filled with an abundance of cartilage throughout the callus. By 10 days, endochondral ossification has begun in the WT fracture but is well underway in the 5-LOKO fracture. At 14 days post-fracture, the 5-LOKO callus appears bridged with bone and has begun to remodel. While the WT callus appears bridged, there is still a large ball of cartilage in the center of the callus. Remodeling continued through 21 days in the fracture calluses of both the WT and 5-LOKO animals.

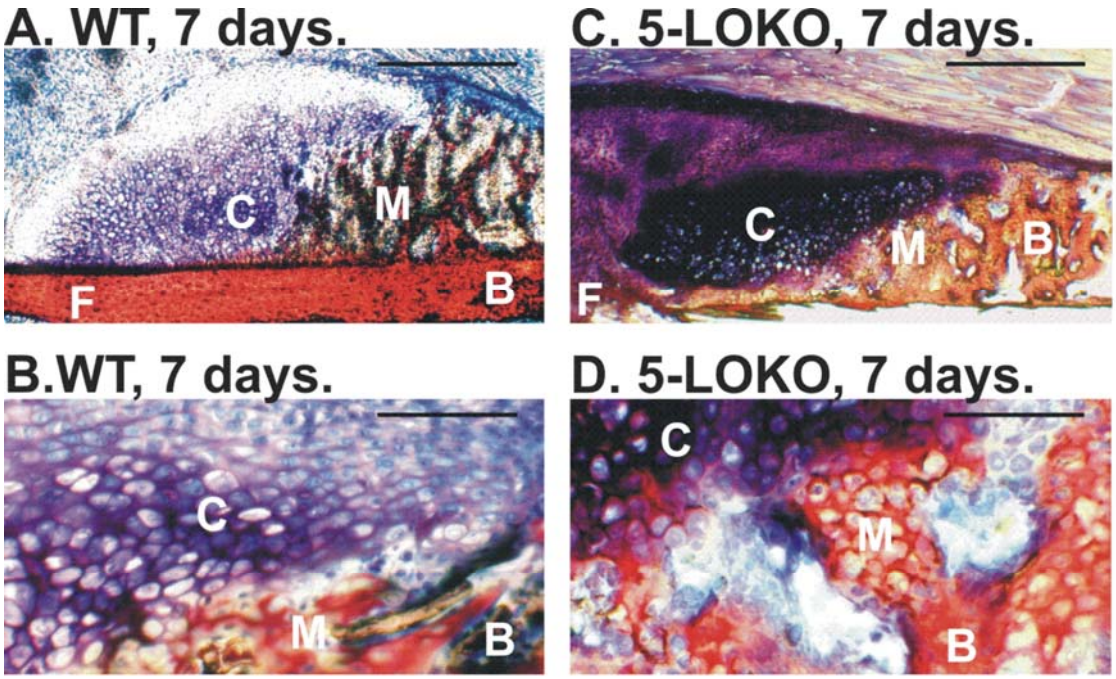

Figure 4.22. Histological Observations of Accelerated Endochondral Ossification During Fracture Repair in 5-LOKO Mice. The callus specimens shown were obtained after 7 days of healing. The fracture (F) is located at the bottom left of panels A and C with femur cortical bone to the bottom right in each. The bar in the upper right of panels A and C is 500 microns long and is 200 microns long in panels B and D. Panel A shows a representative quadrant from a WT fracture callus with normal callus morphology. An area of differentiating chondrocytes was observed (C) that is surrounded on the periphery with mesenchymal cells. An area of mineralized cartilage (M) was observed between the cartilage and areas of new bone formation (B). Panel B shows a magnified view of the cartilage-bone interface in the WT fracture callus showing areas of cartilage (C), mineralized cartilage (M) and new bone(B). Panel C shows a quadrant from the callus a 5-LOKO mouse with a deeply stained area of cartilage (C), a large mineralized cartilage interface (M), and areas of new bone formation in the external callus (B). Panel D shows a magnified view of the cartilage-bone interface in the 5-LOKO fracture callus. Chondrocytes (C), mineralized cartilage (M), and newly formed bone (B) is evident in the 5-LOKO fracture callus.

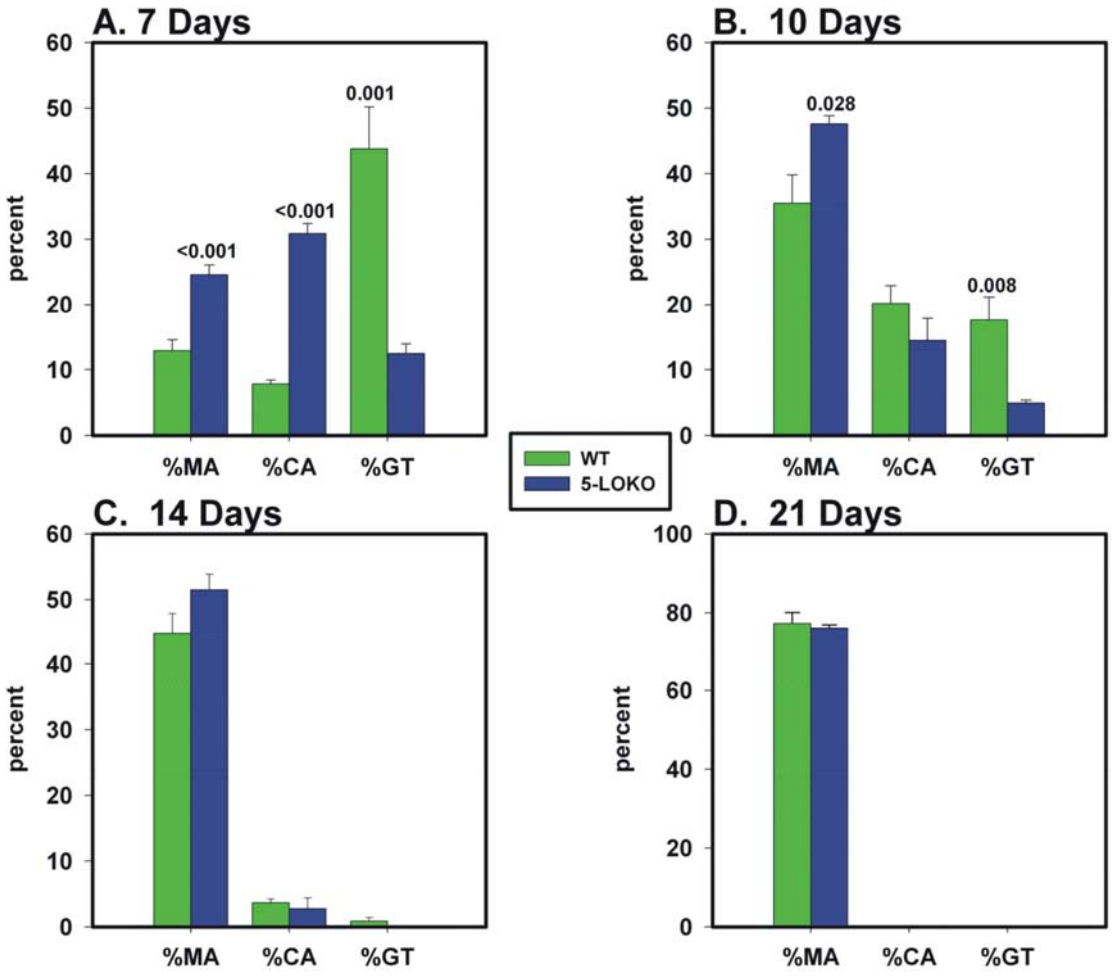

Figure 4.23. Histomorphometric Analysis of 5-LOKO Fracture Calluses. The percent of callus area that was mineralized tissue (%MA), cartilage (%CA), and granulation tissue (%GT) was compared between control and 5-LOKO mice at 7, 10, 14, and 21 days after fracture. Bars represent avg ± SEM. At 7 days, there was almost 4-fold more cartilage in the 5-LOKO callus than in the control callus. Similarly, there was almost 2-fold more mineralized tissue after 7 days and approximately a third more after 10 days in the 5-LOKO mice as compared to the control mice. Femurs from 5 mice of each genotype were used at each time point.

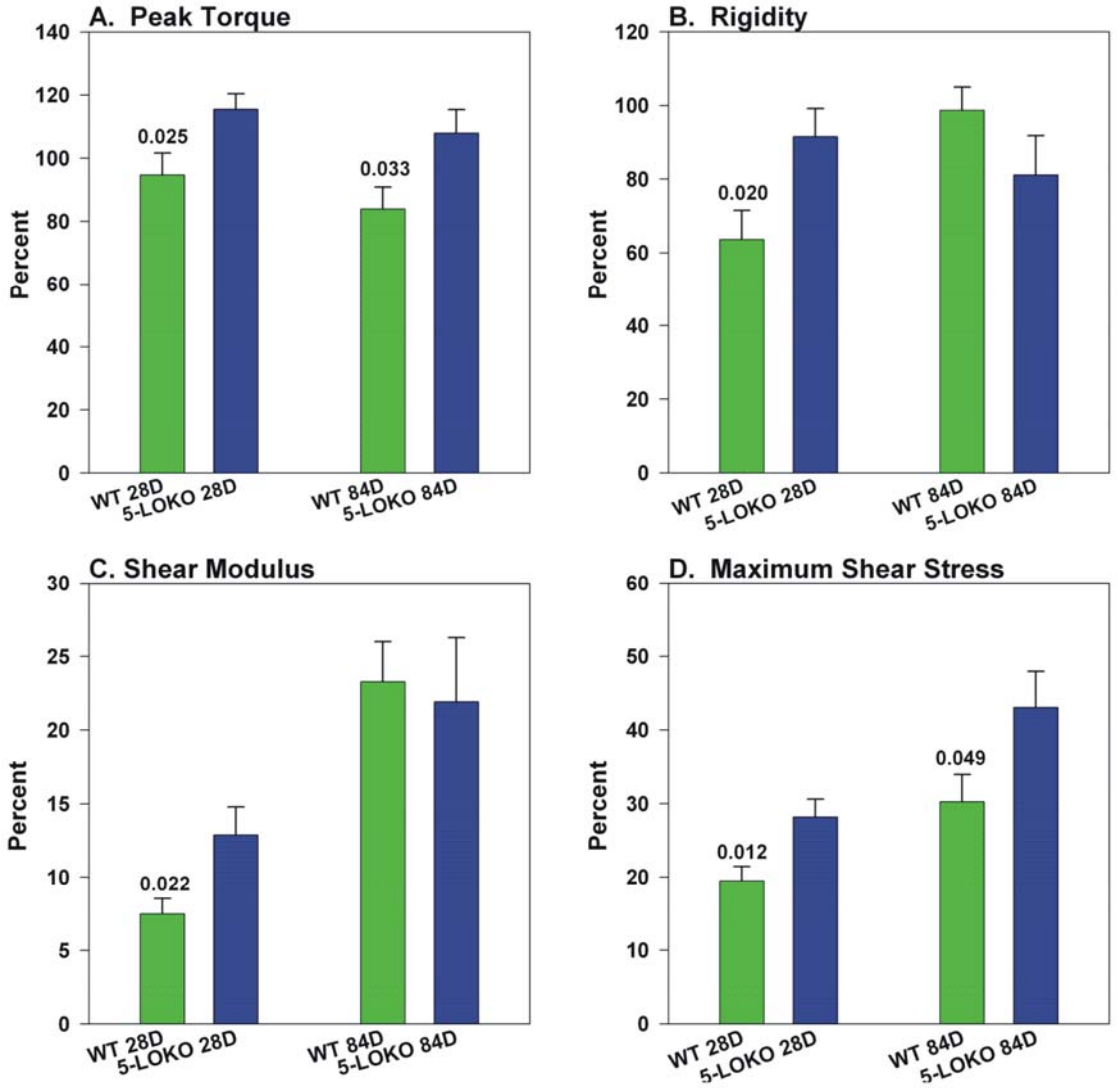

Figure 4.24. Fracture Calluses From 5-LOKO Mice Have Enhanced Mechanical Properties. Fractured and contralateral femurs from WT (28 days n=11; 84 days n=11) and 5-LOKO mice (28 days n=11; 84 days n=8) were mechanically tested to failure in torsion after 28 and 84 days of healing. Peak torque (A), rigidity (B), shear modulus (C), and maximum shear stress (D) were measured or calculated from the force to angular displacement curves generated during the testing procedure and the callus dimensions. Fractured femur values were normalized to the values from the contralateral femur of that mouse as a percentage. Normalized values were compared between genotypes at each time point. All parameters were significantly higher in the 5-LOKO mice than the control mice after 28 days of healing. After 84 days, rigidity and shear modulus in the control mice increased to levels similar to the 5-LOKO mice. However, peak torque and maximum shear stress were still significantly higher in the 5-LOKO mice than in the controls after 3 months of healing.

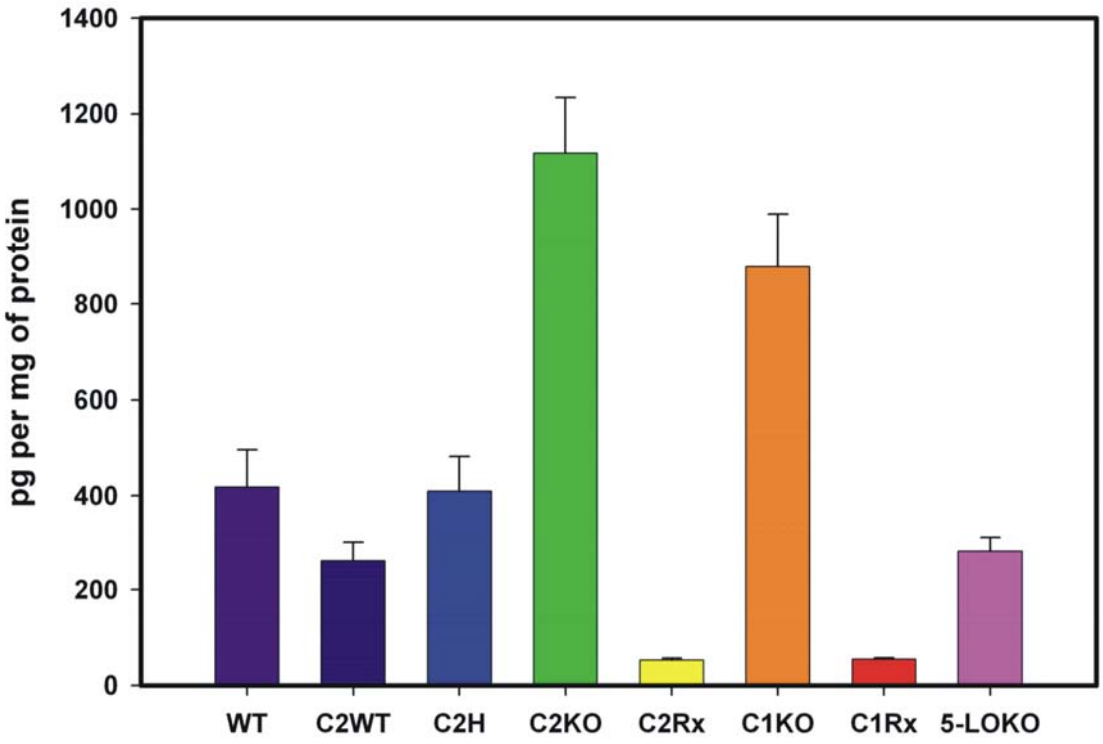

Figure 4.25. Callus PGE_2 Levels are Elevated in COX-2KO and COX-1KO Fractures. Fracture callus PGE_2 levels were measured in WT (n=6), Cox-2WT (C2WT) (n=6), Cox-2Het (C2H) (n=6), Cox-2KO (C2KO) (n=6), Cox-2 treated with rofecoxib (C2Rx) (n=5), Cox-1KO (C1KO) (n=4), Cox-1 treated with SC-560 (C1Rx) (n=3), and 5-LOKO (n=6) mice at 4 days post-fracture. Values were normalized to total callus protein levels. WT, C2WT, C2H and 5-LOKO all have similar values of callus PGE_2. However, loss of COX-2 and COX-1 function results in significantly elevated PGE_2 values ($p < 0.001$). The increased PGE_2 levels in the C2KO and C1KO were COX-1 and COX-2 dependent, respectively, since treatment with rofecoxib or SC-560 significantly reduced PGE_2 levels in these mice ($p < 0.001$) compared to the untreated C1KO and C2KO animals, respectively.

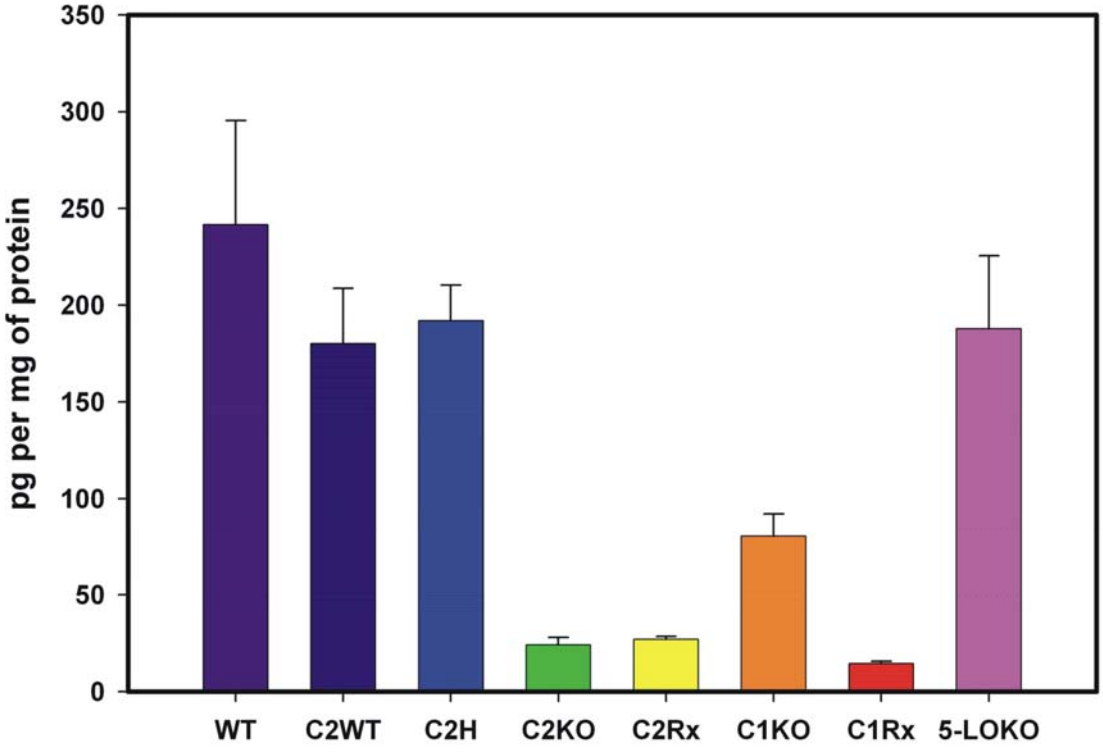

Figure 4.26. Callus $PGF_{2\alpha}$ Levels are Diminished in Cox-2KO Fractures. Fracture callus $PGF_{2\alpha}$ levels were measured in WT (n=6), Cox-2WT (C2WT) (n=6), Cox-2Het (C2H) (n=6), Cox-2KO (C2KO) (n=6), Cox-2 treated with rofecoxib (C2Rx) (n=5), Cox-1KO (C1KO) (n=4), Cox-1 treated with SC-560 (C1Rx) (n=3), and 5-LOKO (n=6) mice at 4 days post-fracture. Values were normalized to total callus protein levels. WT, C2WT, C2H and 5-LOKO all have similar values of callus $PGF_{2\alpha}$. However, loss of COX-2 function results in significantly decreased $PGF_{2\alpha}$ values ($p < 0.001$). The decreased $PGF_{2\alpha}$ levels in the C2KO and C1KO fracture calluses were primarily COX-2 dependent since very little $PGF_{2\alpha}$ was measured in C2KO mice and treating animals with rofecoxib significantly reduced levels of $PGF_{2\alpha}$ in C1KO mice ($p= 0.006$).

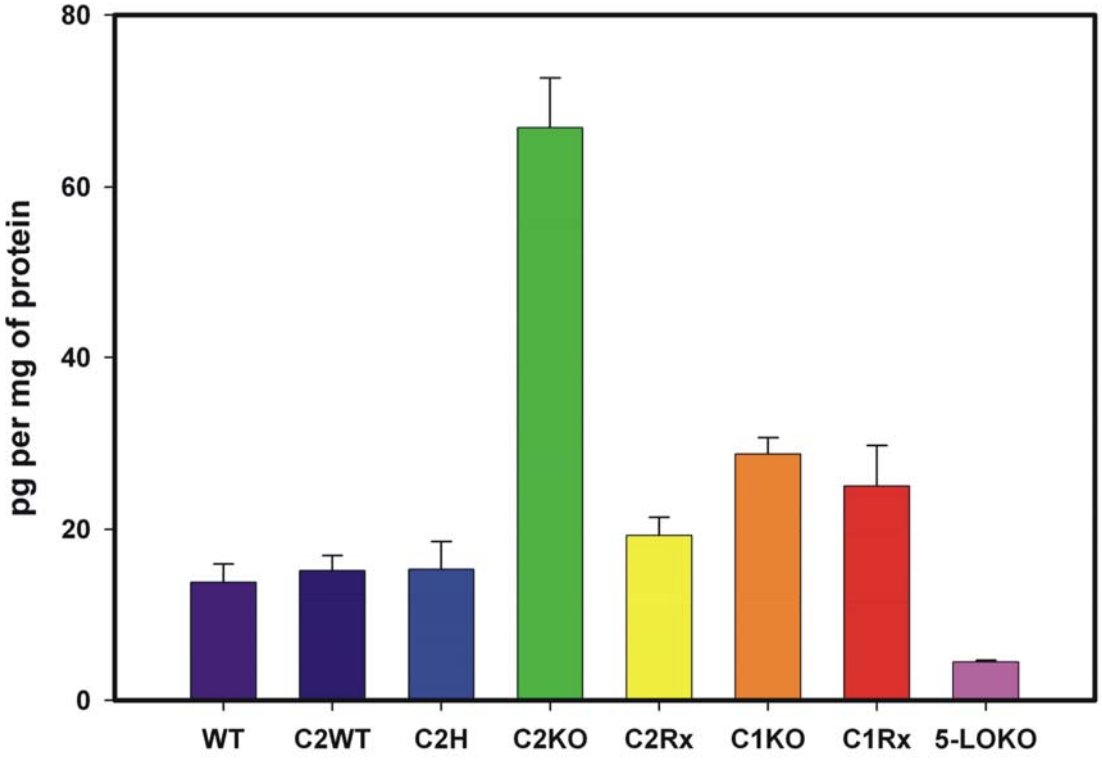

Figure 4.27. Callus LTB_4 Levels are Elevated in Cox-2KO Fractures. Fracture callus LTB_4 levels were measured in WT (n=6), Cox-2WT (C2WT) (n=6), Cox-2Het (C2H) (n=6), Cox-2KO (C2KO) (n=6), Cox-2 treated with rofecoxib (C2Rx) (n=5), Cox-1KO (C1KO) (n=4), Cox-1 treated with SC-560 (C1Rx) (n=3), and 5-LOKO (n=6) mice at 4 days post-fracture. As expected, LTB_4 levels in 5-LOKO animals were significantly lower than all other mice examined ($p < 0.001$). WT, C2WT, C2H, C1KO and C1Rx all had similar values of callus LTB_4. However, loss of COX-2 function resulted in significantly elevated LTB_4 values ($p < 0.001$), suggesting shunting of arachidonic acid had occurred. The increased LTB_4 level was diminished in C2KO mice after treatment with SC-560.

5.0.0 DISCUSSION

5.1.0 Developing and Characterizing a Closed Murine Femoral Fracture Model

The mouse femoral fracture model developed and characterized proved consistent and reliable. The overall success rate of the mouse fracture model was above 75%, with experimental losses due to the mechanical testing preparation accounting for almost 16% of the number of animals used. Poor or comminuted fracture production was minimal and represented only 3.3% of all animals used (Table 4.1).

The murine femoral fracture model described proved to be analogous to the rat closed femur fracture model developed by Bonnarens and Einhorn (209). Fracture healing followed a reproducible order of events, including hematoma formation, inflammation, endochondral ossification and remodeling (Figures 4.2 and 4.3). The processes observed were also similar to those seen in the rat model. However, one observed difference was that bony bridging of the fracture site in the mouse occurred between twenty-one and twenty-eight days post-fracture, while it does not occur until after twenty-eight days in the rat.

The use of the relatively straight femur allowed for the analysis of the torsional mechanical properties of a mouse fracture (Figure 4.5 and Table B1). Temporal variations in the mechanical properties also followed an expected pattern. Peak torque values increased rapidly to reach 82% of the contralateral control femur by twenty-one days post fracture. The increase in torque is most likely because of structural changes occurring in the fractured femur as its cross-sectional area increases at the site of injury (Figure 4.1 and Table B1). However,

rigidity showed a slower increase in values after 28 days of healing. This was consistent with the radiographical and histological data showing that the bridging of the fracture gap with new bone occurred between twenty-one and twenty-eight days post-fracture. Material properties also showed a slower increase in values. These increases were seen after twenty-eight days of healing. In contrast to the structural properties achieving similar values to controls quickly, the maximum shear stress and shear modulus values only reached 35% and 29% of the contralateral control femurs even after eighty-four days of healing post-fracture. While it is assumed that bone remodeling should occur quickly in mice, and therefore lead to increased material properties. The lower material properties observed may be attributed to potential stress shielding by the intramedullary pin. Generally, the structural mechanical properties (peak torque and rigidity) increased faster, as opposed to the material mechanical properties (shear stress and shear modulus), of the healing bones.

Other investigators have used additional murine femoral fracture models since this work began. One report showed a bone defect model developed in the distal metaphysic of the mouse femur (237). The healing process was followed by histomorphometry, peripheral quantitative computed tomography (pQCT), cantilever-bending mechanical testing, and molecular biological analyses. Bone healing in this model mainly occurred by intramembranous ossification, as very little cartilage was observed. Two reports described externally fixed femoral osteotomies. In one, cell proliferation and apoptosis rates during healing were characterized (232). In the other, radiography and four-point bending tests

evaluated fracture healing (236). Both of these reports showed results similar to those found here, with the bridging of the defect occurring at twenty-one days and stiffness values increasing over time.

Murine fracture callus cells also have been used as the a cell source for in vitro culture experiments (229). Another study focused on exploring whether traceable D1-BAG stromal cells would localize to the site of experimentally induced fractures (227). Transplanted bone marrow cells were injected intravenously into mice that sustained stabilized femoral shaft fractures. Callus tissue and marrow were examined histologically at seven, fourteen, twenty-one, twenty-eight, forty-two, fifty-six and seventy days post-fracture. In another report, systemically administered mesenchymal stem cells transfected with plasmids to express IGF-1 or β-galactosidase were quantified in the fracture callus at fourteen, twenty-eight and forty-two days post-fracture (256). Internally fixed, open femur fractures in mice were used to assess the effects of simvastatin on fracture healing (230). Examination of histology at seven, fourteen and twenty-one days post-fracture and mechanical testing by three-point bending was utilized in this experiment. Consistent with the findings here, fractures were found to be bridged at 21 days post fracture. Furthermore, the simvastatin-treatment appeared to affect the early stages of fracture healing by increasing the callus size at 14 days after fracture. However, this effect was eliminated by three weeks post-fracture, as no significance between treated and controls was noted at this time. The role of vascular endothelial growth factor (VEGF) was explored using a soluble form of the VEGF receptor to reduce

circulating levels of VEGF (231). Fractures were examined at seven and fourteen days post-fracture by microcomputer tomography and by histological examination. Finally, one group developed a locking femur nail for mice (235). Peak torque, rigidity and stiffness values were similar to the ones already presented. However, no histological data was presented.

While these reports utilized the murine fracture model, the radiographic, histological and mechanical testing analysis did not extensively characterize the healing pathway and only one report discussed the torsional mechanical properties (235). However, this report was published after the model presented here had already been published (257).

5.2.0 Genetic Background and Fracture Repair

Bone mineral density (BMD) is the most commonly used clinical indication of osteoporosis and fracture risk (73). Studies have shown that torsional strength is proportional to and primarily dependent on mineral content (258,259). Having a higher bone mineral density reduces the risk of a bone fracture. However, there is no correlation on whether or not having a high bone mineral density results in faster fracture healing once bone trauma has occurred. To determine if a high BMD correlated with a stronger or faster bony union following a femoral fracture, one outbred and three inbred strains of mice with previously published bone mineral density values (238) were evaluated for fracture healing capacity.

Radiographical and histological analysis (Figure 4.6-4.7) would first indicate that a high BMD leads to faster fracture repair. By 14 days, the mouse

with the highest BMD (C3H) appears bridged, while all other strains appear to lag behind. Additionally, remodeling appeared to have begun by 28 days in C3H animal. However, histomorphometry and mechanical testing results did not support these initial findings (Figures 4.8-4.14). Histomorphometric measurements showed that C57BL/6 fractures (lowest BMD) had the highest percentage of mineralized tissue and cartilage area at the earliest time point. Also, the C57BL/6 calluses have the least amount of granulation tissue at the earliest time post-fracture. This suggests that the C57BL/6 callus (low BMD) has healed faster than the C3H callus (high BMD).

Mechanical testing supports these findings. Analysis of the mechanical testing properties shows that when the fractured femur was normalized to its control unfractured femur, the C57BL/6 had the highest structural (peak torque and rigidity) and material (maximum shear stress and shear modulus) properties. C3H fractures, while having the highest bone mineral density values, have the weakest normalized mechanical testing properties. This suggests an inverse relationship between bone mineral density and fracture healing success exists. As expected, when comparing the fractured to the unfractured control femur, the C3H animal had significantly greater mechanical testing values. Therefore, a high bone mineral density is valuable in minimizing fracture risk. However, after a fracture is sustained, such as in a high impact accident, a genetic pre-disposition to high bone mineral density may be deleterious to the fracture healing progress.

5.3.0 Cyclooxygenase and Fracture Repair

Because prostaglandins are known to be modulators of bone metabolism, the role of prostaglandin synthesis in bone healing has been of much interest. The most abundant prostaglandin produced by osteoblasts, PGE_2, has been shown to play a crucial role in bone formation, mainly through the EP2 and EP4 prostaglandin receptor subtypes (260-262). Previous experiments that systemically administered PGE_2 showed an increase in bone formation, as well as bone mass (263-266). In the rabbit, blood flow to the surrounding muscle, bone and marrow was increased by PGE_2 infusion (267), while callus formations showed a dose-dependent stimulation response (268). Furthermore, PGE_2 given to canines increased mineralization, indicating accelerated remodeling (269,270). Collectively, there is ample scientific evidence to support the role prostaglandins play in bone metabolism. However, to better understand the role prostaglandins play in fracture repair, it is important to understand how prostaglandins contribute to the fracture repair process.

During the inflammatory stage of fracture healing, pro-inflammatory stimuli, cytokine and growth factors release influence prostaglandin production (114,271,272). Prostaglandins were shown to accumulated in the fracture callus in the first two weeks after injury and are abundantly produced by osteoblasts (27,271,273). During the bone reparative phase, prostaglandins are responsible for increasing the amount and activity of osteoclasts, thereby aiding subsequent bone resorption (274) and PGE_2 is the most potent agonist for stimulating bone resorption and formation (266). Additionally, prostaglandin production in bone

and their future action on bone cells was shown to be indirectly enhanced by COX-2 induction (151,274).

The two recognized isoforms of cyclooxygenase, COX-1 and COX-2, are differentially expressed in bone. COX-1 is constitutively expressed in normal bone and COX-2 is upregulated during the beginning stages of fracture repair and inflammation (27,275-277). Because of these findings, much attention has recently been given to studying how the blocking of prostaglandin synthesis, specifically by non-selective, non-steroidal anti-inflammatory drugs (NSAIDs) and selective COX-2 inhibitors (COXIBs), alters bone healing. Because of their anti-inflammatory and analgesic properties, NSAIDs are widely prescribed to patients with bone and joint ailments and musculoskeletal injuries (278,279). In normal bones, long term NSAID use rarely causes adverse effects and is considered to be therapeutic for bone loss prevention and osteoporosis (280). Furthermore, NSAIDs are useful in preventing heterotopic ossification following joint replacement surgery (281-286). However, the potential side effects associated with traditional NSAID use resulted in the development of selective COX-2 inhibitors that would affect prostaglandin production by the COX-2 pathway, but spare the prostaglandin production associated with the COX-1 pathway that are necessary for normal tissue function (186).

Many preclinical models of fracture repair have evaluated NSAIDs following fracture or osteotomy. For example, impaired bone healing in rats and rabbits resulted after being treated with aspirin, diclofenac, ibuprofen, indomethacin, and tenoxicam (287-304). Recent studies focusing on how

COXIBs effect bone healing have shown similar results (114,305,306). In essence, these studies show a decreased callus size and inferior mechanical properties indicative of inhibited fracture healing.

Because the strong pharmacological data that specific COX-2 inhibitors impair fracture healing, this dissertation sought to determine if the impairment in bone regeneration was caused by a pharmacological dosing side-effect or whether COX-2 had a functional role in bone healing.

The radiographical, histological, histomorphometric, mechanical and callus eicosanoid level information presented here clearly shows Cox-2KO mice have an abnormal repair sequence when compared to controls (Figure 4.15-4.18). Fracture callus levels of PGE_2 were significantly higher ($p<0.001$) in both the Cox-1KO and Cox-2KO animals compared to all other groups. While this may seem counterintuitive, only half of the arachidonic acid pathway is blocked in either of these strains of mice. One possible reason why Cox-2KO mice fail to heal properly is that the excess PGE_2 results in elevated bone resorption. Eicosanoid levels also show that Cox-1KO animals have a high level of $PGF_{2\alpha}$, while Cox-2KO fracture calluses have non-detectable amounts of $PGF_{2\alpha}$. This implies that COX-2 governs $PGF_{2\alpha}$ production. Since chondrogenesis is $PGF_{2\alpha}$ dependent, it follows that Cox-2KO mice would have low chondrocyte populations. This is evident in the histology and histomorphometry results presented (Figures 6.2-6.4). However, Cox-1KO fracture calluses show lower than average levels of $PGF_{2\alpha}$. Therefore, Cox-1KO animals should still produce chondrocytes. It is hypothesized that if the ratio of PGE_2 to $PGF_{2\alpha}$ is less than 1,

healing will occur normally. If the ratio of PGE_2 to $PGF_{2\alpha}$ is greater than 1, then healing will occur abnormally. Because the Cox-1KO levels of PGE_2 are higher than the levels of $PGF_{2\alpha}$, this may explain the high number of non-unions seen in these experiments. However, the difference between the PGE_2 levels and the $PGF_{2\alpha}$ levels is not as drastic in the Cox-1KO mice as with the Cox-2 mice and should occur less often.

Recently, one group published results in contrast to our findings (307). In this randomized blinded study, a stabilized closed-tibial fracture was placed in 8-10 week old male mice. These animals were then placed in one of seven treatment groups to examine the effect of COX-2 inhibitors and non-steroidal anti-inflammatory drugs on fracture healing. Animals in a treatment group received oral NSAIDS delivered in peanut butter chow. Biochemical and three-point biomechanical testing was completed at 28, 56 and 84 days post-fracture. The results of this study found no differences in maximum load or stiffness values between any treatment groups compared to control values and only the animals in the ketorolac group exhibited differences in collagen expression with decreased cartilage formation. However, the data presented in this dissertation does not support the finding of this report, as the Cox-2KO animals examined here showed severe fracture healing delays or complete non-unions.

5.4.0 5-Lipoxygenase and Fracture Repair

Animal studies have confirmed the importance of non-steroidal anti-inflammatory drugs (NSAIDs) on fracture healing (287,288,291-293,308).

Because NSAIDs inhibit cyclooxygenase activity, one explanation for the deleterious effects would be that COX-2 activity induced as part of the inflammatory phase of fracture repair has a necessary function. Experiments have shown that COX-2 selective NSAID treatments in the rat impair fracture healing in the rat and that fracture healing is drastically inhibited in mice lacking COX-2 function (306). In the clinical setting, NSAIDs are prescribed to reduce heterotopic bone formation in humans and retrospective studies show that the use of NSAIDs can lead to an increase of non-unions in humans (309-313).

Prostaglandins induce osteogenesis in animals and humans (314,315). Therefore, one explanation would be that the loss of, or inhibition of, COX-2 activity would reduce bone formation during fracture repair. Little is known about the specific cell types that produce prostaglandins or which cells respond to the prostaglandins during fracture repair. While, *in vitro* data has shown that osteoblasts, chondrocytes and endothelial cells synthesize and respond to prostaglandins (316-331), this has yet to be proven *in vivo* during fracture repair.

This thesis hypothesizes that another mechanism could account for the impaired fracture healing observed in Cox-2KO mice or in other animals treated with NSAIDs. As part of the normal inflammatory response, COX-2 and 5-LO are activated and induced. This leads to the normal production of prostaglandins and leukotrienes (Figure 4.27-Panel A). When COX-2 function is absent, arachidonic acid released by phospholipase A2 activity may potentially be shunted into the 5-LO pathway leading to increase leukotrienes synthesis, a

decrease in prostaglandin synthesis, and ultimately impaired healing (Figure 4.27-Panel B).

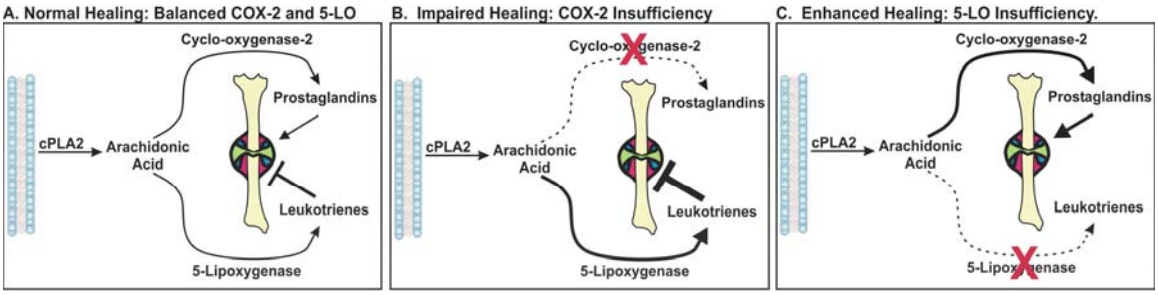

Figure 5.1. Hypothetical Model of COX-2 and 5-LO Function in Fracture Healing (From J. P. O'Connor).

Previous work has shown that *in vitro* treatment with LTB_4 or 5-HETE can reduce osteoblast proliferation and differentiation (332,333). It may be possible that loss of 5-lipoxygenase activity could potentially reduce leukotriene levels, increase prostaglandin levels and accelerate fracture healing (Figure 4.27-Panel C).

Radiographic, histologic, and histomorphometric data support that genetic ablation of 5-LO function accelerates tissue regeneration during fracture healing (Figures 4.19-4.22). While a normal pattern of endochondral ossification was observed, there was significantly more cartilage in the facture site than in control mice by seven days post fracture. In addition, more mineralized tissue was evident in the 5-LOKO mice at seven and ten days post-fracture. This data signifies that bone regeneration occurred through an accelerated endochondral ossification process in the 5-LOKO mice.

In accordance with the radiographic and histomorphometric results, the mechanical data also provided compelling evidence that the 5-LOKO mice experience acelerated healing (Figure 4.23). Normalized peak torque and rigidity values were approximately 20% and 40% higher for the 5-LOKO mice than for the control mice after 28 days of healing. Likewise, after 28 days of healing, maximum shear modulus and shear stress were approximately 70% and 40%, respectively, in the 5-LOKO mice. Peak torque and maximum shear stress remained significantly higher in the 5-LOKO mice even after 84 days post-fracture, demonstrating that the 5-LOKO fracture callus obtained better structural and material properties faster than control mice.

To directly test the hypothesis that in the absence of COX-2, arachidonic acid could shunt into the 5-LO pathway leading to excess leukotriene synthesis, which is potentially responsible for the impairment of bone regeneration during fracture healing, fracture callus levels of eicosanoids were also measured (Figures 4.24-4.26). Callus eicosanoid data showed 5-LOKO mice had significantly reduced levels of LTB_4. This was expected since without 5-LO function, these mice should have no leukotrienes or other 5-LO metabolites being produced. Furthermore, fracture callus leukotriene levels were four-fold higher in the Cox-2KO mice. However, true shunting was not observed, as 5-LOKO mice did not have significantly higher levels of either PGE_2 or $PGF_{2\alpha}$. So, while arachidonic acid was being shunted into the 5-LO pathway in the absence of COX-2, arachidonic acid was not being shunted in the absence of 5-LO. One potential reason for this occurrence is that Five Lipoxygenase Activating Protein

(FLAP) is preventing this shunting from occurring. FLAP is the membrane bound protein required for 5-LO function (334-336). In the absence of 5-LO, $cPLA_2$ still can interact with FLAP, thereby preventing full shunting from happening.

It is therefore proposed that when COX-2 activity is impaired, either genetically or pharmacologically, the excess leukotrienes will impair healing. When 5-LO activity is impaired, the amount of leukotrienes is decreased, thereby accelerating fracture healing. Therefore, the pharmacological inhibition of 5-LO and its other metabolites could be used to accelerate or enhance fracture repair.

6.0.0 CONCLUSIONS

The use of the mouse as a fracture model has proved useful in the field of orthopaedics. With the development of these animals with targeted mutations, it is now possible to study complex genes and phenotypes associated with bone diseases. The further development of a biomechanical testing protocol that would better approximate the mechanical properties of the healing tissue is also important. While the three-point and four-point bending tests are commonly used for biomechanical analyses, these tests are inadequate for fracture healing studies involving small sized specimens. A more accurate biomechanical test for small samples is the torsion test. Therefore, the development and characterization of a murine femoral fracture model suitable for torsional mechanical testing was completed. This model was validated using radiographic, histologic and mechanical testing data. These parameters were selected based on their relevance to previous literature and showed that mouse heals similarly to other published fracture models.

Using this established model, a complex phenotype was then examined to see its role in fracture healing. Mice with different genetic backgrounds were selected to see how bone mineral density values affected fracture healing success. It was found that while bone mineral density may aid in preventing a fracture, the radiographic, histological, and mechanical testing data show a high bone mineral density actually impedes fracture healing success.

The last part of this dissertation focused on how the altering of a single pathway affects fracture healing. The arachidonic acid pathway, its products and

the enzymes mediating their formation play a crucial role in many aspects of human physiology. Leukotrienes and prostaglandins are produced by the activity of three enzymes, 5-lipoxygenase, cyclooxygenase-1 and cyclooxygenase-2, as part of the arachidonic acid pathway. Manipulating this pathway, by the blocking or rerouting of arachidonic acid, proved to be critical in fracture healing. Radiography, histology and mechanical testing showed that mice with a genetic deletion of cycloxygenase-2 (COX-2) showed greatly inhibited fracture healing while mice with a genetic deletion of 5-Lipoxygenase showed accelerated fracture healing. Furthermore, fracture callus eicosanoid levels showed that arachidonic acid reroutes itself under genetic conditions.

The mouse has proven to be an exceptionally valuable research tool involving orthopaedic conditions that involve genetics and complex phenotypes. Biomechanical testing provides a better understanding of healing bone properties. The mouse model along with a suitable mechanical testing protocol allows for the better estimation of key structural and material properties crucial in evaluating fracture healing success. This allows for the development of potential future treatments for fracture healing patients and a better understanding of the normal fracture healing mechanisms responsible for fracture healing success.

Appendix A

Protocols for Decalcified and Calcified Mouse Bone Specimens and Mechanical Testing Equations

Specimen Fixation Protocol for Calcified and Decalcified Samples

Fixation:	
10% Buffered Formalin	24 hours or longer
Decalcification (Decalcified Samples ONLY):	
Wash in running water	10 minutes
Immunocal	change daily for 2 to 4 days
Wash in running water	30 minutes
Dehydration:	
40% EtOH	8 hours
70% EtOH	16 hours
80% EtOH I	8 hours
80% EtOH II	16 hours
90% EtOH I	8 hours
90% EtOH II	16 hours
100% EtOH I	8 hours
100% EtOH II	16 hours
Clearing:	
Hemo-De I	8 hours
Hemo-De II	16 hours
Infiltration:	
Calcified Samples:	
PMMA I	3 to 7 days
PMMA II	3 to 7 days
PMMA III	3 to 7 days
PMMA III	Place tissues in specimen bottle and place bottle in 37°C water bath
Decalcified Samples:	
Paraffin I	Overnight
Paraffin II	Overnight

Polymethylmethacrylate (PMMA) Solutions

PMMA I

100 mL Polymethylmethacrylate Monomer

PMMA II

100 mL Polymethylmethacrylate Monomer
1 gram dry benzoyl peroxide

PMMA III

100 ml Polymethylmethacrylate Monomer
2.5 grams dry benzoyl peroxide

Masson's Trichrome

Reagents and Equipment Required:

Bouin's solution
Weigert's Iron Hematoxylin Set. Prepare working solution according to label instructions.
Acetic Acid, 1%. Prepare by diluting 1 part Acetic Acid with 9 parts water
Biebrich Scarlet-Acid Fuchsin Solution. Biebrich scarlet, 0.9%, acid fuchsin 0.1%, in acetic acid, 1%
Phosphomolybdic Acid Solution, Phosphomolybdic Acid, 10%
Aniline Blue Solution, Aniline blue, 2.4% and acetic acid 2%

To Prepare Working Phosphotungstic/Phosphomolybdic Acid Solution:

Mix 1 volume of Phosphotungstic Acid Solution and 1 volume Phosphomolybdic Acid Solution with 2 volumes of deionized water. Discard after one use.

Standard Procedure:

1. Deparaffinize slides to deionized water.
2. Mordant in preheated Bouin's solution at 56ºC for 15 minutes or at room temperature overnight.
3. Cool slides in tap water contained in a Coplin jar.
4. Wash in running tap water to remove yellow color from sections.
5. Stain in Working Weigert's Iron Hematoxylin Solution for 5 minutes.
6. Wash in running tap water for 5 minutes.
7. Rinse in deionized water.
8. Stain in Biebrich Scarlet-Acid Fuschin for 5 minutes
9. Rinse in deionized water.
10. Place slides in working Phosphotungstic/Phosphomolybdic Acid Solution for 5 minutes.
11. Place slides in Aniline Blue Solution for 5 minutes
12. Place slides in Acetic Acid, 1%, for 2 minutes. Discard Solution.
13. Rinse Slides, dehydrate through alcohol, clear in xylene and mount

Results of stain:

Cytoplasm and muscle fibers- red
Collagen- blue

Stevenel's Blue and Van Geison's Picro-Fuchsin (SVG)

Stevenel's Blue Stain:

Solution 1:
1 g of Methylene Blue (Fisher: M-291)
75 mL of distilled water
Solution 2:
1.5 g of Potassium Permanganate
75 mL of distilled water

Mix solutions 1 and 2 and place in a boiling water bath until the precipitate dissolves. Allow the stain to reach room temperature, then filter.

Van Geison Picro-Fuchsin:

0.1 g of Acid Fuchsin
10 mL of distilled water
100 mL of saturated Picric Acid

Mix the Acid Fuchsin with the distilled water to obtain a 1% aqueous solution. Mix the solution with the Picric Acid.

Standard Procedure:

1. Soak in Stevenel's Blue in a water bath at 60 C for the following times:
    a. 10 minutes for bone,
    b. 1 minute 20 seconds for soft tissue
    c. 2 minutes for muscle
2. Rinse in distilled water in a water in a water bath at 60 C and blot dry
3. Soak in Van Geison's Picro-Fuchsin for 2 minutes for all tissue types at room temperature.
4. Rinse in 100% ethanol.

Results of stain:

Cells and extracellular structures not mineralized- shades of blue
Collagen fibers- green to green-blue
Bone-orange or purple
Osteoid- yellow-green
Muscle fibers- blue to blue-green

Mechanical Testing Data Equations

Polar Moment of Inertia (J)

$J= [\pi(ab^3+a^3b-(a-t)(b-t)^3-(a-t)^3(b-t)]/4$

a = maximum callus or diaphyseal radius
b = minimum callus or diaphyseal radius
t = is the average bone thickness

Torsional Rigidity (R)

$R= (T_{max} \times L)/\varphi$

T_{max} = maximum peak torque value
L = working gauge length
φ = angle at failure in radians

Shear Stress (τ)

$T= (T_{max} \times c)/J$

T_{max} = maximum peak torque value
c = maximum callus or diaphyseal radius
J = polar moment of inertia

Shear Modulus (G)

$G= (T_{max} \times L)/ (J \times \varphi)$

T_{max} = maximum peak torque value
L = working gauge length
J = polar moment of inertia
φ = angle of failure in radians

Cross-Sectional Area (A)

$A= ab\pi$

a = maximum callus or diaphyseal radius
b = minimum callus or diaphyseal radius

Appendix B

Analysis and Statistical Summary Tables for Mechanical and Histomorphometrical Data

Table B1. Summary of ICR Mouse Femur Mechanical Testing Data.

	Pooled Control Femurs	Fractured Femurs (Time Post-Fracture)			
		21 Days	28 Days	42 Days	84 Days
Sample Size (n)	68	18	18	15	17
Cross-sectional Area (mm^2)					
Fractured		8.84 ± 1.80	8.22 ± 1.44	5.02 ± 1.28	4.41 ± 0.71
Control	2.10 ± 0.27	2.22 ± 0.27	1.96 ± 0.24	1.95 ± 0.20	2.24 ± 0.24
Percent* **		403 ± 93	420 ± 63	256 ± 52	198 ± 33
paired t-test	—	<0.001	<0.001	<0.001	<0.001
Peak Torque (Nmm)					
Fractured		36.0 ± 11.0	33.9 ± 10.0	34.2 ± 8.6	42.8 ± 10.8
Control	43.8 ± 14.2	38.23 ± 12.39	46.34 ± 11.23	43.00 ± 13.09	47.60 ± 18.45
Percent		102 ± 39	75 ± 22	84 ± 27	100 ± 39
paired t-test	—	0.497	<0.001	0.013	0.28
Rigidity (Nmm^2)					
Fractured		567 ± 235	483 ± 226	563 ± 309	1,105 ± 415
Control	991.0 ± 425.8	940 ± 426	924 ± 344	1,117 ± 527	1,005 ± 419
Percent		69 ± 32	54 ± 23	55 ± 27	128 ± 65
paired t-test	—	0.002	<0.001	<0.001	0.44
Shear Stress (MPa)					
Fractured		13.0 ± 5.0	13.6 ± 4.6	30.2 ± 13.6	44.4 ± 16.8
Control	160.0 ± 61.2	127 ± 57	187 ± 40	178 ± 65	152 ± 66
Percent		12 ± 6	8 ± 3	19 ± 11	35 ± 21
paired t-test	—	<0.001	<0.001	<0.001	<0.001
Shear Modulus (GPa)					
Fractured		0.12 ± 0.06	0.11 ± 0.06	0.36 ± 0.22	0.82 ± 0.41
Control	3.94 ± 1.99	3.39 ± 2.12	4.21 ± 1.67	4.99 ± 2.43	3.31 ± 1.34
Percent		5 ± 3	3 ±1	8 ± 5	29 ± 18
paired t-test	—	<0.001	<0.001	<0.001	<0.001
Angle at Failure (degrees)					
Fractured		22.6 ± 9.3	25.6 ± 10.9	19.2 ± 10.6	11.0 ± 3.9
Control	13.8 ± 6.1	12.8 ± 4.4	16.1 ± 5.4	11.8 ± 6.4	14.3 ± 7.6
Percent		203 ± 134	163 ± 61	1.83 ± 1.32	91 ± 41
paired t-test		<0.001	<0.001	0.02	0.07
Polar Moment of Inertia (J) (mm^4)					
Fractured		5.4 ± 2.0	4.8 ± 1.5	1.9 ± 1.0	1.5 ± 0.5
Control	0.27 ± 0.09	0.31 ± 0.09	0.23 ± 0.06	0.23 ± 0.05	0.31 ± 0.09
Percent		1,878 ± 863	532,120 ± 595	819 ± 322	494 ± 191
paired t-test		<0.001	<0.001	<0.001	<0.001
Gage Length (mm)					
Fractured		5.6 ± 1.0	5.6 ± 1.5	4.3 ± 0.90	4.7 ± 1.1
Control	4.9 ± 1.0	5.0 ± 0.8	5.2 ± 1.2	4.6 ± 0.9	4.7 ± 1.1
Percent		115 ± 32	107 ± 20	95 ± 23	103 ± 26
paired t-test		0.14	0.24	0.18	0.95

Values shown for all parameters are the mean and standard deviation. Values for each parameter are listed from all the contra-lateral control femurs. Statistical comparisons were made by comparing fracture to control femur values within a time point (paired t-test). Mean percentage values and standard deviations were calculated from the percent fracture to control values for each animal.

Table B2. Inbred Mouse Fracture Callus Histomorphometrical Measurements Summary.

ICR Histomorphometry Measurements

Time Point	n		TA (mm^2)	B (mm^2)	MA (mm^2)	CA (mm^2)	GT (mm^2)	Void	CALLUS (mm^2)	% MA/CALLUS	% CA/CALLUS	% GT/CALLUS
7 Days	6	AVERAGE	14.04	2.67	0.00	0.72	7.27	3.38	11.37	0.00	6.23	63.73
		SD	1.31	0.24	0.00	0.35	1.14	0.39	1.41	0.00	2.53	4.10
		SEM	0.54	0.10	0.00	0.14	0.47	0.16	0.58	0.00	1.03	1.68
10 Days	4	AVERAGE	14.26	3.17	0.88	1.46	5.74	3.02	11.10	7.87	13.47	50.93
		SD	1.05	0.53	0.39	0.58	2.01	0.27	1.51	3.44	5.60	11.22
		SEM	0.52	0.26	0.20	0.29	1.00	0.14	0.75	1.72	2.80	5.61
14 Days	5	AVERAGE	16.53	3.08	3.86	1.93	5.28	2.39	13.45	28.54	14.45	39.62
		SD	1.99	0.72	1.25	0.36	0.99	0.81	2.29	6.61	1.81	6.71
		SEM	0.89	0.32	0.56	0.16	0.44	0.36	1.02	2.96	0.81	3.00
21 Days	3	AVERAGE	14.90	3.05	6.84	1.04	1.07	2.90	11.85	57.91	8.82	8.75
		SD	0.75	0.39	0.64	0.07	0.94	0.41	0.62	7.64	0.90	7.64
		SEM	0.43	0.23	0.37	0.04	0.54	0.24	0.36	4.41	0.52	4.41
28 Days	3	AVERAGE	12.71	2.27	8.40	0.00	0.00	2.04	10.44	81.05	0.00	0.00
		SD	1.42	0.31	0.70	0.00	0.00	1.09	1.28	8.50	0.00	0.00
		SEM	0.82	0.18	0.40	0.00	0.00	0.63	0.74	4.91	0.00	0.00
42 Days	4	AVERAGE	9.28	2.11	5.70	0.00	0.00	1.47	7.17	79.74	0.00	0.00
		SD	1.10	0.47	0.69	0.00	0.00	0.36	1.03	2.23	0.00	0.00
		SEM	0.55	0.24	0.35	0.00	0.00	0.18	0.51	1.12	0.00	0.00

C3H Histomorphometry Measurements

Time Point	n		TA (mm^2)	B (mm^2)	MA (mm^2)	CA (mm^2)	GT (mm^2)	Void	CALLUS (mm^2)	% MA/CALLUS	% CA/CALLUS	% GT/CALLUS
7 Days	4	AVERAGE	8.72	3.67	0.00	0.47	3.73	0.85	5.05	0.00	10.51	69.85
		SD	1.88	0.18	0.00	0.06	1.94	0.05	2.00	0.00	3.81	13.65
		SEM	0.94	0.09	0.00	0.03	0.97	0.03	1.00	0.00	1.90	6.82
10 Days	4	AVERAGE	13.31	4.22	0.15	2.87	5.00	1.07	9.09	1.67	31.30	55.14
		SD	0.83	0.53	0.31	0.62	0.46	0.39	0.76	3.34	4.81	5.20
		SEM	0.41	0.26	0.16	0.31	0.23	0.20	0.38	1.67	2.40	2.60
14 Days	5	AVERAGE	13.44	3.36	3.94	0.79	0.50	4.85	10.08	39.16	8.00	5.13
		SD	0.89	0.64	1.26	0.12	0.28	1.44	1.20	11.66	2.15	2.96
		SEM	0.36	0.26	0.52	0.05	0.12	0.59	0.49	4.76	0.88	1.21
21 Days	4	AVERAGE	13.40	3.61	6.20	0.12	0.20	2.88	9.79	63.20	1.39	2.15
		SD	2.15	0.70	1.43	0.14	0.29	1.19	1.70	7.69	1.66	3.29
		SEM	1.07	0.35	0.71	0.07	0.14	0.49	0.85	3.84	0.83	1.65
28 Days	8	AVERAGE	10.78	4.02	5.86	0.00	0.00	0.91	6.77	86.26	0.00	0.00
		SD	1.28	0.93	1.17	0.00	0.00	0.35	1.13	6.42	0.00	0.00
		SEM	0.45	0.33	0.42	0.00	0.00	0.12	0.40	2.27	0.00	0.00
42 Days	9	AVERAGE	8.07	2.71	3.54	0.00	0.00	1.83	5.37	65.68	0.00	0.00
		SD	1.08	0.60	0.90	0.00	0.00	0.58	0.96	10.83	0.00	0.00
		SEM	0.36	0.20	0.30	0.00	0.00	0.19	0.32	3.61	0.00	0.00

DBA/2 Histomorphometry Measurements

Time Point	n		TA (mm^2)	B (mm^2)	MA (mm^2)	CA (mm^2)	GT (mm^2)	Void	CALLUS (mm^2)	% MA/CALLUS	% CA/CALLUS	% GT/CALLUS
7 Days	3	AVERAGE	7.67	2.36	0.00	0.21	2.40	2.71	5.31	0.00	4.02	46.56
		SD	1.39	0.32	0.00	0.02	0.37	1.13	1.25	0.00	0.69	10.65
		SEM	0.80	0.19	0.00	0.01	0.22	0.66	0.72	0.00	0.40	6.15
10 Days	4	AVERAGE	8.58	2.75	0.00	1.91	1.91	2.01	5.83	0.00	34.00	32.58
		SD	0.98	0.42	0.00	0.64	0.50	1.20	0.82	0.00	14.44	6.75
		SEM	0.49	0.21	0.00	0.32	0.25	0.60	0.41	0.00	7.22	3.37
14 Days	3	AVERAGE	12.27	2.63	1.90	2.40	1.01	4.33	9.64	21.13	24.05	9.88
		SD	2.42	0.34	0.90	1.17	0.65	1.27	2.08	12.10	6.68	4.16
		SEM	1.40	0.20	0.52	0.68	0.38	0.74	1.20	6.98	3.85	2.40
21 Days	5	AVERAGE	9.21	2.12	4.34	0.51	0.48	1.76	7.09	62.42	6.78	6.41
		SD	1.66	0.48	0.94	0.31	0.29	0.95	1.32	15.62	3.87	3.63
		SEM	0.74	0.21	0.42	0.14	0.13	0.43	0.59	6.99	1.73	1.62
28 Days	4	AVERAGE	7.52	2.46	3.94	0.05	0.00	1.06	5.05	79.42	0.87	0.00
		SD	1.24	0.46	1.75	0.10	0.00	1.40	1.49	26.38	1.74	0.00
		SEM	0.62	0.23	0.88	0.05	0.00	0.70	0.75	13.19	0.87	0.00
42 Days	8	AVERAGE	5.33	1.73	2.70	0.00	0.00	0.90	3.60	76.18	0.00	0.00
		SD	0.64	0.29	0.44	0.00	0.00	0.65	0.58	14.88	0.00	0.00
		SEM	0.23	0.10	0.16	0.00	0.00	0.23	0.20	5.26	0.00	0.00

C57BL/6 Histomorphometry Measurements

Time Point	n		TA (mm^2)	B (mm^2)	MA (mm^2)	CA (mm^2)	GT (mm^2)	Void	CALLUS (mm^2)	% MA/CALLUS	% CA/CALLUS	% GT/CALLUS
7 Days	3	AVERAGE	9.13	2.10	0.56	0.48	4.39	1.60	7.03	8.04	6.82	62.22
		SD	0.82	0.70	0.22	0.04	1.01	0.68	0.23	3.25	0.74	13.33
		SEM	0.48	0.40	0.13	0.03	0.58	0.39	0.13	1.88	0.43	7.70
10 Days	4	AVERAGE	13.38	2.52	1.75	2.02	1.92	5.16	10.86	16.02	18.68	17.57
		SD	0.78	0.51	0.46	0.11	0.54	0.15	0.90	3.51	0.81	3.95
		SEM	0.39	0.26	0.23	0.05	0.27	0.07	0.45	1.76	0.40	1.97
14 Days	5	AVERAGE	15.56	2.54	6.74	1.73	1.08	3.46	13.02	51.26	13.19	8.58
		SD	1.25	0.46	1.65	0.57	0.44	0.53	1.14	8.43	3.49	4.01
		SEM	0.56	0.21	0.74	0.25	0.20	0.24	0.51	3.77	1.56	1.79
21 Days	5	AVERAGE	16.40	2.78	10.54	0.10	0.00	2.99	13.62	76.40	0.82	0.00
		SD	2.58	0.62	3.11	0.13	0.00	0.44	2.82	7.23	1.14	0.00
		SEM	1.15	0.28	1.39	0.06	0.00	0.20	1.26	3.23	0.51	0.00
28 Days	7	AVERAGE	15.44	2.39	9.98	0.00	0.00	3.07	13.05	76.11	0.00	0.00
		SD	1.94	0.24	1.97	0.00	0.00	0.77	1.90	6.60	0.00	0.00
		SEM	0.74	0.09	0.75	0.00	0.00	0.29	0.72	2.49	0.00	0.00
42 Days	9	AVERAGE	12.84	2.37	7.36	0.00	0.00	3.10	10.46	69.76	0.00	0.00
		SD	2.34	0.34	2.08	0.00	0.00	0.86	2.15	9.33	0.00	0.00
		SEM	0.78	0.11	0.70	0.00	0.00	0.29	0.72	3.11	0.00	0.00

Table B3. Statistical Summary for Inbred Mouse Fracture Callus Histomorphometrical Measurements.

7 Day % Mineralized Area (ANOVA p <0.001)				
	ICR	C3H	DBA/2	C57BL/6
ICR	----------	1.000	1.000	<0.001
C3H		----------	1.000	<0.001
DBA/2			----------	<0.001
C57BL/6				----------

7 Day % Cartilage Area (ANOVA p = 0.032)				
	ICR	C3H	DBA/2	C57BL/6
ICR	----------	0.023	0.241	0.749
C3H		----------	0.006	0.082
DBA/2			----------	0.202
C57BL/6				----------

7 Day % Granulation Tissue Area (ANOVA p =0.063)				
	ICR	C3H	DBA/2	C57BL/6
ICR	----------	N/A	N/A	N/A
C3H		----------	N/A	N/A
DBA/2			----------	N/A
C57BL/6				----------

10 Day % Mineralized Area (ANOVA p <0.001)				
	ICR	C3H	DBA/2	C57BL/6
ICR	----------	0.012	0.003	0.002
C3H		----------	0.442	<0.001
DBA/2			----------	<0.001
C57BL/6				----------

10 Day % Cartilage Area (ANOVA p = 0.010)				
	ICR	C3H	DBA/2	C57BL/6
ICR	----------	0.009	0.004	0.382
C3H		----------	0.647	0.048
DBA/2			----------	0.021
C57BL/6				----------

10 Day % Granulation Tissue Area (ANOVA p <0.001)				
	ICR	C3H	DBA/2	C57BL/6
ICR	----------	0.432	0.004	<0.001
C3H		----------	<0.001	<0.001
DBA/2			----------	0.013
C57BL/6				----------

14 Day % Mineralized Area (ANOVA p =0.003)				
	ICR	C3H	DBA/2	C57BL/6
ICR	----------	0.093	0.315	0.002
C3H		----------	0.020	0.059
DBA/2			----------	<0.001
C57BL/6				----------

14 Day % Cartilage Area (ANOVA p <0.001)				
	ICR	C3H	DBA/2	C57BL/6
ICR	----------	0.007	0.002	0.567
C3H		----------	<0.001	0.024
DBA/2			----------	<0.001
C57BL/6				----------

14 Day % Granulation Tissue Area (ANOVA p <0.001)				
	ICR	C3H	DBA/2	C57BL/6
ICR	----------	<0.001	<0.001	<0.001
C3H		----------	0.168	0.238
DBA/2			----------	0.706
C57BL/6				----------

21 Day % Mineralized Area (ANOVA p = 0.111)				
	ICR	C3H	DBA/2	C57BL/6
ICR	----------	N/A	N/A	N/A
C3H		----------	N/A	N/A
DBA/2			----------	N/A
C57BL/6				----------

21 Day % Cartilage Area (ANOVA p <0.001)				
	ICR	C3H	DBA/2	C57BL/6
ICR	----------	0.001	0.264	<0.001
C3H		----------	0.005	0.726
DBA/2			----------	0.002
C57BL/6				----------

21 Day % Granulation Tissue Area (ANOVA p = 0.030				
	ICR	C3H	DBA/2	C57BL/6
ICR	----------	0.047	0.429	0.009
C3H		----------	0.131	0.432
DBA/2			----------	0.023
C57BL/6				----------

28 Day % Mineralized Area (ANOVA p = 0.480)				
	ICR	C3H	DBA/2	C57BL/6
ICR	----------	N/A	N/A	N/A
C3H		----------	N/A	N/A
DBA/2			----------	N/A
C57BL/6				----------

28 Day % Cartilage Area (ANOVA p = 0.216)				
	ICR	C3H	DBA/2	C57BL/6
ICR	----------	N/A	N/A	N/A
C3H		----------	N/A	N/A
DBA/2			----------	N/A
C57BL/6				----------

28 Day % Granulation Tissue Area (ANOVA p = 1.000)				
	ICR	C3H	DBA/2	C57BL/6
ICR	----------	N/A	N/A	N/A
C3H		----------	N/A	N/A
DBA/2			----------	N/A
C57BL/6				----------

42 Day Percent Mineralized Area (ANOVA p = 0.123)				
	ICR	C3H	DBA/2	C57BL/6
ICR	----------	N/A	N/A	N/A
C3H		----------	N/A	N/A
DBA/2			----------	N/A
C57BL/6				----------

42 Day % Cartilage Area (ANOVA p = 1.000)				
	ICR	C3H	DBA/2	C57BL/6
ICR	----------	N/A	N/A	N/A
C3H		----------	N/A	N/A
DBA/2			----------	N/A
C57BL/6				----------

42 Day % Granulation Tissue Area (ANOVA p = 1.000)				
	ICR	C3H	DBA/2	C57BL/6
ICR	----------	N/A	N/A	N/A
C3H		----------	N/A	N/A
DBA/2			----------	N/A
C57BL/6				----------

Table B4. Summary of Inbred Mouse Femur Mechanical Testing Data.

Strain	n		Peak Torque (Nmm)		%P	Area (mm^2)		%A	Polar Moment of Inertia (J)		Gage Length (mm)		Rigidity (Nmm^2/rad)		%R	Shear Modulus (GPa)		%G	Maximum Shear Stress (MPa)		%S
			Left	Right		Left	Right		Left	Right	Left	Right	Left	Right		Left	Right		Left	Right	
ICR	13	Average	44.94	37.19	84.70	2.36	9.59	409.18	0.38	6.21	4.82	5.39	1471.95	1027.75	72.29	3.35	0.15	4.42	118.06	12.88	11.32
		SD	8.68	11.25	25.46	0.27	2.31	96.94	0.10	2.84	0.93	0.99	582.23	492.48	29.14	1.33	0.10	2.40	24.10	4.87	4.39
		SEM	2.41	3.12	7.06	0.08	0.64	26.89	0.03	0.79	0.26	0.27	161.48	136.59	8.08	0.37	0.03	0.67	6.68	1.35	1.22
C3H	11	Average	39.57	21.47	56.21	2.02	7.71	382.26	0.14	4.16	5.33	5.67	1354.40	542.61	43.58	10.63	0.15	1.52	252.67	9.57	3.94
		SD	6.69	3.72	14.90	0.20	1.15	51.83	0.04	1.30	0.95	1.39	433.81	138.90	17.65	5.46	0.07	0.62	48.80	2.82	1.49
		SEM	2.02	1.12	4.49	0.06	0.35	15.63	0.01	0.39	0.29	0.42	130.80	41.88	5.32	1.65	0.02	0.19	14.71	0.85	0.45
DBA/2	11	Average	27.30	19.84	74.08	1.48	6.48	439.31	0.15	2.96	4.47	5.63	905.65	486.21	61.03	6.08	0.20	3.54	158.28	12.72	7.88
		SD	5.41	6.28	24.31	0.11	1.45	101.67	0.02	1.24	1.02	1.50	311.12	186.64	33.23	2.05	0.12	2.19	29.72	6.55	3.49
		SEM	1.63	1.90	7.33	0.03	0.44	30.66	0.01	0.37	0.31	0.45	93.81	56.28	10.02	0.62	0.04	0.66	8.96	1.98	1.05
C57BL/6	11	Average	32.69	31.78	98.11	2.10	8.52	412.18	0.32	4.12	4.27	4.77	980.22	835.28	89.22	3.36	0.22	7.48	99.02	15.18	15.59
		SD	3.81	9.09	29.45	0.26	1.56	93.80	0.08	1.32	0.80	0.81	400.52	344.80	33.75	1.88	0.11	3.93	20.90	6.24	6.36
		SEM	1.15	2.74	8.88	0.08	0.47	28.28	0.02	0.40	0.24	0.25	120.76	103.96	10.18	0.57	0.03	1.18	6.30	1.88	1.92

Table B5. Statistical Summary for Raw and Normalized Inbred Mouse Femur Mechanical Testing Data.

Peak Torque (Nmm) (ANOVA p <0.001)					Peak Torque (Nmm) (p <0.001)					Normalized Mechanical Properties ((Fx/Control)*100)				
LEFT					RIGHT					Normalized Peak Torque (%) (ANOVA p = 0.002)				
	ICR	C3H	DBA/2	C57BL/6		ICR	C3H	DBA/2	C57BL/6		ICR	C3H	DBA/2	C57BL/6
ICR	---	0.051	**<0.001**	**<0.001**	ICR	---	**<0.001**	**<0.001**	0.118	ICR	---	**0.006**	0.290	0.183
C3H		---	**<0.001**	**0.018**	C3H		---	0.647	**0.006**	C3H		---	0.090	**<0.001**
DBA/2			---	0.059	DBA/2			---	**0.002**	DBA/2			---	**0.025**
C57BL/6				---	C57BL/6				---	C57BL/6				---
Rigidity (Nmm^2) (ANOVA p = 0.008)					Rigidity (Nmm^2/rad) (ANOVA p <0.001)					Normalized Rigidity (%) (ANOVA p = 0.006)				
	ICR	C3H	DBA/2	C57BL/6		ICR	C3H	DBA/2	C57BL/6		ICR	C3H	DBA/2	C57BL/6
ICR	---	0.528	**0.004**	**0.011**	ICR	---	**<0.001**	**<0.001**	0.165	ICR	---	**0.021**	0.351	0.164
C3H		---	**0.024**	0.058	C3H		---	0.693	**0.045**	C3H		---	0.168	**<0.001**
DBA/2			---	0.700	DBA/2			---	**0.018**	DBA/2			---	**0.029**
C57BL/6				---	C57BL/6				---	C57BL/6				---
Shear Modulus (GPa) (ANOVA p <0.001)					Shear Modulus (GPa) (ANOVA p = 0.241)					Normalized Shear Modulus (%) (ANOVA p <0.001)				
	ICR	C3H	DBA/2	C57BL/6		ICR	C3H	DBA/2	C57BL/6		ICR	C3H	DBA/2	C57BL/6
ICR	---	**<0.001**	**0.036**	0.997	ICR	---	NA	NA	NA	ICR	---	**0.009**	0.411	**0.006**
C3H		---	**0.001**	**<0.001**	C3H		---	NA	NA	C3H		---	0.071	**<0.001**
DBA/2			---	**0.044**	DBA/2			---	NA	DBA/2			---	**<0.001**
C57BL/6				---	C57BL/6				---	C57BL/6				---
Shear Stress (MPa) (ANOVA p <0.001)					Shear Stress (MPa) (ANOVA p = 0.118)					Normalized Shear Stress (%) (ANOVA p < 0.001)				
	ICR	C3H	DBA/2	C57BL/6		ICR	C3H	DBA/2	C57BL/6		ICR	C3H	DBA/2	C57BL/6
ICR	---	**<0.001**	**0.004**	0.158	ICR	---	NA	NA	NA	ICR	---	**<0.001**	0.058	**0.020**
C3H		---	**<0.001**	**<0.001**	C3H		---	NA	NA	C3H		---	**0.038**	**<0.001**
DBA/2			---	**<0.001**	DBA/2			---	NA	DBA/2			---	**<0.001**
C57BL/6				---	C57BL/6				---	C57BL/6				---

Table B6. Weight Normalized Inbred Mouse Femur Mechanical Testing Data Summary.

Strain	n		Peak Torque (Nmm)/g		Rigidity (Nmm^2)/g		Shear Modulus (MPa)/g		Shear Stress (MPa)/g	
			Left	Right	Left	Right	Left	Right	Left	Right
ICR	13	Average	1.19	0.99	38.23	27.20	88.51	4.09	3.15	0.34
		SD	0.27	0.32	13.05	13.33	36.63	2.92	0.80	0.14
		SEM	0.07	0.09	3.62	3.70	10.16	0.81	0.22	0.04
C3H	11	Average	1.36	0.74	47.01	18.88	373.73	5.08	8.74	0.33
		SD	0.19	0.15	16.38	5.39	212.43	2.42	1.88	0.10
		SEM	0.06	0.05	4.94	1.62	64.05	0.73	0.57	0.03
DBA/2	11	Average	1.04	0.76	34.67	18.72	234.38	7.75	6.05	0.48
		SD	0.24	0.26	13.27	7.65	92.66	4.49	1.39	0.23
		SEM	0.07	0.08	4.00	2.31	27.94	1.35	0.42	0.07
C57BL/6	11	Average	1.05	1.00	31.65	27.19	108.66	7.10	3.18	0.48
		SD	0.20	0.26	14.34	13.08	65.77	3.79	0.84	0.18
		SEM	0.06	0.08	4.33	3.95	19.83	1.14	0.25	0.05

Table B7. Statistical Summary for Weight Normalized Inbred Mouse Femur Mechanical Testing.

LEFT					RIGHT				
Peak Torque/ Weight (Nmm/g) (ANOVA p = 0.007)					Peak Torque/ Weight (Nmm/g) (ANOVA p = 0.025)				
	ICR	C3H	DBA/2	C57BL/6		ICR	C3H	DBA/2	C57BL/6
ICR	----------	0.082	0.117	0.141	ICR	----------	**0.027**	**0.035**	0.867
C3H		----------	**0.002**	0.010	C3H		----------	0.907	**0.022**
DBA/2			----------	0.922	DBA/2			----------	**0.030**
C57BL/6				----------	C57BL/6				----------
Rigidity/ Weight (N/mm^{2}g) (ANOVA p = 0.082)					Rigidity/ Weight (N/mm^{2}g) (ANOVA p = 0.081)				
	ICR	C3H	DBA/2	C57BL/6		ICR	C3H	DBA/2	C57BL/6
ICR	----------	NA	NA	NA	ICR	----------	NA	NA	NA
C3H		----------	NA	NA	C3H		----------	NA	NA
DBA/2			----------	NA	DBA/2			----------	NA
C57BL/6				----------	C57BL/6				----------
Shear Modulus/ Weight (GPa/g) (ANOVA p <0.001)					Shear Modulus/ Weight (GPa/g) (ANOVA p = 0.048)				
	ICR	C3H	DBA/2	C57BL/6		ICR	C3H	DBA/2	C57BL/6
ICR	----------	**<0.001**	**0.005**	0.682	ICR	----------	0.491	**0.014**	**0.040**
C3H		----------	**0.009**	**<0.001**	C3H		----------	0.078	0.178
DBA/2			----------	**0.017**	DBA/2			----------	0.666
C57BL/6				----------	C57BL/6				----------
Shear Stress/ Weight (MPa/g) (ANOVA p <0.001)					Shear Stress/ Weight (MPa/g) (ANOVA p = 0.060)				
	ICR	C3H	DBA/2	C57BL/6		ICR	C3H	DBA/2	C57BL/6
ICR	----------	**<0.001**	**<0.001**	0.950	ICR	----------	NA	NA	NA
C3H		----------	**<0.001**	**<0.001**	C3H		----------	NA	NA
DBA/2			----------	**<0.001**	DBA/2			----------	NA
C57BL/6				----------	C57BL/6				----------

Table B8. Summary of Inbred Mouse Femur Mechanical Testing Data Normalized to Femur Cross-Sectional Area.

Strain	n		Peak Torque (N/mm^2)		Rigidity (N/mm^4)		Shear Modulus (GPa/mm^2)		Shear Stress (MPa/mm^2)	
			Left	Right	Left	Right	Left	Right	Left	Right
ICR	13	Average	19.15	4.07	446.89	115.24	1.46	0.02	51.37	1.48
		SD	3.37	1.42	239.59	65.86	0.71	0.01	14.52	0.77
		SEM	0.93	0.39	66.45	18.27	0.20	0.00	4.03	0.21
C3H	11	Average	19.54	2.83	683.43	72.72	5.52	0.02	127.46	1.31
		SD	2.70	0.60	250.77	25.39	3.38	0.01	34.32	0.57
		SEM	0.81	0.18	75.61	7.65	1.02	0.00	10.35	0.17
DBA/2	11	Average	18.46	3.30	611.20	81.82	4.15	0.04	107.80	2.21
		SD	3.42	1.51	200.59	40.56	1.44	0.03	22.05	1.54
		SEM	1.03	0.46	60.48	12.23	0.44	0.01	6.65	0.46
C57BL/6	11	Average	15.81	3.90	482.33	100.92	1.68	0.03	48.65	1.92
		SD	2.69	1.52	232.45	44.20	1.07	0.02	14.39	1.05
		SEM	0.81	0.46	70.09	13.33	0.32	0.01	4.34	0.32

Table B9. Statistical Summary for Cross-Sectional Area Normalized Inbred Mouse Femur Mechanical Testing.

LEFT					RIGHT				
Peak Torque/ Area (N/mm^2) (ANOVA p = 0.028)					Peak Torque/ Area (N/mm^2) (ANOVA p = 0.112)				
	ICR	C3H	DBA/2	C57BL/6		ICR	C3H	DBA/2	C57BL/6
ICR	----------	0.761	0.588	**0.011**	ICR	----------	NA	NA	NA
C3H		----------	0.418	**0.009**	C3H		----------	NA	NA
DBA/2			----------	**0.050**	DBA/2			----------	NA
C57BL/6				----------	C57BL/6				----------
Rigidity/ Area (N/mm^4) (ANOVA p = 0.062)					Rigidity/ Area (N/mm^4) (ANOVA p = 0.140)				
	ICR	C3H	DBA/2	C57BL/6		ICR	C3H	DBA/2	C57BL/6
ICR	----------	NA	NA	NA	ICR	----------	NA	NA	NA
C3H		----------	NA	NA	C3H		----------	NA	NA
DBA/2			----------	NA	DBA/2			----------	NA
C57BL/6				----------	C57BL/6				----------
Shear Modulus/ Area (GPa/mm^2) (ANOVA p <0.001)					Shear Modulus/ Area (GPa/mm^2) (ANOVA p = 0.099)				
	ICR	C3H	DBA/2	C57BL/6		ICR	C3H	DBA/2	C57BL/6
ICR	----------	**<0.001**	**0.001**	0.780	ICR	----------	NA	NA	NA
C3H		----------	0.099	**<0.001**	C3H		----------	NA	NA
DBA/2			----------	**0.004**	DBA/2			----------	NA
C57BL/6				----------	C57BL/6				----------
Shear Stress/ Area (MPa/mm^2) (ANOVA p <0.001)					Shear Stress/ Area (MPa/mm^2) (ANOVA p = 0.164)				
	ICR	C3H	DBA/2	C57BL/6		ICR	C3H	DBA/2	C57BL/6
ICR	----------	**<0.001**	**<0.001**	0.769	ICR	----------	NA	NA	NA
C3H		----------	**0.047**	**<0.001**	C3H		----------	NA	NA
DBA/2			----------	**<0.001**	DBA/2			----------	NA
C57BL/6				----------	C57BL/6				----------

Table B10. Summary of Inbred Mouse Femur Mechanical Testing Data Normalized to Bone Mineral Density.

Strain	n		Peak Torque (Nmm)/(g/cm^2))		Rigidity (N/mm)/(g/cm^2)		Shear Modulus (GPa)/(g/cm^2)		Shear Stress (MPa)/(g/cm^2)	
			Left	Right	Left	Right	Left	Right	Left	Right
C3H	11	Average	47.67	25.87	1631.80	653.75	12.81	176.17	304.42	11.53
		SD	8.06	4.48	522.66	167.35	6.58	83.84	58.79	3.40
		SEM	2.43	1.35	157.59	50.46	1.98	25.28	17.73	1.03
DBA/2	11	Average	47.07	34.21	1561.47	838.30	10.49	350.73	272.89	21.93
		SD	9.32	10.83	536.42	321.80	3.54	211.80	51.24	11.30
		SEM	2.81	3.27	161.74	97.03	1.07	63.86	15.45	3.41
C57BL/6	11	Average	72.66	70.62	2178.27	1856.18	7.46	491.31	220.05	33.72
		SD	8.47	20.20	890.05	766.21	4.18	247.88	46.44	13.87
		SEM	2.55	6.09	268.36	231.02	1.26	74.74	14.00	4.18

Table B11. Statistical Summary for Bone Mineral Density Normalized Inbred Mechanical Testing.

LEFT				RIGHT			
Peak Torque/BMD (Nmm)/(g/cm^2) (ANOVA p <0.001)				**Peak Torque/BMD (Nmm)/(g/cm^2) (ANOVA p <0.001)**			
	C3H	DBA/2	C57BL/6		C3H	DBA/2	C57BL/6
C3H	----------	0.872	**<0.001**	C3H	----------	0.157	**<0.001**
DBA/2		----------	**<0.001**	DBA/2		----------	**<0.001**
C57BL/6			----------	C57BL/6			----------
Rigidity (Nmm^2)/(g/cm2) (ANOVA p = 0.078)				**Rigidity (Nmm2)/(g/cm2) (ANOVA p <0.001)**			
	C3H	DBA/2	C57BL/6		C3H	DBA/2	C57BL/6
C3H	----------	NA	NA	C3H	----------	0.384	**<0.001**
DBA/2		----------	NA	DBA/2		----------	**<0.001**
C57BL/6			----------	C57BL/6			----------
Shear Modulus (GPa)/(g/cm^2) (ANOVA p = 0.053)				**Shear Modulus (GPa)/(g/cm2) (ANOVA p = 0.003)**			
	C3H	DBA/2	C57BL/6		C3H	DBA/2	C57BL/6
C3H	----------	NA	NA	C3H	----------	**0.044**	**<0.001**
DBA/2		----------	NA	DBA/2		----------	0.100
C57BL/6			----------	C57BL/6			----------
Shear Stress (MPa)/(g/cm^2) (ANOVA p = 0.003)				**Shear Stress (MPa)/(g/cm^2) (ANOVA p <0.001)**			
	C3H	DBA/2	C57BL/6		C3H	DBA/2	C57BL/6
C3H	----------	0.169	**<0.001**	C3H	----------	**0.027**	**<0.001**
DBA/2		----------	**0.025**	DBA/2		----------	**0.013**
C57BL/6			----------	C57BL/6			----------

Table B12. Cox-1KO Mouse Fracture Callus Histomorphometry Measurements.

Time Point	n		TA (mm^2)	B (mm^2)	MA (mm^2)	CA (mm^2)	GT (mm^2)	Void	CALLUS (mm^2)	% MA/CALLUS	% CA/CALLUS	% GT/CALLUS
7 Days	4	AVERAGE	9.49	2.67	0.45	0.45	3.14	2.77	6.82	6.82	6.60	47.02
		SD	1.19	0.36	0.20	0.13	0.89	1.18	1.21	3.09	0.92	16.13
		SEM	0.59	0.18	0.10	0.06	0.45	0.59	0.60	1.55	0.46	8.07
10 Days	4	AVERAGE	14.35	3.16	2.92	1.97	3.56	2.74	11.19	25.80	17.74	31.63
		SD	0.85	0.63	1.03	0.52	0.76	0.93	0.96	7.30	5.22	4.68
		SEM	0.43	0.32	0.52	0.26	0.38	0.46	0.48	3.65	2.61	2.34
14 Days	3	AVERAGE	16.92	4.00	5.20	1.96	1.45	4.31	12.93	40.38	14.99	11.27
		SD	1.78	0.44	0.40	0.86	0.08	0.82	1.48	2.12	5.75	0.84
		SEM	1.03	0.26	0.23	0.50	0.05	0.47	0.86	1.22	3.32	0.49
21 Days	4	AVERAGE	15.37	3.08	7.70	0.00	0.00	4.59	12.29	62.29	0.00	0.00
		SD	1.92	0.37	1.74	0.00	0.00	0.56	2.26	3.21	0.00	0.00
		SEM	0.96	0.19	0.87	0.00	0.00	0.28	1.13	1.60	0.00	0.00
28 Days	4	AVERAGE	10.55	2.32	4.81	0.00	0.00	3.41	8.23	57.83	0.00	0.00
		SD	1.21	0.12	1.38	0.00	0.00	0.72	1.17	10.34	0.00	0.00
		SEM	0.60	0.06	0.69	0.00	0.00	0.36	0.58	5.17	0.00	0.00
42 Days	3	AVERAGE	10.88	2.29	4.06	0.00	0.00	4.52	8.58	47.76	0.00	0.00
		SD	1.90	0.42	0.48	0.00	0.00	1.08	1.49	4.33	0.00	0.00
		SEM	1.10	0.24	0.28	0.00	0.00	0.62	0.86	2.50	0.00	0.00
84 Days	4	AVERAGE	8.87	2.10	3.42	0.00	0.00	3.36	6.77	50.60	0.00	0.00
		SD	2.03	0.25	1.67	0.00	0.00	1.58	2.24	14.55	0.00	0.00
		SEM	1.02	0.13	0.83	0.00	0.00	0.79	1.12	7.27	0.00	0.00

Table B13. Cox-2KO Mouse Fracture Callus Histomorphometry Measurements.

Time Point	n		TA (mm^2)	B (mm^2)	MA (mm^2)	CA (mm^2)	GT (mm^2)	Void	CALLUS (mm^2)	% MA/CALLUS	% CA/CALLUS	% GT/CALLUS
7 Days	3	AVERAGE	8.90	2.03	0.00	0.20	4.63	2.03	6.87	0.00	2.97	67.42
		SD	0.27	0.11	0.00	0.08	0.57	0.56	0.19	0.00	1.21	7.81
		SEM	0.16	0.06	0.00	0.05	0.33	0.32	0.11	0.00	0.70	4.51
10 Days	5	AVERAGE	11.01	3.12	0.52	0.86	3.68	2.83	7.89	6.64	10.99	46.54
		SD	1.56	0.80	0.59	0.48	1.79	1.48	1.76	7.00	5.54	18.62
		SEM	0.70	0.36	0.26	0.21	0.80	0.66	0.79	3.13	2.48	8.33
14 Days	3	AVERAGE	12.39	2.68	2.67	0.89	3.28	2.87	9.71	27.41	8.88	33.74
		SD	1.41	1.02	1.30	0.61	0.77	0.63	0.80	13.13	5.49	7.26
		SEM	0.82	0.59	0.75	0.35	0.45	0.36	0.46	7.58	3.17	4.19
21 Days	4	AVERAGE	14.50	2.93	5.59	0.49	1.93	3.57	11.57	48.66	4.26	16.94
		SD	2.01	0.66	0.81	0.18	0.20	1.46	1.49	7.62	1.61	3.15
		SEM	1.00	0.33	0.41	0.09	0.10	0.73	0.75	3.81	0.81	1.58
28 Days	4	AVERAGE	12.89	2.56	5.92	0.09	1.23	3.09	10.33	58.01	1.03	12.12
		SD	1.52	0.53	1.22	0.18	1.19	1.52	1.55	13.86	2.06	12.25
		SEM	0.76	0.26	0.61	0.09	0.60	0.76	0.78	6.93	1.03	6.12
42 Days	4	AVERAGE	12.34	1.96	6.09	0.18	0.54	3.57	10.38	60.24	1.40	4.24
		SD	1.80	0.23	0.91	0.36	1.08	0.92	1.61	14.61	2.80	8.49
		SEM	0.90	0.12	0.46	0.18	0.54	0.46	0.80	7.30	1.40	4.25
84 Days	4	AVERAGE	7.63	1.73	3.36	0.00	0.00	2.53	5.89	57.97	0.00	0.00
		SD	1.73	0.46	0.36	0.00	0.00	0.96	1.30	6.00	0.00	0.00
		SEM	0.87	0.23	0.18	0.00	0.00	0.48	0.65	3.00	0.00	0.00

Table B14. Cox-2HET Mouse Fracture Callus Histomorphometry Measurements.

Time Point	n		TA (mm^2)	B (mm^2)	MA (mm^2)	CA (mm^2)	GT (mm^2)	Void	CALLUS (mm^2)	% MA/CALLUS	% CA/CALLUS	% GT/CALLUS
7 Days	4	AVERAGE	9.06	2.24	0.47	0.63	1.72	4.00	6.82	7.03	9.28	25.38
		SD	1.02	0.19	0.09	0.07	0.48	0.94	1.09	2.16	0.82	6.71
		SEM	0.51	0.09	0.04	0.04	0.24	0.47	0.55	1.08	0.41	3.35
10 Days	7	AVERAGE	14.72	3.79	1.90	2.38	3.56	3.09	10.94	17.88	21.78	31.99
		SD	2.74	0.56	0.87	0.81	1.42	0.82	2.81	7.23	4.27	7.30
		SEM	1.03	0.21	0.33	0.31	0.54	0.32	1.06	2.73	1.61	2.76
14 Days	5	AVERAGE	14.04	2.59	5.50	1.26	1.57	3.12	11.45	48.07	10.92	14.22
		SD	1.10	0.66	1.26	0.56	0.69	0.99	1.46	9.22	4.56	6.41
		SEM	0.49	0.30	0.57	0.25	0.31	0.44	0.65	4.12	2.04	2.87
21 Days	3	AVERAGE	15.65	3.10	9.06	0.00	0.04	3.46	12.56	72.40	0.00	0.37
		SD	1.03	0.63	1.28	0.00	0.07	1.23	1.66	7.92	0.00	0.65
		SEM	0.59	0.36	0.74	0.00	0.04	0.71	0.96	4.57	0.00	0.38
28 Days	7	AVERAGE	13.14	2.65	6.30	0.14	0.19	3.85	10.48	60.24	1.36	1.89
		SD	1.44	0.28	1.05	0.22	0.33	1.03	1.63	6.56	1.96	3.42
		SEM	0.55	0.11	0.40	0.08	0.13	0.39	0.62	2.48	0.74	1.29
42 Days	5	AVERAGE	9.04	1.68	4.65	0.00	0.00	2.71	7.36	62.38	0.00	0.00
		SD	1.84	0.44	1.47	0.00	0.00	0.43	1.57	6.97	0.00	0.00
		SEM	0.82	0.20	0.66	0.00	0.00	0.19	0.70	3.12	0.00	0.00
84 Days	7	AVERAGE	8.60	1.46	2.88	0.00	0.00	4.26	7.14	39.02	0.00	0.00
		SD	1.44	0.17	1.14	0.00	0.00	0.61	1.43	10.03	0.00	0.00
		SEM	0.54	0.06	0.43	0.00	0.00	0.23	0.54	3.79	0.00	0.00

Table B15. Cox-2WT Mouse Fracture Callus Histomorphometry Measurements.

Time Point	n		TA (mm^2)	B (mm^2)	MA (mm^2)	CA (mm^2)	GT (mm^2)	Void	CALLUS (mm^2)	% MA/CALLUS	% CA/CALLUS	% GT/CALLUS
7 Days	5	AVERAGE	8.96	2.36	0.55	0.59	1.27	4.20	6.60	8.10	9.38	19.84
		SD	1.03	0.36	0.22	0.21	0.49	1.26	1.26	2.22	4.22	9.00
		SEM	0.46	0.16	0.10	0.09	0.22	0.56	0.56	0.99	1.89	4.03
10 Days	3	AVERAGE	15.20	2.36	2.73	2.40	2.22	5.50	12.84	21.07	18.62	17.29
		SD	0.69	0.26	1.25	1.34	0.01	0.76	0.49	9.23	10.12	0.73
		SEM	0.40	0.15	0.72	0.78	0.00	0.44	0.28	5.33	5.84	0.42
14 Days	5	AVERAGE	16.57	2.91	7.18	1.38	0.99	4.12	13.67	50.43	10.58	7.81
		SD	2.71	0.91	3.25	0.43	0.58	0.29	2.91	14.56	4.65	5.41
		SEM	1.21	0.41	1.46	0.19	0.26	0.13	1.30	6.51	2.08	2.42
21 Days	4	AVERAGE	16.18	2.50	9.54	0.21	0.00	3.93	13.68	69.75	1.20	0.00
		SD	2.94	0.22	2.56	0.42	0.00	1.38	3.10	7.45	2.41	0.00
		SEM	1.47	0.11	1.28	0.21	0.00	0.69	1.55	3.73	1.20	0.00
28 Days	6	AVERAGE	12.69	2.55	6.31	0.00	0.00	3.83	10.14	62.05	0.00	0.00
		SD	1.71	0.63	1.64	0.00	0.00	1.07	1.74	9.57	0.00	0.00
		SEM	0.70	0.26	0.67	0.00	0.00	0.44	0.71	3.91	0.00	0.00
42 Days	3	AVERAGE	8.59	1.45	2.79	0.00	0.00	4.35	7.14	39.04	0.00	0.00
		SD	0.33	0.26	0.62	0.00	0.00	0.61	0.18	8.38	0.00	0.00
		SEM	0.19	0.15	0.36	0.00	0.00	0.35	0.11	4.84	0.00	0.00
84 Days	3	AVERAGE	8.72	1.44	2.96	0.00	0.00	4.32	7.28	39.71	0.00	0.00
		SD	1.85	0.25	1.16	0.00	0.00	0.78	1.78	8.63	0.00	0.00
		SEM	1.07	0.15	0.67	0.00	0.00	0.45	1.03	4.98	0.00	0.00

Table B16. Summary of Cyclooxygenase Deficient Mouse Femur Mechanical Testing Data.

	Strain	n		Peak Torque (Nmm)		%P	Area (mm^2)		%A	Polar Moment of Inertia (J)		Gage Length (mm)		Rigidity (Nmm^2)		%R	Shear Modulus (GPa)		%G	Shear Stress (MPa)		%S
				Left	Right		Left	Right		Left	Right	Left	Right	Left	Right		Left	Right		Left	Right	
28 Days	Cox-1KO	11	Average	37.73	26.87	80.85	1.55	5.84	377.66	0.17	2.25	4.34	4.37	1042.80	629.58	67.47	6.30	0.31	5.53	179.31	18.99	11.64
			SD	11.97	7.74	38.48	0.11	1.05	75.57	0.03	0.74	0.67	0.83	586.46	278.12	35.02	3.62	0.17	3.65	48.82	6.02	5.28
			SEM	3.61	2.34	11.60	0.03	0.32	22.78	0.01	0.22	0.20	0.25	176.82	83.86	10.56	1.09	0.05	1.10	14.72	1.81	1.59
	Cox-2WT	9	Average	39.21	30.32	77.38	1.36	6.49	477.51	0.12	2.74	4.90	4.28	1134.61	711.16	67.41	9.64	0.29	3.52	239.71	19.72	8.19
			SD	2.88	5.78	13.45	0.11	1.42	88.91	0.02	1.07	0.92	0.92	201.95	296.48	39.04	2.86	0.16	2.72	29.90	7.04	2.77
			SEM	0.96	1.93	4.48	0.04	0.47	29.64	0.01	0.36	0.31	0.31	67.32	98.83	13.01	0.95	0.05	0.91	9.97	2.35	0.92
	Cox-2HET	10	Average	41.10	33.65	85.18	1.61	7.46	463.53	0.18	3.48	4.46	5.01	1075.93	900.97	88.75	6.08	0.26	4.57	186.66	17.81	9.60
			SD	8.48	8.45	28.95	0.11	0.94	53.81	0.03	0.73	0.79	0.76	280.93	364.39	42.69	1.62	0.10	2.11	44.34	6.72	2.61
			SEM	2.68	2.67	9.15	0.04	0.30	17.02	0.01	0.23	0.25	0.24	88.84	115.23	13.50	0.51	0.03	0.67	14.02	2.12	0.83
	Cox-2KO	9	Average	37.35	12.10	35.64	1.46	7.11	483.96	0.14	3.20	4.16	4.85	849.89	172.33	22.63	5.83	0.07	1.19	198.05	7.06	3.65
			SD	10.94	5.00	20.82	0.15	1.83	103.32	0.03	1.44	0.46	0.83	363.18	60.99	10.13	1.88	0.05	0.70	51.71	4.32	2.00
			SEM	3.65	1.67	6.94	0.05	0.61	34.44	0.01	0.48	0.15	0.28	121.06	20.33	3.38	0.63	0.02	0.23	17.24	1.44	0.67

	Strain	n		Peak Torque (Nmm)		%P	Area (mm^2)		%A	Polar Moment of Inertia (J)		Gage Length (mm)		Rigidity (Nmm^2)		%R	Shear Modulus (GPa)		%G	Shear Stress (MPa)		%S
				Left	Right		Left	Right		Left	Right	Left	Right	Left	Right		Left	Right		Left	Right	
84 Days	Cox-1KO	13	Average	33.77	30.14	91.48	1.57	3.14	200.39	0.17	0.78	5.00	4.36	836.50	990.22	137.70	4.98	1.75	45.77	160.82	54.61	36.72
			SD	6.08	7.47	25.09	0.10	0.99	61.64	0.02	0.49	0.92	0.61	296.37	268.69	68.04	1.78	1.09	44.16	34.67	20.13	19.44
			SEM	1.69	2.07	6.96	0.03	0.28	17.10	0.01	0.14	0.26	0.17	82.20	74.52	18.87	0.49	0.30	12.25	9.62	5.58	5.39
	Cox-2WT	10	Average	32.45	31.91	97.72	1.55	3.52	227.50	0.17	1.00	4.70	4.69	920.89	817.56	98.49	6.04	1.00	19.72	155.39	48.60	31.70
			SD	7.99	10.00	15.31	0.19	1.10	63.79	0.04	0.72	0.74	0.79	359.30	309.54	46.31	2.86	0.53	13.57	28.86	18.21	10.73
			SEM	2.53	3.16	4.84	0.06	0.35	20.17	0.01	0.23	0.23	0.25	113.62	97.89	14.65	0.91	0.17	4.29	9.13	5.76	3.39
	Cox-2HET	14	Average	31.07	27.27	89.41	1.54	3.32	215.96	0.16	0.85	4.63	4.77	925.13	829.50	98.53	6.22	1.19	21.30	155.98	45.62	29.94
			SD	5.64	5.03	18.32	0.21	0.82	45.18	0.05	0.40	0.98	1.03	331.73	259.17	39.54	3.10	0.63	13.29	46.80	17.90	9.40
			SEM	1.51	1.34	4.90	0.06	0.22	12.08	0.01	0.11	0.26	0.27	88.66	69.27	10.57	0.83	0.17	3.55	12.51	4.79	2.51
	Cox-2KO	8	Average	28.42	27.64	101.12	1.55	3.59	233.41	0.17	0.94	4.59	4.37	834.45	614.97	74.83	4.99	0.68	14.09	139.48	39.66	31.06
			SD	7.56	6.66	29.40	0.21	0.73	47.52	0.05	0.36	0.43	0.46	323.68	308.58	25.50	1.28	0.31	6.36	42.77	14.90	16.81
			SEM	2.68	2.35	10.40	0.08	0.26	16.80	0.02	0.13	0.15	0.16	114.44	109.10	9.02	0.45	0.11	2.25	15.12	5.27	5.94

Table B17. 5-LOKO and 5-LOWT Mouse Fracture Callus Histomorphometry Measurements.

5-LOKO Histomorphometry Measurements												
Time Point	n		TA (mm^2)	B (mm^2)	MA (mm^2)	CA (mm^2)	GT (mm^2)	Void	CALLUS (mm^2)	% MA/CALLUS	% CA/CALLUS	% GT/CALLUS
7 Days	5	AVERAGE	12.70	2.22	2.57	3.22	1.31	3.37	10.47	24.56	30.84	12.48
		SD	0.54	0.30	0.31	0.28	0.37	0.50	0.42	3.33	3.46	3.29
		SEM	0.24	0.13	0.14	0.13	0.17	0.22	0.19	1.49	1.55	1.47
10 Days	5	AVERAGE	12.73	1.68	5.25	1.57	0.54	3.69	11.05	47.57	14.46	4.93
		SD	1.27	0.31	0.57	0.79	0.09	1.05	1.26	2.86	7.53	1.01
		SEM	0.57	0.14	0.25	0.35	0.04	0.47	0.56	1.28	3.37	0.45
14 Days	5	AVERAGE	14.74	2.31	6.38	0.35	0.00	5.71	12.43	51.46	2.73	0.00
		SD	1.09	0.54	0.65	0.49	0.00	1.20	1.22	5.38	3.71	0.00
		SEM	0.49	0.24	0.29	0.22	0.00	0.54	0.55	2.41	1.66	0.00
21 Days	5	AVERAGE	11.68	1.66	7.59	0.00	0.00	2.43	10.02	75.72	0.00	0.00
		SD	1.02	0.36	0.79	0.00	0.00	0.34	0.98	2.55	0.00	0.00
		SEM	0.46	0.16	0.36	0.00	0.00	0.15	0.44	1.14	0.00	0.00

5-LOWT Histomorphometry Measurements												
Time Point	n		TA (mm2)	B (mm2)	MA (mm2)	CA (mm2)	GT (mm2)	Void	CALLUS (mm2)	% MA/CALLUS	% CA/CALLUS	% GT/CALLUS
7 Days	5	AVERAGE	11.71	2.77	1.18	0.72	3.81	3.24	8.94	12.89	7.84	43.75
		SD	2.17	0.44	0.46	0.26	1.11	1.25	1.96	3.76	1.31	14.36
		SEM	0.97	0.20	0.21	0.12	0.50	0.56	0.88	1.68	0.59	6.42
10 Days	5	AVERAGE	14.47	2.75	4.16	2.35	2.09	3.13	11.72	35.49	20.16	17.60
		SD	0.99	0.86	1.17	0.67	1.04	0.55	0.78	9.67	6.13	7.95
		SEM	0.44	0.38	0.53	0.30	0.47	0.24	0.35	4.32	2.74	3.56
14 Days	5	AVERAGE	16.26	2.04	6.33	0.53	0.11	7.24	14.21	44.66	3.63	0.85
		SD	1.36	0.21	1.04	0.23	0.17	1.15	1.26	7.14	1.37	1.28
		SEM	0.61	0.09	0.46	0.10	0.08	0.51	0.56	3.19	0.61	0.57
21 Days	5	AVERAGE	13.22	2.19	8.49	0.00	0.00	2.54	11.03	77.26	0.00	0.00
		SD	0.77	0.32	0.52	0.00	0.00	0.88	0.89	6.26	0.00	0.00
		SEM	0.35	0.14	0.23	0.00	0.00	0.40	0.40	2.80	0.00	0.00

Table B18. Summary of 5-LOKO and 5-LOWT Mouse Femur Mechanical Testing Data.

	Strain	n		Peak Torque (Nmm)		%P	Area (mm^2)		%A	Polar Moment of Inertia (J)		Gage Length (mm)		Rigidity (Nmm^2)		%R	Shear Modulus (GPa)		%G	Shear Stress (MPa)		%S
				Left	Right		Left	Right		Left	Right	Left	Right	Left	Right		Left	Right		Left	Right	
28 Days	5-LOKO	11	Average	24.84	28.56	115.49	1.49	4.56	308.37	0.16	1.29	4.26	4.14	687.80	614.77	91.52	4.24	0.52	12.88	126.37	34.50	28.15
			SD	4.94	6.30	16.32	0.09	0.93	71.42	0.02	0.42	0.54	0.44	168.48	191.80	25.37	1.02	0.22	6.30	27.69	8.96	8.20
			SEM	1.49	1.90	4.92	0.03	0.28	21.53	0.01	0.13	0.16	0.13	50.80	57.83	7.65	0.31	0.06	1.90	8.35	2.70	2.47
	WT	11	Average	31.89	29.63	94.64	1.63	5.57	344.06	0.20	1.79	4.69	4.58	819.41	490.94	63.59	4.24	0.30	7.48	143.59	26.96	19.46
			SD	5.00	5.58	23.33	0.12	1.09	73.72	0.03	0.57	0.48	0.44	200.11	175.06	26.44	1.03	0.12	3.51	29.91	6.59	6.53
			SEM	1.51	1.68	7.04	0.04	0.33	22.23	0.01	0.17	0.14	0.13	60.34	52.78	7.97	0.31	0.04	1.06	9.02	1.99	1.97
84 Days	5-LOKO	8	Average	23.84	24.97	107.90	1.40	2.85	204.19	0.14	0.58	4.94	4.53	645.22	492.57	81.12	4.53	0.94	21.91	129.58	53.28	43.06
			SD	5.66	3.51	21.38	0.07	0.41	33.44	0.02	0.14	0.52	0.32	156.87	116.15	30.28	0.82	0.44	12.34	29.40	12.24	12.86
			SEM	2.00	1.24	7.56	0.03	0.15	11.82	0.01	0.05	0.18	0.11	55.46	41.07	10.71	0.29	0.15	4.36	10.40	4.33	4.90
	WT	11	Average	37.19	29.72	83.92	1.71	3.96	233.14	0.21	1.03	4.65	4.35	784.48	756.95	98.63	3.75	0.80	23.29	155.96	43.78	30.25
			SD	8.39	4.90	22.90	0.11	0.92	57.14	0.03	0.40	0.61	0.63	208.16	184.49	21.01	1.18	0.24	8.99	37.43	14.33	12.33
			SEM	2.53	1.48	6.91	0.03	0.28	17.23	0.01	0.12	0.18	0.19	62.76	55.63	6.33	0.36	0.07	2.71	11.29	4.32	3.72

References

1. Cho TJ, Gerstenfeld LC, Einhorn TA 2002 Differential temporal expression of members of the transforming growth factor beta superfamily during murine fracture healing. J Bone Miner Res 17(3):513-20.
2. Einhorn TA 1998 The cell and molecular biology of fracture healing. Clin Orthop (355 Suppl):S7-21.
3. Reddi AH 2001 Bone morphogenetic proteins: from basic science to clinical applications. J Bone Joint Surg Am 83-A Suppl 1(Pt 1):S1-6.
4. Sandberg MM, Aro HT, Vuorio EI 1993 Gene expression during bone repair. Clin Orthop Relat Res (289):292-312.
5. Greenbaum MA, Kanat IO 1993 Current concepts in bone healing. Review of the literature. J Am Podiatr Med Assoc 83(3):123-9.
6. Crenshaw A 1992 General principles of fracture treatment. In: Crenshaw A (ed.) Campbell's Operative Orthopaedics, 8th ed. Mosby-Year Book, St. Louis.
7. McKibbin B 1978 The biology of fracture healing in long bones. J Bone Joint Surg Br 60-B(2):150-62.
8. Cruess R, Dumont J 1975 Healing of Bone, Tendon and Ligament. In: Rockwood C, Green D (eds.) Fractures. J.B. Lippincott, Philadelphia, pp 97.
9. Frost HM 1989 The biology of fracture healing. An overview for clinicians. Part I. Clin Orthop (248):283-93.
10. Brighton CT, Hunt RM 1991 Early histological and ultrastructural changes in medullary fracture callus. J Bone Joint Surg Am 73(6):832-47.
11. Bolander ME 1992 Regulation of fracture repair by growth factors. Proc Soc Exp Biol Med 200(2):165-70.
12. Einhorn TA, Majeska RJ, Rush EB, Levine PM, Horowitz MC 1995 The expression of cytokine activity by fracture callus. J Bone Miner Res 10(8):1272-81.
13. Mizuno K, Mineo K, Tachibana T, Sumi M, Matsubara T, Hirohata K 1990 The osteogenetic potential of fracture haematoma. Subperiosteal and intramuscular transplantation of the haematoma. J Bone Joint Surg Br 72(5):822-9.
14. Fisher LW, Termine JD 1985 Noncollagenous proteins influencing the local mechanisms of calcification. Clin Orthop Relat Res (200):362-85.
15. Einhorn TA, Trippel SB 1997 Growth factor treatment of fractures. Instr Course Lect 46:483-6.
16. Jingushi S, Joyce ME, Bolander ME 1992 Genetic expression of extracellular matrix proteins correlates with histologic changes during fracture repair. J Bone Miner Res 7(9):1045-55.
17. Topping RE, Bolander ME, Balian G 1994 Type X collagen in fracture callus and the effects of experimental diabetes. Clin Orthop Relat Res (308):220-8.

18. Becker RO, Murray DG 1967 A method for producing cellular dedifferentiation by means of very small electrical currents. Trans N Y Acad Sci 29(5):606-15.
19. Einhorn TA, Hirschman A, Kaplan C, Nashed R, Devlin VJ, Warman J 1989 Neutral protein-degrading enzymes in experimental fracture callus: a preliminary report. J Orthop Res 7(6):792-805.
20. Barnes GL, Kostenuik PJ, Gerstenfeld LC, Einhorn TA 1999 Growth factor regulation of fracture repair. J Bone Miner Res 14(11):1805-15.
21. Steinbrech DS, Mehrara BJ, Saadeh PB, Greenwald JA, Spector JA, Gittes GK, Longaker MT 2000 VEGF expression in an osteoblast-like cell line is regulated by a hypoxia response mechanism. Am J Physiol Cell Physiol 278(4):C853-60.
22. Rydziel S, Varghese S, Canalis E 1997 Transforming growth factor beta1 inhibits collagenase 3 expression by transcriptional and post-transcriptional mechanisms in osteoblast cultures. J Cell Physiol 170(2):145-52.
23. Lee FY, Choi YW, Behrens FF, DeFouw DO, Einhorn TA 1998 Programmed removal of chondrocytes during endochondral fracture healing. J Orthop Res 16(1):144-50.
24. Gerber HP, Vu TH, Ryan AM, Kowalski J, Werb Z, Ferrara N 1999 VEGF couples hypertrophic cartilage remodeling, ossification and angiogenesis during endochondral bone formation. Nat Med 5(6):623-8.
25. Hollinger J, Wong ME 1996 The integrated processes of hard tissue regeneration with special emphasis on fracture healing. Oral Surg Oral Med Oral Pathol Oral Radiol Endod 82(6):594-606.
26. Le AX, Miclau T, Hu D, Helms JA 2001 Molecular aspects of healing in stabilized and non-stabilized fractures. J Orthop Res 19(1):78-84.
27. Gerstenfeld LC, Cullinane DM, Barnes GL, Graves DT, Einhorn TA 2003 Fracture healing as a post-natal developmental process: molecular, spatial, and temporal aspects of its regulation. J Cell Biochem 88(5):873-84.
28. Solheim E 1998 Growth factors in bone. Int Orthop 22(6):410-6.
29. Massague J, Attisano L, Wrana JL 1994 The TGF-beta family and its composite receptors. Trends Cell Biol 4(5):172-8.
30. Bostrom MP 1998 Expression of bone morphogenetic proteins in fracture healing. Clin Orthop Relat Res (355 Suppl):S116-23.
31. Lieberman JR, Daluiski A, Einhorn TA 2002 The role of growth factors in the repair of bone. Biology and clinical applications. J Bone Joint Surg Am 84-A(6):1032-44.
32. Heldin CH, Miyazono K, ten Dijke P 1997 TGF-beta signalling from cell membrane to nucleus through SMAD proteins. Nature 390(6659):465-71.
33. Mundy GR 1996 Regulation of bone formation by bone morphogenetic proteins and other growth factors. Clin Orthop Relat Res (324):24-8.
34. Sakou T 1998 Bone morphogenetic proteins: from basic studies to clinical approaches. Bone 22(6):591-603.

35. Fujii M, Takeda K, Imamura T, Aoki H, Sampath TK, Enomoto S, Kawabata M, Kato M, Ichijo H, Miyazono K 1999 Roles of bone morphogenetic protein type I receptors and Smad proteins in osteoblast and chondroblast differentiation. Mol Biol Cell 10(11):3801-13.
36. Onishi T, Ishidou Y, Nagamine T, Yone K, Imamura T, Kato M, Sampath TK, ten Dijke P, Sakou T 1998 Distinct and overlapping patterns of localization of bone morphogenetic protein (BMP) family members and a BMP type II receptor during fracture healing in rats. Bone 22(6):605-12.
37. ten Dijke P, Fu J, Schaap P, Roelen BA 2003 Signal transduction of bone morphogenetic proteins in osteoblast differentiation. J Bone Joint Surg Am 85-A Suppl 3:34-8.
38. Cheng H, Jiang W, Phillips FM, Haydon RC, Peng Y, Zhou L, Luu HH, An N, Breyer B, Vanichakarn P, Szatkowski JP, Park JY, He TC 2003 Osteogenic activity of the fourteen types of human bone morphogenetic proteins (BMPs). J Bone Joint Surg Am 85-A(8):1544-52.
39. Deckers MM, van Bezooijen RL, van der Horst G, Hoogendam J, van Der Bent C, Papapoulos SE, Lowik CW 2002 Bone morphogenetic proteins stimulate angiogenesis through osteoblast-derived vascular endothelial growth factor A. Endocrinology 143(4):1545-53.
40. Peng H, Wright V, Usas A, Gearhart B, Shen HC, Cummins J, Huard J 2002 Synergistic enhancement of bone formation and healing by stem cell-expressed VEGF and bone morphogenetic protein-4. J Clin Invest 110(6):751-9.
41. Valdimarsdottir G, Goumans MJ, Rosendahl A, Brugman M, Itoh S, Lebrin F, Sideras P, ten Dijke P 2002 Stimulation of Id1 expression by bone morphogenetic protein is sufficient and necessary for bone morphogenetic protein-induced activation of endothelial cells. Circulation 106(17):2263-70.
42. Lind M 1998 Growth factor stimulation of bone healing. Effects on osteoblasts, osteomies, and implants fixation. Acta Orthop Scand Suppl 283:2-37.
43. Wang JS 1996 Basic fibroblast growth factor for stimulation of bone formation in osteoinductive or conductive implants. Acta Orthop Scand Suppl 269:1-33.
44. Friesel RE, Maciag T 1995 Molecular mechanisms of angiogenesis: fibroblast growth factor signal transduction. Faseb J 9(10):919-25.
45. Jingushi S, Heydemann A, Kana SK, Macey LR, Bolander ME 1990 Acidic fibroblast growth factor (aFGF) injection stimulates cartilage enlargement and inhibits cartilage gene expression in rat fracture healing. J Orthop Res 8(3):364-71.
46. Rodan SB, Wesolowski G, Thomas K, Rodan GA 1987 Growth stimulation of rat calvaria osteoblastic cells by acidic fibroblast growth factor. Endocrinology 121(6):1917-23.
47. Xu X, Weinstein M, Li C, Deng C 1999 Fibroblast growth factor receptors (FGFRs) and their roles in limb development. Cell Tissue Res 296(1):33-43.

48. Nakamura T, Hara Y, Tagawa M, Tamura M, Yuge T, Fukuda H, Nigi H 1998 Recombinant human basic fibroblast growth factor accelerates fracture healing by enhancing callus remodeling in experimental dog tibial fracture. J Bone Miner Res 13(6):942-9.
49. Dionne CA, Jaye M, Schlessinger J 1991 Structural diversity and binding of FGF receptors. Ann N Y Acad Sci 638:161-6.
50. Deng C, Wynshaw-Boris A, Zhou F, Kuo A, Leder P 1996 Fibroblast growth factor receptor 3 is a negative regulator of bone growth. Cell 84(6):911-21.
51. Dietz F, Muschler G 2000 Update on the genetic basis of disorders with orthopaedic manifestations. In: Buckwalter J, Einhorn T, Simon S (eds.) Orthopaedic Basic Science. AAOS, Rosemont, pp 114.
52. Canalis E, Varghese S, McCarthy TL, Centrella M 1992 Role of platelet derived growth factor in bone cell function. Growth Regul 2(4):151-5.
53. Claesson-Welsh L, Heldin CH 1989 Platelet-derived growth factor. Three isoforms that bind to two distinct cell surface receptors. Acta Oncol 28(3):331-4.
54. Heldin CH, Westermark B 1987 PDGF-like growth factors in autocrine stimulation of growth. J Cell Physiol Suppl Suppl 5:31-4.
55. Andrew JG, Hoyland JA, Freemont AJ, Marsh DR 1995 Platelet-derived growth factor expression in normally healing human fractures. Bone 16(4):455-60.
56. Millis DL 1999 Bone- and non-bone-derived growth factors and effects on bone healing. Vet Clin North Am Small Anim Pract 29(5):1221-46.
57. Linder BL, Chernoff A, Kaplan KL, Goodman DS 1979 Release of platelet-derived growth factor from human platelets by arachidonic acid. Proc Natl Acad Sci U S A 76(8):4107-11.
58. Canalis E 1980 Effect of insulinlike growth factor I on DNA and protein synthesis in cultured rat calvaria. J Clin Invest 66(4):709-19.
59. Prisell PT, Edwall D, Lindblad JB, Levinovitz A, Norstedt G 1993 Expression of insulin-like growth factors during bone induction in rat. Calcif Tissue Int 53(3):201-5.
60. Andrew JG, Hoyland J, Freemont AJ, Marsh D 1993 Insulinlike growth factor gene expression in human fracture callus. Calcif Tissue Int 53(2):97-102.
61. Bak B, Jorgensen PH, Andreassen TT 1990 Dose response of growth hormone on fracture healing in the rat. Acta Orthop Scand 61(1):54-7.
62. Gerstenfeld LC, Cho TJ, Kon T, Aizawa T, Tsay A, Fitch J, Barnes GL, Graves DT, Einhorn TA 2003 Impaired fracture healing in the absence of TNF-alpha signaling: the role of TNF-alpha in endochondral cartilage resorption. J Bone Miner Res 18(9):1584-92.
63. Kon T, Cho TJ, Aizawa T, Yamazaki M, Nooh N, Graves D, Gerstenfeld LC, Einhorn TA 2001 Expression of osteoprotegerin, receptor activator of NF-kappaB ligand (osteoprotegerin ligand) and related proinflammatory cytokines during fracture healing. J Bone Miner Res 16(6):1004-14.

64. Visse R, Nagase H 2003 Matrix metalloproteinases and tissue inhibitors of metalloproteinases: structure, function, and biochemistry. Circ Res 92(8):827-39.
65. Shapiro SD 1998 Matrix metalloproteinase degradation of extracellular matrix: biological consequences. Curr Opin Cell Biol 10(5):602-8.
66. Stamenkovic I 2003 Extracellular matrix remodelling: the role of matrix metalloproteinases. J Pathol 200(4):448-64.
67. Lehmann W, Edgar CM, Wang K, Cho TJ, Barnes GL, Kakar S, Graves DT, Rueger JM, Gerstenfeld LC, Einhorn TA 2005 Tumor necrosis factor alpha (TNF-alpha) coordinately regulates the expression of specific matrix metalloproteinases (MMPS) and angiogenic factors during fracture healing. Bone 36(2):300-10.
68. Ferrara N, Keyt B 1997 Vascular endothelial growth factor: basic biology and clinical implications. Exs 79:209-32.
69. Raisz LG 2005 Pathogenesis of osteoporosis: concepts, conflicts, and prospects. J Clin Invest 115(12):3318-25.
70. Dalle Carbonare L, Giannini S 2004 Bone microarchitecture as an important determinant of bone strength. J Endocrinol Invest 27(1):99-105.
71. Lanyon L, Armstrong V, Ong D, Zaman G, Price J 2004 Is estrogen receptor alpha key to controlling bones' resistance to fracture? J Endocrinol 182(2):183-91.
72. Roschger P, Matsuo K, Misof BM, Tesch W, Jochum W, Wagner EF, Fratzl P, Klaushofer K 2004 Normal mineralization and nanostructure of sclerotic bone in mice overexpressing Fra-1. Bone 34(5):776-82.
73. Nguyen TV, Center JR, Pocock NA, Eisman JA 2004 Limited utility of clinical indices for the prediction of symptomatic fracture risk in postmenopausal women. Osteoporos Int 15(1):49-55.
74. Klein RF 2002 Genetic regulation of bone mineral density in mice. J Musculoskelet Neuronal Interact 2(3):232-6.
75. Evans RA, Marel GM, Lancaster EK, Kos S, Evans M, Wong SY 1988 Bone mass is low in relatives of osteoporotic patients. Ann Intern Med 109(11):870-3.
76. Jouanny P, Guillemin F, Kuntz C, Jeandel C, Pourel J 1995 Environmental and genetic factors affecting bone mass. Similarity of bone density among members of healthy families. Arthritis Rheum 38(1):61-7.
77. Kelly PJ, Harris M 1995 Genetic regulation of peak bone mass. Acta Paediatr Suppl 411:24-9; discussion 30.
78. Pocock NA, Eisman JA, Hopper JL, Yeates MG, Sambrook PN, Eberl S 1987 Genetic determinants of bone mass in adults. A twin study. J Clin Invest 80(3):706-10.
79. Slemenda CW, Christian JC, Williams CJ, Norton JA, Johnston CC, Jr. 1991 Genetic determinants of bone mass in adult women: a reevaluation of the twin model and the potential importance of gene interaction on heritability estimates. J Bone Miner Res 6(6):561-7.
80. Smith DM, Nance WE, Kang KW, Christian JC, Johnston CC, Jr. 1973 Genetic factors in determining bone mass. J Clin Invest 52(11):2800-8.

81. Morrison NA, Qi JC, Tokita A, Kelly PJ, Crofts L, Nguyen TV, Sambrook PN, Eisman JA 1994 Prediction of bone density from vitamin D receptor alleles. Nature 367(6460)**:**284-7.
82. Looney JE, Yoon HK, Fischer M, Farley SM, Farley JR, Wergedal JE, Baylink DJ 1995 Lack of a high prevalence of the BB vitamin D receptor genotype in severely osteoporotic women. J Clin Endocrinol Metab 80(7)**:**2158-62.
83. Hustmyer FG, Peacock M, Hui S, Johnston CC, Christian J 1994 Bone mineral density in relation to polymorphism at the vitamin D receptor gene locus. J Clin Invest 94(5)**:**2130-4.
84. Howard G, Nguyen T, Morrison N, Watanabe T, Sambrook P, Eisman J, Kelly PJ 1995 Genetic influences on bone density: physiological correlates of vitamin D receptor gene alleles in premenopausal women. J Clin Endocrinol Metab 80(9)**:**2800-5.
85. Bailey DW 1979 Definition of Inbred Strains. In: Altman PL, Katz DD (eds.) Inbred and Genetically Defined Strains of Laboratory Animals, vol. 1: Mouse and Rat. Federation of American Societies for Experimental Biology, Bethesda.
86. Cohen C 1979 Inbred Animals: History, Uses, and Classification. In: Altman PL, Katz DD (eds.) Inbred and Genetically Defined Strains of Laboratory Animals, vol. 1: Mouse and Rat. Federation of American Societies for Experimental Biology, Bethesda.
87. Koller DL, Liu G, Econs MJ, Hui SL, Morin PA, Joslyn G, Rodriguez LA, Conneally PM, Christian JC, Johnston CC, Jr., Foroud T, Peacock M 2001 Genome screen for quantitative trait loci underlying normal variation in femoral structure. J Bone Miner Res 16(6)**:**985-91.
88. Beamer WG, Shultz KL, Churchill GA, Frankel WN, Baylink DJ, Rosen CJ, Donahue LR 1999 Quantitative trait loci for bone density in C57BL/6J and CAST/EiJ inbred mice. Mamm Genome 10(11)**:**1043-9.
89. Beamer WG, Shultz KL, Donahue LR, Churchill GA, Sen S, Wergedal JR, Baylink DJ, Rosen CJ 2001 Quantitative trait loci for femoral and lumbar vertebral bone mineral density in C57BL/6J and C3H/HeJ inbred strains of mice. J Bone Miner Res 16(7)**:**1195-206.
90. Volkman SK, Galecki AT, Burke DT, Miller RA, Goldstein SA 2004 Quantitative trait loci that modulate femoral mechanical properties in a genetically heterogeneous mouse population. J Bone Miner Res 19(9)**:**1497-505.
91. Klein RF, Mitchell SR, Phillips TJ, Belknap JK, Orwoll ES 1998 Quantitative trait loci affecting peak bone mineral density in mice. J Bone Miner Res 13(11)**:**1648-56.
92. Drake TA, Hannani K, Kabo JM, Villa V, Krass K, Lusis AJ 2001 Genetic loci influencing natural variations in femoral bone morphometry in mice. J Orthop Res 19(4)**:**511-7.
93. Hornby SB, Evans GP, Hornby SL, Pataki A, Glatt M, Green JR 2003 Long-term zoledronic acid treatment increases bone structure and

mechanical strength of long bones of ovariectomized adult rats. Calcif Tissue Int 72(4):519-27.
94. Myers VS, Jr. 1965 Confusing radiologic variations at the distal end of the radius of the horse. J Am Vet Med Assoc 147(12):1310-2.
95. Gao H, Ji B, Jager IL, Arzt E, Fratzl P 2003 Materials become insensitive to flaws at nanoscale: lessons from nature. Proc Natl Acad Sci U S A 100(10):5597-600.
96. Shapiro R, Heaney RP 2003 Co-dependence of calcium and phosphorus for growth and bone development under conditions of varying deficiency. Bone 32(5):532-40.
97. Funk CD 2001 Prostaglandins and leukotrienes: advances in eicosanoid biology. Science 294(5548):1871-5.
98. Bergstroem S, Danielsson H, Samuelsson B 1964 The Enzymatic Formation of Prostaglandin E2 from Arachidonic Acid Prostaglandins and Related Factors 32. Biochim Biophys Acta 90:207-10.
99. Samuelsson B 1983 Leukotrienes: mediators of immediate hypersensitivity reactions and inflammation. Science 220(4597):568-75.
100. Pace-Asciak CR, Granstrom E, Samuelsson B 1983 Arachidonic acid epoxides. Isolation and structure of two hydroxy epoxide intermediates in the formation of 8,11,12- and 10,11,12-trihydroxyeicosatrienoic acids. J Biol Chem 258(11):6835-40.
101. Samuelsson B, Dahlen SE, Lindgren JA, Rouzer CA, Serhan CN 1987 Leukotrienes and lipoxins: structures, biosynthesis, and biological effects. Science 237(4819):1171-6.
102. Henderson WR, Jr. 1994 The role of leukotrienes in inflammation. Ann Intern Med 121(9):684-97.
103. Serhan CN 1994 Lipoxin biosynthesis and its impact in inflammatory and vascular events. Biochim Biophys Acta 1212(1):1-25.
104. Peppelenbosch MP, Tertoolen LG, Hage WJ, de Laat SW 1993 Epidermal growth factor-induced actin remodeling is regulated by 5-lipoxygenase and cyclooxygenase products. Cell 74(3):565-75.
105. Capodici C, Pillinger MH, Han G, Philips MR, Weissmann G 1998 Integrin-dependent homotypic adhesion of neutrophils. Arachidonic acid activates Raf-1/Mek/Erk via a 5-lipoxygenase- dependent pathway. J Clin Invest 102(1):165-75.
106. Tsujii M, DuBois RN 1995 Alterations in cellular adhesion and apoptosis in epithelial cells overexpressing prostaglandin endoperoxide synthase 2. Cell 83(3):493-501.
107. Tong WG, Ding XZ, Witt RC, Adrian TE 2002 Lipoxygenase inhibitors attenuate growth of human pancreatic cancer xenografts and induce apoptosis through the mitochondrial pathway. Mol Cancer Ther 1(11):929-35.
108. Romano M, Catalano A, Nutini M, D'Urbano E, Crescenzi C, Claria J, Libner R, Davi G, Procopio A 2001 5-lipoxygenase regulates malignant mesothelial cell survival: involvement of vascular endothelial growth factor. Faseb J 15(13):2326-36.

109. Tsujii M, Kawano S, Tsuji S, Sawaoka H, Hori M, DuBois RN 1998 Cyclooxygenase regulates angiogenesis induced by colon cancer cells. Cell 93(5)**:**705-16.
110. Constantini S, Tamir J, Gomori MJ, Shohami E 1993 Tumor prostaglandin levels correlate with edema around supratentorial meningiomas. Neurosurgery 33(2)**:**204-10; discussion 211.
111. Black KL, Hoff JT, McGillicuddy JE, Gebarski SS 1986 Increased leukotriene C4 and vasogenic edema surrounding brain tumors in humans. Ann Neurol 19(6)**:**592-5.
112. Soberman RJ, Christmas P 2003 The organization and consequences of eicosanoid signaling. J Clin Invest 111(8)**:**1107-13.
113. Dubois RN, Abramson SB, Crofford L, Gupta RA, Simon LS, Van De Putte LB, Lipsky PE 1998 Cyclooxygenase in biology and disease. Faseb J 12(12)**:**1063-73.
114. Zhang X, Schwarz EM, Young DA, Puzas JE, Rosier RN, O'Keefe RJ 2002 Cyclooxygenase-2 regulates mesenchymal cell differentiation into the osteoblast lineage and is critically involved in bone repair. J Clin Invest 109(11)**:**1405-15.
115. Breyer RM, Bagdassarian CK, Myers SA, Breyer MD 2001 Prostanoid receptors: subtypes and signaling. Annu Rev Pharmacol Toxicol 41**:**661-90.
116. Smith WL, DeWitt DL, Garavito RM 2000 Cyclooxygenases: structural, cellular, and molecular biology. Annu Rev Biochem 69**:**145-82.
117. Fujishima H, Sanchez Mejia RO, Bingham CO, 3rd, Lam BK, Sapirstein A, Bonventre JV, Austen KF, Arm JP 1999 Cytosolic phospholipase A2 is essential for both the immediate and the delayed phases of eicosanoid generation in mouse bone marrow-derived mast cells. Proc Natl Acad Sci U S A 96(9)**:**4803-7.
118. Gilroy DW, Newson J, Sawmynaden P, Willoughby DA, Croxtall JD 2004 A novel role for phospholipase A2 isoforms in the checkpoint control of acute inflammation. Faseb J 18(3)**:**489-98.
119. Hawkey CJ 1999 COX-2 inhibitors. Lancet 353(9149)**:**307-14.
120. Davies P, Bailey PJ, Goldenberg MM, Ford-Hutchinson AW 1984 The role of arachidonic acid oxygenation products in pain and inflammation. Annu Rev Immunol 2**:**335-57.
121. Vane JR 1971 Inhibition of prostaglandin synthesis as a mechanism of action for aspirin-like drugs. Nat New Biol 231(25)**:**232-5.
122. Vane JR, Botting RM 1997 Mechanism of action of aspirin-like drugs. Semin Arthritis Rheum 26(6 Suppl 1)**:**2-10.
123. Vane JR, Bakhle YS, Botting RM 1998 Cyclooxygenases 1 and 2. Annu Rev Pharmacol Toxicol 38**:**97-120.
124. Raz A, Wyche A, Needleman P 1989 Temporal and pharmacological division of fibroblast cyclooxygenase expression into transcriptional and translational phases. Proc Natl Acad Sci U S A 86(5)**:**1657-61.

125. Fu JY, Masferrer JL, Seibert K, Raz A, Needleman P 1990 The induction and suppression of prostaglandin H2 synthase (cyclooxygenase) in human monocytes. J Biol Chem 265(28)**:**16737-40.
126. Picot D, Loll PJ, Garavito RM 1994 The X-ray crystal structure of the membrane protein prostaglandin H2 synthase-1. Nature 367(6460)**:**243-9.
127. Luong C, Miller A, Barnett J, Chow J, Ramesha C, Browner MF 1996 Flexibility of the NSAID binding site in the structure of human cyclooxygenase-2. Nat Struct Biol 3(11)**:**927-33.
128. Kawaguchi H, Raisz LG, Voznesensky OS, Alander CB, Hakeda Y, Pilbeam CC 1994 Regulation of the two prostaglandin G/H synthases by parathyroid hormone, interleukin-1, cortisol, and prostaglandin E2 in cultured neonatal mouse calvariae. Endocrinology 135(3)**:**1157-64.
129. Simmons DL, Levy DB, Yannoni Y, Erikson RL 1989 Identification of a phorbol ester-repressible v-src-inducible gene. Proc Natl Acad Sci U S A 86(4)**:**1178-82.
130. Kujubu DA, Fletcher BS, Varnum BC, Lim RW, Herschman HR 1991 TIS10, a phorbol ester tumor promoter-inducible mRNA from Swiss 3T3 cells, encodes a novel prostaglandin synthase/cyclooxygenase homologue. J Biol Chem 266(20)**:**12866-72.
131. O'Banion MK, Sadowski HB, Winn V, Young DA 1991 A serum- and glucocorticoid-regulated 4-kilobase mRNA encodes a cyclooxygenase-related protein. J Biol Chem 266(34)**:**23261-7.
132. Wong WY, Richards JS 1991 Evidence for two antigenically distinct molecular weight variants of prostaglandin H synthase in the rat ovary. Mol Endocrinol 5(9)**:**1269-79.
133. Xie WL, Chipman JG, Robertson DL, Erikson RL, Simmons DL 1991 Expression of a mitogen-responsive gene encoding prostaglandin synthase is regulated by mRNA splicing. Proc Natl Acad Sci U S A 88(7)**:**2692-6.
134. Fletcher BS, Kujubu DA, Perrin DM, Herschman HR 1992 Structure of the mitogen-inducible TIS10 gene and demonstration that the TIS10-encoded protein is a functional prostaglandin G/H synthase. J Biol Chem 267(7)**:**4338-44.
135. Golden BD, Abramson SB 1999 Selective cyclooxygenase-2 inhibitors. Rheum Dis Clin North Am 25(2)**:**359-78.
136. Scheiman JM 1996 NSAIDs, gastrointestinal injury, and cytoprotection. Gastroenterol Clin North Am 25(2)**:**279-98.
137. Zambraski EJ 1995 The effects of nonsteroidal anti-inflammatory drugs on renal function: experimental studies in animals. Semin Nephrol 15(3)**:**205-13.
138. Breyer MD, Jacobson HR, Breyer RM 1996 Functional and molecular aspects of renal prostaglandin receptors. J Am Soc Nephrol 7(1)**:**8-17.
139. Burch JW, Stanford N, Majerus PW 1978 Inhibition of platelet prostaglandin synthetase by oral aspirin. J Clin Invest 61(2)**:**314-9.
140. Crofford LJ 1997 COX-1 and COX-2 tissue expression: implications and predictions. J Rheumatol Suppl 49**:**15-9.

141. Anderson GD, Hauser SD, McGarity KL, Bremer ME, Isakson PC, Gregory SA 1996 Selective inhibition of cyclooxygenase (COX)-2 reverses inflammation and expression of COX-2 and interleukin 6 in rat adjuvant arthritis. J Clin Invest 97(11):2672-9.
142. Harris RC, McKanna JA, Akai Y, Jacobson HR, Dubois RN, Breyer MD 1994 Cyclooxygenase-2 is associated with the macula densa of rat kidney and increases with salt restriction. J Clin Invest 94(6):2504-10.
143. Guan Y, Chang M, Cho W, Zhang Y, Redha R, Davis L, Chang S, DuBois RN, Hao CM, Breyer M 1997 Cloning, expression, and regulation of rabbit cyclooxygenase-2 in renal medullary interstitial cells. Am J Physiol 273(1 Pt 2):F18-26.
144. Kaufmann WE, Worley PF, Pegg J, Bremer M, Isakson P 1996 COX-2, a synaptically induced enzyme, is expressed by excitatory neurons at postsynaptic sites in rat cerebral cortex. Proc Natl Acad Sci U S A 93(6):2317-21.
145. Tocco G, Freire-Moar J, Schreiber SS, Sakhi SH, Aisen PS, Pasinetti GM 1997 Maturational regulation and regional induction of cyclooxygenase-2 in rat brain: implications for Alzheimer's disease. Exp Neurol 144(2):339-49.
146. Narko K, Ritvos O, Ristimaki A 1997 Induction of cyclooxygenase-2 and prostaglandin F2alpha receptor expression by interleukin-1beta in cultured human granulosa-luteal cells. Endocrinology 138(9):3638-44.
147. Chakraborty I, Das SK, Wang J, Dey SK 1996 Developmental expression of the cyclo-oxygenase-1 and cyclo-oxygenase-2 genes in the peri-implantation mouse uterus and their differential regulation by the blastocyst and ovarian steroids. J Mol Endocrinol 16(2):107-22.
148. Yang ZM, Das SK, Wang J, Sugimoto Y, Ichikawa A, Dey SK 1997 Potential sites of prostaglandin actions in the periimplantation mouse uterus: differential expression and regulation of prostaglandin receptor genes. Biol Reprod 56(2):368-79.
149. Miettinen S, Fusco FR, Yrjanheikki J, Keinanen R, Hirvonen T, Roivainen R, Narhi M, Hokfelt T, Koistinaho J 1997 Spreading depression and focal brain ischemia induce cyclooxygenase-2 in cortical neurons through N-methyl-D-aspartic acid-receptors and phospholipase A2. Proc Natl Acad Sci U S A 94(12):6500-5.
150. Amin AR, Attur M, Patel RN, Thakker GD, Marshall PJ, Rediske J, Stuchin SA, Patel IR, Abramson SB 1997 Superinduction of cyclooxygenase-2 activity in human osteoarthritis-affected cartilage. Influence of nitric oxide. J Clin Invest 99(6):1231-7.
151. Tai H, Miyaura C, Pilbeam CC, Tamura T, Ohsugi Y, Koishihara Y, Kubodera N, Kawaguchi H, Raisz LG, Suda T 1997 Transcriptional induction of cyclooxygenase-2 in osteoblasts is involved in interleukin-6-induced osteoclast formation. Endocrinology 138(6):2372-9.
152. Onoe Y, Miyaura C, Kaminakayashiki T, Nagai Y, Noguchi K, Chen QR, Seo H, Ohta H, Nozawa S, Kudo I, Suda T 1996 IL-13 and IL-4 inhibit

bone resorption by suppressing cyclooxygenase-2-dependent prostaglandin synthesis in osteoblasts. J Immunol 156(2)**:**758-64.
153. Cohn SM, Schloemann S, Tessner T, Seibert K, Stenson WF 1997 Crypt stem cell survival in the mouse intestinal epithelium is regulated by prostaglandins synthesized through cyclooxygenase-1. J Clin Invest 99(6)**:**1367-79.
154. Langenbach R, Morham SG, Tiano HF, Loftin CD, Ghanayem BI, Chulada PC, Mahler JF, Lee CA, Goulding EH, Kluckman KD, Kim HS, Smithies O 1995 Prostaglandin synthase 1 gene disruption in mice reduces arachidonic acid-induced inflammation and indomethacin-induced gastric ulceration. Cell 83(3)**:**483-92.
155. Hedi H, Norbert G 2004 5-Lipoxygenase Pathway, Dendritic Cells, and Adaptive Immunity. J Biomed Biotechnol 2004(2)**:**99-105.
156. Peters-Golden M, Brock TG 2001 Intracellular compartmentalization of leukotriene synthesis: unexpected nuclear secrets. FEBS Lett 487(3)**:**323-6.
157. Rouzer CA, Shimizu T, Samuelsson B 1985 On the nature of the 5-lipoxygenase reaction in human leukocytes: characterization of a membrane-associated stimulatory factor. Proc Natl Acad Sci U S A 82(22)**:**7505-9.
158. Radmark O 2002 Arachidonate 5-lipoxygenase. Prostaglandins Other Lipid Mediat 68-69**:**211-34.
159. Gronert K, Clish CB, Romano M, Serhan CN 1999 Transcellular regulation of eicosanoid biosynthesis. Methods Mol Biol 120**:**119-44.
160. Radmark O, Shimizu T, Jornvall H, Samuelsson B 1984 Leukotriene A4 hydrolase in human leukocytes. Purification and properties. J Biol Chem 259(20)**:**12339-45.
161. Yoshimoto T, Soberman RJ, Spur B, Austen KF 1988 Properties of highly purified leukotriene C4 synthase of guinea pig lung. J Clin Invest 81(3)**:**866-71.
162. Serhan CN 1997 Lipoxins and novel aspirin-triggered 15-epi-lipoxins (ATL): a jungle of cell-cell interactions or a therapeutic opportunity? Prostaglandins 53(2)**:**107-37.
163. Serhan CN, Sheppard KA 1990 Lipoxin formation during human neutrophil-platelet interactions. Evidence for the transformation of leukotriene A4 by platelet 12-lipoxygenase in vitro. J Clin Invest 85(3)**:**772-80.
164. Fiore S, Serhan CN 1990 Formation of lipoxins and leukotrienes during receptor-mediated interactions of human platelets and recombinant human granulocyte/macrophage colony-stimulating factor-primed neutrophils. J Exp Med 172(5)**:**1451-7.
165. Romano M, Chen XS, Takahashi Y, Yamamoto S, Funk CD, Serhan CN 1993 Lipoxin synthase activity of human platelet 12-lipoxygenase. Biochem J 296 (Pt 1)**:**127-33.
166. Romano M, Serhan CN 1992 Lipoxin generation by permeabilized human platelets. Biochemistry 31(35)**:**8269-77.

167. Papayianni A, Serhan CN, Phillips ML, Rennke HG, Brady HR 1995 Transcellular biosynthesis of lipoxin A4 during adhesion of platelets and neutrophils in experimental immune complex glomerulonephritis. Kidney Int 47(5):1295-302.
168. Edenius C, Haeggstrom J, Lindgren JA 1988 Transcellular conversion of endogenous arachidonic acid to lipoxins in mixed human platelet-granulocyte suspensions. Biochem Biophys Res Commun 157(2):801-7.
169. Goldman DW, Goetzl EJ 1982 Specific binding of leukotriene B4 to receptors on human polymorphonuclear leukocytes. J Immunol 129(4):1600-4.
170. Goldman DW, Goetzl EJ 1984 Heterogeneity of human polymorphonuclear leukocyte receptors for leukotriene B4. Identification of a subset of high affinity receptors that transduce the chemotactic response. J Exp Med 159(4):1027-41.
171. Kato K, Yokomizo T, Izumi T, Shimizu T 2000 Cell-specific transcriptional regulation of human leukotriene B(4) receptor gene. J Exp Med 192(3):413-20.
172. Yokomizo T, Kato K, Hagiya H, Izumi T, Shimizu T 2001 Hydroxyeicosanoids bind to and activate the low affinity leukotriene B4 receptor, BLT2. J Biol Chem 276(15):12454-9.
173. Kamohara M, Takasaki J, Matsumoto M, Saito T, Ohishi T, Ishii H, Furuichi K 2000 Molecular cloning and characterization of another leukotriene B4 receptor. J Biol Chem 275(35):27000-4.
174. Christie PE, Henderson WR, Jr. 2002 Lipid inflammatory mediators: leukotrienes, prostaglandins, platelet-activating factor. Clin Allergy Immunol 16:233-54.
175. Lynch KR, O'Neill GP, Liu Q, Im DS, Sawyer N, Metters KM, Coulombe N, Abramovitz M, Figueroa DJ, Zeng Z, Connolly BM, Bai C, Austin CP, Chateauneuf A, Stocco R, Greig GM, Kargman S, Hooks SB, Hosfield E, Williams DL, Jr., Ford-Hutchinson AW, Caskey CT, Evans JF 1999 Characterization of the human cysteinyl leukotriene CysLT1 receptor. Nature 399(6738):789-93.
176. Gronert K, Martinsson-Niskanen T, Ravasi S, Chiang N, Serhan CN 2001 Selectivity of recombinant human leukotriene D(4), leukotriene B(4), and lipoxin A(4) receptors with aspirin-triggered 15-epi-LXA(4) and regulation of vascular and inflammatory responses. Am J Pathol 158(1):3-9.
177. Mellor EA, Maekawa A, Austen KF, Boyce JA 2001 Cysteinyl leukotriene receptor 1 is also a pyrimidinergic receptor and is expressed by human mast cells. Proc Natl Acad Sci U S A 98(14):7964-9.
178. Mancini JA, Abramovitz M, Cox ME, Wong E, Charleson S, Perrier H, Wang Z, Prasit P, Vickers PJ 1993 5-lipoxygenase-activating protein is an arachidonate binding protein. FEBS Lett 318(3):277-81.
179. Katzung Be 2001 Basic and Clinical Pharmacology, 8th ed. McGraw-Hill, New York.
180. Schafer AI 1995 Effects of nonsteroidal antiinflammatory drugs on platelet function and systemic hemostasis. J Clin Pharmacol 35(3):209-19.

181. Patrono C 1994 Aspirin as an antiplatelet drug. N Engl J Med 330(18):1287-94.
182. Cryer B, Feldman M 1998 Cyclooxygenase-1 and cyclooxygenase-2 selectivity of widely used nonsteroidal anti-inflammatory drugs. Am J Med 104(5):413-21.
183. Griffin MR 1998 Epidemiology of nonsteroidal anti-inflammatory drug-associated gastrointestinal injury. Am J Med 104(3A):23S-29S; discussion 41S-42S.
184. Gabriel SE, Fehring RA 1992 Trends in the utilization of non-steroidal anti-inflammatory drugs in the United States, 1986-1990. J Clin Epidemiol 45(9):1041-4.
185. Nishida T, Tsujii M, Tsuji S 2004 [Are COX-2 inhibitors truly able to prevent NSAIDs-associated ulcer?]. Nippon Rinsho 62(3):561-5.
186. Elder CL, Dahners LE, Weinhold PS 2001 A cyclooxygenase-2 inhibitor impairs ligament healing in the rat. Am J Sports Med 29(6):801-5.
187. Drazen JM, Israel E, O'Byrne PM 1999 Treatment of asthma with drugs modifying the leukotriene pathway. N Engl J Med 340(3):197-206.
188. Drazen J 1998 Clinical pharmacology of leukotriene receptor antagonists and 5-lipoxygenase inhibitors. Am J Respir Crit Care Med 157(6 Pt 2):S233-7; discussion S247-8.
189. Bernstein PR 1998 Chemistry and structure--activity relationships of leukotriene receptor antagonists. Am J Respir Crit Care Med 157(6 Pt 2):S220-5; discussion S225-6, S247-8.
190. Aharony D 1998 Pharmacology of leukotriene receptor antagonists. Am J Respir Crit Care Med 157(6 Pt 2):S214-8; discussion S218-9, S247-8.
191. Schultz R 1972 The Language of Fractures. Williams and Wilkins, Baltimore.
192. Reichel H, Lebek S, Alter C, Hein W 1998 Biomechanical and densitometric bone properties after callus distraction in sheep. Clin Orthop Relat Res (357):237-46.
193. Robertson DM, Smith DC, Das SK, Kumar A 1980 Microdensitometry as a clinical tool for diagnosing the progress of fracture healing. J Oral Surg 38(10):740-3.
194. Milne EN 1974 Electronic magnification of the x-ray image. Radiology 113(3):521-8.
195. Rao GU, Clark RL 1970 Radiographic magnification versus optical magnification. Radiology 94(1):196.
196. Eriksen E, Axelrod D, Melsen Fse 1994 Bone histomorphometry. In: EF E (ed.), 1st ed. Raven Press Ltd, New York.
197. An Y, Barfield W, Knets I 2000 Methods of Evaluation for Bone Dimensions, Densities, Contents, Morphology, and Structures. In: An Y, Draughn R (eds.) Mechanical Testing of Bone and the Bone-Implant Interface, 1st ed. CRC Press, Boca Raton, pp 103-118.
198. Gerstenfeld LC, Wronski TJ, Hollinger JO, Einhorn TA 2005 Application of histomorphometric methods to the study of bone repair. J Bone Miner Res 20(10):1715-22.

199. An Y, Bell T 1999 Mechanical Properties and Testing Methods of Bone. In: An Y, Friedman R (eds.) Animal Models in Orthopaedic Research, 1st ed. CRC Press, Boca Raton.
200. Turner CH, Burr DB 1993 Basic biomechanical measurements of bone: a tutorial. Bone 14(4):595-608.
201. Bronk JT, Ilstrup D, An K-N 1995 Further characterization of the Bonnarens and Einhorn rat femur fracture model. Trans Orthop Res Soc. 20:587.
202. Arnoczky S, Wilson J 1986 Experimental Surgery of the Skeletal System. In: Gay W, Heavner J (eds.) Methods of Animal Experimentation, vol. VII. Academic Press, London, pp 67-108.
203. An Y, Friedman R 1999 Animal Selections in Orthopaedic Research. In: An Y, Friedman R (eds.) Animal Models in Orthopaedic Research, 1st ed. CRC Press, Boca Raton, pp 39-57.
204. White AA, 3rd, Panjabi MM, Southwick WO 1977 The four biomechanical stages of fracture repair. J Bone Joint Surg Am 59(2):188-92.
205. An Y, Friedman R, Draughn R 1999 Animal Models of Bone Fracture or Osteotomy. In: An Y, Friedman R (eds.) Animal Models in Orthopaedic Research, 1st ed. CRC Press, Boca Raton, pp 197-217.
206. Nunamaker DM 1998 Experimental models of fracture repair. Clin Orthop Relat Res (355 Suppl):S56-65.
207. Egermann M, Goldhahn J, Schneider E 2005 Animal models for fracture treatment in osteoporosis. Osteoporos Int 16 Suppl 2:S129-38.
208. Kelly PJ, Montgomery RJ, Bronk JT 1990 Reaction of the circulatory system to injury and regeneration. Clin Orthop Relat Res (254):275-88.
209. Bonnarens F, Einhorn TA 1984 Production of a standard closed fracture in laboratory animal bone. J Orthop Res 2(1):97-101.
210. Ekeland A, Engesaeter LB, Langeland N 1981 Mechanical properties of fractured and intact rat femora evaluated by bending, torsional and tensile tests. Acta Orthop Scand 52(6):605-13.
211. Ferretti JL, Capozza RF, Mondelo N, Zanchetta JR 1993 Interrelationships between densitometric, geometric, and mechanical properties of rat femora: inferences concerning mechanical regulation of bone modeling. J Bone Miner Res 8(11):1389-96.
212. Lepola V, Vaananen K, Jalovaara P 1993 The effect of immobilization on the torsional strength of the rat tibia. Clin Orthop Relat Res (297):55-61.
213. Mosekilde L, Danielsen CC, Sogaard CH, Thorling E 1994 The effect of long-term exercise on vertebral and femoral bone mass, dimensions, and strength--assessed in a rat model. Bone 15(3):293-301.
214. Peng Z, Tuukkanen J, Zhang H, Jamsa T, Vaananen HK 1994 The mechanical strength of bone in different rat models of experimental osteoporosis. Bone 15(5):523-32.
215. Raab DM, Smith EL, Crenshaw TD, Thomas DP 1990 Bone mechanical properties after exercise training in young and old rats. J Appl Physiol 68(1):130-4.

216. Isefuku S, Joyner CJ, Reed AA, Simpson AH 2004 Distraction osteogenesis in the Cbfa-1+/- mouse. J Orthop Res 22(6):1276-82.
217. Paccione MF, Warren SM, Spector JA, Greenwald JA, Bouletreau PJ, Longaker MT 2001 A mouse model of mandibular osteotomy healing. J Craniofac Surg 12(5):444-50.
218. Yamagiwa H, Tokunaga K, Hayami T, Hatano H, Uchida M, Endo N, Takahashi HE 1999 Expression of metalloproteinase-13 (Collagenase-3) is induced during fracture healing in mice. Bone 25(2):197-203.
219. Bourque WT, Gross M, Hall BK 1992 A reproducible method for producing and quantifying the stages of fracture repair. Lab Anim Sci 42(4):369-74.
220. Hiltunen A, Vuorio E, Aro HT 1993 A standardized experimental fracture in the mouse tibia. J Orthop Res 11(2):305-12.
221. Hiltunen A, Aro HT, Vuorio E 1993 Regulation of extracellular matrix genes during fracture healing in mice. Clin Orthop (297):23-7.
222. Fujii H, Kitazawa R, Maeda S, Mizuno K, Kitazawa S 1999 Expression of platelet-derived growth factor proteins and their receptor alpha and beta mRNAs during fracture healing in the normal mouse. Histochem Cell Biol 112(2):131-8.
223. Uusitalo H, Hiltunen A, Ahonen M, Gao TJ, Lefebvre V, Harley V, Kahari VM, Vuorio E 2001 Accelerated up-regulation of L-Sox5, Sox6, and Sox9 by BMP-2 gene transfer during murine fracture healing. J Bone Miner Res 16(10):1837-45.
224. Colnot C, Thompson Z, Miclau T, Werb Z, Helms JA 2003 Altered fracture repair in the absence of MMP9. Development 130(17):4123-33.
225. Nakayama T, Toguchida J, Wadayama B, Kanoe H, Aizawa S, Sasaki MS, Nakamura T 1996 Fracture healing is a process independent of p53 function. In Vivo 10(6):553-8.
226. Buzdon MM, Napolitano LM, Shi HJ, Ceresoli DM, Rauniya R, Bass BL 1999 Femur fracture induces site-specific changes in T-cell immunity. J Surg Res 82(2):201-8.
227. Devine MJ, Mierisch CM, Jang E, Anderson PC, Balian G 2002 Transplanted bone marrow cells localize to fracture callus in a mouse model. J Orthop Res 20(6):1232-9.
228. Napolitano LM, Koruda MJ, Meyer AA, Baker CC 1996 The impact of femur fracture with associated soft tissue injury on immune function and intestinal permeability. Shock 5(3):202-7.
229. Bhandari M, Schemitsch EH 2002 Bone formation following intramedullary femoral reaming is decreased by indomethacin and antibodies to insulin-like growth factors. J Orthop Trauma 16(10):717-22.
230. Skoglund B, Forslund C, Aspenberg P 2002 Simvastatin improves fracture healing in mice. J Bone Miner Res 17(11):2004-8.
231. Street J, Bao M, deGuzman L, Bunting S, Peale FV, Jr., Ferrara N, Steinmetz H, Hoeffel J, Cleland JL, Daugherty A, van Bruggen N, Redmond HP, Carano RA, Filvaroff EH 2002 Vascular endothelial growth factor stimulates bone repair by promoting angiogenesis and bone turnover. Proc Natl Acad Sci U S A 99(15):9656-61.

232. Li G, White G, Connolly C, Marsh D 2002 Cell proliferation and apoptosis during fracture healing. J Bone Miner Res 17(5):791-9.
233. Chhabra A, Zijerdi D, Zhang J, Kline A, Balian G, Hurwitz S 2005 BMP-14 deficiency inhibits long bone fracture healing: a biochemical, histologic, and radiographic assessment. J Orthop Trauma 19(9):629-34.
234. Ramasamy JG, Akkus O 2006 Local variations in the micromechanical properties of mouse femur: The involvement of collagen fiber orientation and mineralization. J Biomech.
235. Holstein JH, Menger MD, Culemann U, Meier C, Pohlemann T 2005 Development of a locking femur nail for mice. J Biomech.
236. Cheung KM, Kaluarachi K, Andrew G, Lu W, Chan D, Cheah KS 2003 An externally fixed femoral fracture model for mice. J Orthop Res 21(4):685-90.
237. Uusitalo H, Rantakokko J, Ahonen M, Jamsa T, Tuukkanen J, KaHari V, Vuorio E, Aro HT 2001 A metaphyseal defect model of the femur for studies of murine bone healing. Bone 28(4):423-9.
238. Beamer WG, Donahue LR, Rosen CJ, Baylink DJ 1996 Genetic variability in adult bone density among inbred strains of mice. Bone 18(5):397-403.
239. Smith WL, Eling TE, Kulmacz RJ, Marnett LJ, Tsai A 1992 Tyrosyl radicals and their role in hydroperoxide-dependent activation and inactivation of prostaglandin endoperoxide synthase. Biochemistry 31(1):3-7.
240. Ruf HH, Raab-Brill U, Blau C 1993 A model for the catalytic mechanism of prostaglandin endoperoxide synthase. Biochem Soc Trans 21 (Pt 3)(3):739-44.
241. Shimokawa T, Smith WL 1992 Prostaglandin endoperoxide synthase. The aspirin acetylation region. J Biol Chem 267(17):12387-92.
242. Morham SG, Langenbach R, Loftin CD, Tiano HF, Vouloumanos N, Jennette JC, Mahler JF, Kluckman KD, Ledford A, Lee CA, Smithies O 1995 Prostaglandin synthase 2 gene disruption causes severe renal pathology in the mouse. Cell 83(3):473-82.
243. Norwood VF, Morham SG, Smithies O 2000 Postnatal development and progression of renal dysplasia in cyclooxygenase-2 null mice. Kidney Int 58(6):2291-300.
244. Chen XS, Sheller JR, Johnson EN, Funk CD 1994 Role of leukotrienes revealed by targeted disruption of the 5-lipoxygenase gene. Nature 372(6502):179-82.
245. Ramirez-Solis R, Davis AC, Bradley A 1993 Gene targeting in embryonic stem cells. Methods Enzymol 225:855-78.
246. Dinchuk JE, Car BD, Focht RJ, Johnston JJ, Jaffee BD, Covington MB, Contel NR, Eng VM, Collins RJ, Czerniak PM, et al. 1995 Renal abnormalities and an altered inflammatory response in mice lacking cyclooxygenase II. Nature 378(6555):406-9.
247. Li GQ, Xia HH, Chen MH, Gu Q, Wang JD, Peng JZ, Chan AO, Cho CH, So HL, Lam SK, Hu PJ, Liang YJ, Lin HL, Berg DE, Feng ZH, Langenbach R, Wong BC 2006 Effects of cyclooxygenase-1 and -2 gene disruption on

Helicobacter pylori-induced gastric inflammation. J Infect Dis 193(7):1037-46.
248. Mehrabian M, Allayee H, Wong J, Shi W, Wang XP, Shaposhnik Z, Funk CD, Lusis AJ 2002 Identification of 5-lipoxygenase as a major gene contributing to atherosclerosis susceptibility in mice. Circ Res 91(2):120-6.
249. Baron R, Vigney A, Neff L, Silvergate A, Santa Maria A 1983 Processing of undecalcified bone specimens for bone histomorphometry. In: Recker RR (ed.) Bone Histomorphometry: Techniques and Interpretation. CRC Press Inc., Boca Raton, FL, pp 13-35.
250. Maniatopoulos C, Rodriguez A, Deporter DA, Melcher AH 1986 An improved method for preparing histological sections of metallic implants. Int J Oral Maxillofac Implants 1(1):31-7.
251. Engesaeter LB, Ekeland A, Langeland N 1978 Methods for testing the mechanical properties of the rat femur. Acta Orthop Scand 49(6):512-8.
252. Bell GH, Cuthbertson DP, Orr J 1941 Strength and size of bone in relation to calcium intake. J Physiol 100(3):299-317.
253. Popov E 1968 Introduction to Mechanics of Materials. Prentice-Hall, Inc., Englewood Cliffs.
254. Smith PK, Krohn RI, Hermanson GT, Mallia AK, Gartner FH, Provenzano MD, Fujimoto EK, Goeke NM, Olson BJ, Klenk DC 1985 Measurement of protein using bicinchoninic acid. Anal Biochem 150(1):76-85.
255. Bonewald LF, Flynn M, Qiao M, Dallas MR, Mundy GR, Boyce BF 1997 Mice lacking 5-lipoxygenase have increased cortical bone thickness. Adv Exp Med Biol 433:299-302.
256. Shen FH, Visger JM, Balian G, Hurwitz SR, Diduch DR 2002 Systemically administered mesenchymal stromal cells transduced with insulin-like growth factor-I localize to a fracture site and potentiate healing. J Orthop Trauma 16(9):651-9.
257. Manigrasso MB, O'Connor JP 2004 Characterization of a closed femur fracture model in mice. J Orthop Trauma 18(10):687-95.
258. Currey JD 1984 Effects of differences in mineralization on the mechanical properties of bone. Philos Trans R Soc Lond B Biol Sci 304(1121):509-18.
259. Currey JD 2003 The many adaptations of bone. J Biomech 36(10):1487-95.
260. Akhter MP, Cullen DM, Gong G, Recker RR 2001 Bone biomechanical properties in prostaglandin EP1 and EP2 knockout mice. Bone 29(2):121-5.
261. Akhter MP, Cullen DM, Pan LC 2006 Bone biomechanical properties in EP4 knockout mice. Calcif Tissue Int 78(6):357-62.
262. Flanagan AM, Chambers TJ 1992 Stimulation of bone nodule formation in vitro by prostaglandins E1 and E2. Endocrinology 130(1):443-8.
263. Marks SC, Jr., Miller S 1988 Local infusion of prostaglandin E1 stimulates mandibular bone formation in vivo. J Oral Pathol 17(9-10):500-5.
264. Ringel RE, Brenner JI, Haney PJ, Burns JE, Moulton AL, Berman MA 1982 Prostaglandin-induced periostitis: a complication of long-term PGE1

infusion in an infant with congenital heart disease. Radiology 142(3):657-8.
265. Suponitzky I, Weinreb M 1998 Differential effects of systemic prostaglandin E2 on bone mass in rat long bones and calvariae. J Endocrinol 156(1):51-7.
266. Yang RS, Liu TK, Lin-Shiau SY 1993 Increased bone growth by local prostaglandin E2 in rats. Calcif Tissue Int 52(1):57-61.
267. Keller J, Hansen ES, He SZ, Kjaersgaard-Andersen P, Bunger C 1991 Early hemodynamic response to tibial osteotomy in rabbits: influence of indomethacin and prostaglandin E2. J Orthop Res 9(4):539-44.
268. Keller J 1996 Effects of indomethacin and local prostaglandin E2 on fracture healing in rabbits. Dan Med Bull 43(4):317-29.
269. Norrdin RW, Shih MS 1988 Systemic effects of prostaglandin E2 on vertebral trabecular remodeling in beagles used in a healing study. Calcif Tissue Int 42(6):363-8.
270. Shih MS, Norrdin RW 1986 Effect of prostaglandin E2 on rib fracture healing in beagles: histomorphometric study on periosteum adjacent to the fracture site. Am J Vet Res 47(7):1561-4.
271. Gajraj NM 2003 The effect of cyclooxygenase-2 inhibitors on bone healing. Reg Anesth Pain Med 28(5):456-65.
272. Gerstenfeld LC, Einhorn TA 2004 COX inhibitors and their effects on bone healing. Expert Opin Drug Saf 3(2):131-6.
273. Dekel S, Lenthall G, Francis MJ 1981 Release of prostaglandins from bone and muscle after tibial fracture. An experimental study in rabbits. J Bone Joint Surg Br 63-B(2):185-9.
274. Raisz LG 1999 Prostaglandins and bone: physiology and pathophysiology. Osteoarthritis Cartilage 7(4):419-21.
275. Mungo DV, Zhang X, O'Keefe RJ, Rosier RN, Puzas JE, Schwarz EM 2002 COX-1 and COX-2 expression in osteoid osteomas. J Orthop Res 20(1):159-62.
276. Miyauchi M, Hiraoka M, Oka H, Sato S, Kudo Y, Ogawa I, Noguchi K, Ishikawa I, Takata T 2004 Immuno-localization of COX-1 and COX-2 in the rat molar periodontal tissue after topical application of lipopolysaccharide. Arch Oral Biol 49(9):739-46.
277. Mohammed SI, Khan KN, Sellers RS, Hayek MG, DeNicola DB, Wu L, Bonney PL, Knapp DW 2004 Expression of cyclooxygenase-1 and 2 in naturally-occurring canine cancer. Prostaglandins Leukot Essent Fatty Acids 70(5):479-83.
278. Brooks PM, Day RO 1991 Nonsteroidal antiinflammatory drugs--differences and similarities. N Engl J Med 324(24):1716-25.
279. Vaile JH, Davis P 1998 Topical NSAIDs for musculoskeletal conditions. A review of the literature. Drugs 56(5):783-99.
280. Bauer DC, Orwoll ES, Fox KM, Vogt TM, Lane NE, Hochberg MC, Stone K, Nevitt MC 1996 Aspirin and NSAID use in older women: effect on bone mineral density and fracture risk. Study of Osteoporotic Fractures Research Group. J Bone Miner Res 11(1):29-35.

281. Burssens A, Thiery J, Kohl P, Molderez A, Haazen L 1995 Prevention of heterotopic ossification with tenoxicam following total hip arthroplasty: a double-blind, placebo-controlled dose-finding study. Acta Orthop Belg 61(3):205-11.
282. Kjaersgaard-Andersen P, Nafei A, Teichert G, Kristensen O, Schmidt SA, Keller J, Lucht U 1993 Indomethacin for prevention of heterotopic ossification. A randomized controlled study in 41 hip arthroplasties. Acta Orthop Scand 64(6):639-42.
283. Moed BR, Resnick RB, Fakhouri AJ, Nallamothu B, Wagner RA 1994 Effect of two nonsteroidal antiinflammatory drugs on heterotopic bone formation in a rabbit model. J Arthroplasty 9(1):81-7.
284. Persson PE, Sodemann B, Nilsson OS 1998 Preventive effects of ibuprofen on periarticular heterotopic ossification after total hip arthroplasty. A randomized double-blind prospective study of treatment time. Acta Orthop Scand 69(2):111-5.
285. Vielpeau C, Joubert JM, Hulet C 1999 Naproxen in the prevention of heterotopic ossification after total hip replacement. Clin Orthop Relat Res (369):279-88.
286. Wahlstrom O, Risto O, Djerf K, Hammerby S 1991 Heterotopic bone formation prevented by diclofenac. Prospective study of 100 hip arthroplasties. Acta Orthop Scand 62(5):419-21.
287. Allen HL, Wase A, Bear WT 1980 Indomethacin and aspirin: effect of nonsteroidal anti-inflammatory agents on the rate of fracture repair in the rat. Acta Orthop Scand 51(4):595-600.
288. Altman RD, Latta LL, Keer R, Renfree K, Hornicek FJ, Banovac K 1995 Effect of nonsteroidal antiinflammatory drugs on fracture healing: a laboratory study in rats. J Orthop Trauma 9(5):392-400.
289. Bo J, Sudmann E, Marton PF 1976 Effect of indomethacin on fracture healing in rats. Acta Orthop Scand 47(6):588-99.
290. Brown KM, Saunders MM, Kirsch T, Donahue HJ, Reid JS 2004 Effect of COX-2-specific inhibition on fracture-healing in the rat femur. J Bone Joint Surg Am 86-A(1):116-23.
291. Engesaeter LB, Sudmann B, Sudmann E 1992 Fracture healing in rats inhibited by locally administered indomethacin. Acta Orthop Scand 63(3):330-3.
292. Hogevold HE, Grogaard B, Reikeras O 1992 Effects of short-term treatment with corticosteroids and indomethacin on bone healing. A mechanical study of osteotomies in rats. Acta Orthop Scand 63(6):607-11.
293. Sudmann E, Dregelid E, Bessesen A, Morland J 1979 Inhibition of fracture healing by indomethacin in rats. Eur J Clin Invest 9(5):333-9.
294. Bichara J, Greenwell H, Drisko C, Wittwer JW, Vest TM, Yancey J, Goldsmith J, Rebitski G 1999 The effect of postsurgical naproxen and a bioabsorbable membrane on osseous healing in intrabony defects. J Periodontol 70(8):869-77.
295. Giordano V, Giordano M, Knackfuss IG, Apfel MI, Gomes RD 2003 Effect of tenoxicam on fracture healing in rat tibiae. Injury 34(2):85-94.

296. Jaffre B, Watrin A, Loeuille D, Gillet P, Netter P, Laugier P, Saied A 2003 Effects of antiinflammatory drugs on arthritic cartilage: a high-frequency quantitative ultrasound study in rats. Arthritis Rheum 48(6)**:**1594-601.
297. Keller J, Bunger C, Andreassen TT, Bak B, Lucht U 1987 Bone repair inhibited by indomethacin. Effects on bone metabolism and strength of rabbit osteotomies. Acta Orthop Scand 58(4)**:**379-83.
298. Lindholm TS, Tornkvist H 1981 Inhibitory effect on bone formation and calcification exerted by the anti-inflammatory drug ibuprofen. An experimental study on adult rat with fracture. Scand J Rheumatol 10(1)**:**38-42.
299. Obeid G, Zhang X, Wang X 1992 Effect of ibuprofen on the healing and remodeling of bone and articular cartilage in the rabbit temporomandibular joint. J Oral Maxillofac Surg 50(8)**:**843-9; discussion 849-50.
300. Riew KD, Long J, Rhee J, Lewis S, Kuklo T, Kim YJ, Yukawa Y, Zhu Y 2003 Time-dependent inhibitory effects of indomethacin on spinal fusion. J Bone Joint Surg Am 85-A(4)**:**632-4.
301. Sato S, Kim T, Arai T, Maruyama S, Tajima M, Utsumi N 1986 Comparison between the effects of dexamethasone and indomethacin on bone wound healing. Jpn J Pharmacol 42(1)**:**71-8.
302. Sudmann E, Bang G 1979 Indomethacin-induced inhibition of haversian remodelling in rabbits. Acta Orthop Scand 50(6 Pt 1)**:**621-7.
303. Beck A, Krischak G, Sorg T, Augat P, Farker K, Merkel U, Kinzl L, Claes L 2003 Influence of diclofenac (group of nonsteroidal anti-inflammatory drugs) on fracture healing. Arch Orthop Trauma Surg 123(7)**:**327-32.
304. Tornkvist H, Lindholm TS 1980 Effect of ibuprofen on mass and composition of fracture callus and bone. An experimental study on adult rat. Scand J Rheumatol 9(3)**:**167-71.
305. Goodman S, Ma T, Trindade M, Ikenoue T, Matsuura I, Wong N, Fox N, Genovese M, Regula D, Smith RL 2002 COX-2 selective NSAID decreases bone ingrowth in vivo. J Orthop Res 20(6)**:**1164-9.
306. Simon AM, Manigrasso MB, O'Connor JP 2002 Cyclo-oxygenase 2 function is essential for bone fracture healing. J Bone Miner Res 17(6)**:**963-76.
307. Mullis BH, Copland ST, Weinhold PS, Miclau T, Lester GE, Bos GD 2006 Effect of COX-2 inhibitors and non-steroidal anti-inflammatory drugs on a mouse fracture model. Injury 37(9)**:**827-37.
308. Huo MH, Troiano NW, Pelker RR, Gundberg CM, Friedlaender GE 1991 The influence of ibuprofen on fracture repair: biomechanical, biochemical, histologic, and histomorphometric parameters in rats. J Orthop Res 9(3)**:**383-90.
309. Pritchett JW 1995 Ketorolac prophylaxis against heterotopic ossification after hip replacement. Clin Orthop Relat Res (314)**:**162-5.
310. Moore KD, Goss K, Anglen JO 1998 Indomethacin versus radiation therapy for prophylaxis against heterotopic ossification in acetabular fractures: a randomised, prospective study. J Bone Joint Surg Br 80(2)**:**259-63.

311. Burd TA, Lowry KJ, Anglen JO 2001 Indomethacin compared with localized irradiation for the prevention of heterotopic ossification following surgical treatment of acetabular fractures. J Bone Joint Surg Am 83-A(12)**:**1783-8.
312. Burd TA, Hughes MS, Anglen JO 2003 Heterotopic ossification prophylaxis with indomethacin increases the risk of long-bone nonunion. J Bone Joint Surg Br 85(5)**:**700-5.
313. Giannoudis PV, MacDonald DA, Matthews SJ, Smith RM, Furlong AJ, De Boer P 2000 Nonunion of the femoral diaphysis. The influence of reaming and non-steroidal anti-inflammatory drugs. J Bone Joint Surg Br 82(5)**:**655-8.
314. Ueda K, Saito A, Nakano H, Aoshima M, Yokota M, Muraoka R, Iwaya T 1980 Cortical hyperostosis following long-term administration of prostaglandin E1 in infants with cyanotic congenital heart disease. J Pediatr 97(5)**:**834-6.
315. Jee WS, Ueno K, Deng YP, Woodbury DM 1985 The effects of prostaglandin E2 in growing rats: increased metaphyseal hard tissue and cortico-endosteal bone formation. Calcif Tissue Int 37(2)**:**148-57.
316. Yamaguchi DT, Green J, Merritt BS, Kleeman CR, Muallem S 1989 Modulation of osteoblast function by prostaglandins. Am J Physiol 257(5 Pt 2)**:**F755-61.
317. Hakeda Y, Hotta T, Kurihara N, Ikeda E, Maeda N, Yagyu Y, Kumegawa M 1987 Prostaglandin E1 and F2 alpha stimulate differentiation and proliferation, respectively, of clonal osteoblastic MC3T3-E1 cells by different second messengers in vitro. Endocrinology 121(6)**:**1966-74.
318. Feyen JH, Di Bon A, van der Plas A, Lowik CW, Nijweide PJ 1985 Effects of exogenous prostanoids on the proliferation of osteoblast-like cells in vitro. Prostaglandins 30(5)**:**827-40.
319. Partridge NC, Hillyard CJ, Nolan RD, Martin TJ 1985 Regulation of prostaglandin production by osteoblast-rich calvarial cells. Prostaglandins 30(3)**:**527-39.
320. Chyun YS, Raisz LG 1984 Stimulation of bone formation by prostaglandin E2. Prostaglandins 27(1)**:**97-103.
321. Feyen JH, van der Wilt G, Moonen P, Di Bon A, Nijweide PJ 1984 Stimulation of arachidonic acid metabolism in primary cultures of osteoblast-like cells by hormones and drugs. Prostaglandins 28(6)**:**769-81.
322. Nolan RD, Partridge NC, Godfrey HM, Martin TJ 1983 Cyclo-oxygenase products of arachidonic acid metabolism in rat osteoblasts in culture. Calcif Tissue Int 35(3)**:**294-7.
323. Hakeda Y, Harada S, Matsumoto T, Tezuka K, Higashino K, Kodama H, Hashimoto-Goto T, Ogata E, Kumegawa M 1991 Prostaglandin F2 alpha stimulates proliferation of clonal osteoblastic MC3T3-E1 cells by up-regulation of insulin-like growth factor I receptors. J Biol Chem 266(31)**:**21044-50.
324. Klein-Nulend J, Burger EH, Semeins CM, Raisz LG, Pilbeam CC 1997 Pulsating fluid flow stimulates prostaglandin release and inducible

prostaglandin G/H synthase mRNA expression in primary mouse bone cells. J Bone Miner Res 12(1):45-51.
325. Woodiel FN, Fall PM, Raisz LG 1996 Anabolic effects of prostaglandins in cultured fetal rat calvariae: structure-activity relations and signal transduction pathway. J Bone Miner Res 11(9):1249-55.
326. Li TF, Zuscik MJ, Ionescu AM, Zhang X, Rosier RN, Schwarz EM, Drissi H, O'Keefe RJ 2004 PGE2 inhibits chondrocyte differentiation through PKA and PKC signaling. Exp Cell Res 300(1):159-69.
327. Jakob M, Demarteau O, Suetterlin R, Heberer M, Martin I 2004 Chondrogenesis of expanded adult human articular chondrocytes is enhanced by specific prostaglandins. Rheumatology (Oxford) 43(7):852-7.
328. Kosher RA, Walker KH 1983 The effect of prostaglandins on in vitro limb cartilage differentiation. Exp Cell Res 145(1):145-53.
329. Chepenik KP, Ho WC, Waite BM, Parker CL 1984 Arachidonate metabolism during chondrogenesis in vitro. Calcif Tissue Int 36(2):175-81.
330. Diaz-Flores L, Gutierrez R, Valladares F, Varela H, Perez M 1994 Intense vascular sprouting from rat femoral vein induced by prostaglandins E1 and E2. Anat Rec 238(1):68-76.
331. Jiang H, Weyrich AS, Zimmerman GA, McIntyre TM 2004 Endothelial cell confluence regulates cyclooxygenase-2 and prostaglandin E2 production that modulate motility. J Biol Chem 279(53):55905-13.
332. Ren W, Dziak R 1991 Effects of leukotrienes on osteoblastic cell proliferation. Calcif Tissue Int 49(3):197-201.
333. Traianedes K, Dallas MR, Garrett IR, Mundy GR, Bonewald LF 1998 5-Lipoxygenase metabolites inhibit bone formation in vitro. Endocrinology 139(7):3178-84.
334. Miller DK, Gillard JW, Vickers PJ, Sadowski S, Leveille C, Mancini JA, Charleson P, Dixon RA, Ford-Hutchinson AW, Fortin R, et al. 1990 Identification and isolation of a membrane protein necessary for leukotriene production. Nature 343(6255):278-81.
335. Byrum RS, Goulet JL, Griffiths RJ, Koller BH 1997 Role of the 5-lipoxygenase-activating protein (FLAP) in murine acute inflammatory responses. J Exp Med 185(6):1065-75.
336. Flamand N, Lefebvre J, Surette ME, Picard S, Borgeat P 2006 Arachidonic acid regulates the translocation of 5-lipoxygenase to the nuclear membranes in human neutrophils. J Biol Chem 281(1):129-36.

CURRICULUM VITA

Michaele Beth Manigrasso
30 Asbury Avenue
Atlantic Highlands, NJ 07716-1414
Email: mbmanigr8@aol.com

Education:

Ph.D **"The Development and Application of the Murine Femoral Fracture Model to Examine the Effects of Genetics on Long Bone Fracture Healing"**
Biomedical Engineering, Anticipated October 2006
Rutgers University, New Brunswick, New Jersey and University of Medicine and Dentistry of New Jersey- New Jersey Medical School

Principal Advisor: J. Patrick O'Connor Ph.D.
Committee: J. Russell Parsons, Ph.D
Robert Harten, Ph.D.
Vinciane Gaussin, Ph.D
David Denhardt, Ph.D

B.S. **Syracuse University**
Syracuse, NY
Bioengineering, May 1997

Research Experience:

2000-Present **University of Medicine & Dentistry of New Jersey- New Jersey Medical School. Department of Orthopaedics**
Newark, NJ

1999-2000 **Department of Biomedical Engineering- Rutgers University**
Piscataway, NJ
Graduate research assistant- Examined how signal processing with visual evoked potentials (VEP's) are assessed in humans.

1998-1999 **JFK Rehabilitation Institute**
Edison, NJ
Prosthetic training program student internship- Measured, designed and fitted upper and lower extremity prosthetic devices.

1995-1997 **Syracuse University- Institute for Sensory Research**
Syracuse, NY
Undergraduate research assistant- Used vibrotactile psychophysics to examine how Pacinian corpuscles use recruitment in pain reception.

Publications:

Manigrasso MB and O'Connor JP. Characterization of a Closed Femur Fracture Model in Mice. Journal of Orthopaedic Trauma. 2004 Nov-Dec;18(10):687-95.

Simon AM, **Manigrasso MB**, and O'Connor JP. Cyclooxygenase-2 function is Essential For Bone Fracture Healing. Journal of Bone and Mineral Research. 2002 June; 17: 963-976.